FABRICATION OF SURFACES WITH CONTROLLED WETTING PROPERTIES ON POROUS SUBSTRATES USING NON-FLUORINATED CHEMICALS

A Dissertation
Presented to
The Academic Faculty

by

Zhenguan Tang

In Partial Fulfillment
Of the Requirements for the Degree
Doctor of Philosophy in the
School of Chemical and Biomolecular Engineering

Georgia Institute of Technology
May 2016

FABRICATION OF SURFACES WITH CONTROLLED WETTING PROPERTIES ON POROUS SUBSTRATES BY USING NON-FLUORINATED CHEMICALS

Approved by:

Dr. Victor Breedveld, Co-Advisor
School of Chemical and Biomolecular Engineering
Georgia Institute of Technology

Dr. Dennis Hess, Co-Advisor
School of Chemical and Biomolecular Engineering
Georgia Institute of Technology

Dr. Norman Marsolan
School of Chemical and Biomolecular Engineering
Georgia Institute of Technology

Dr. David Bucknall
School of Materials Science and Engineering
Georgia Institute of Technology

Dr. Amy Blakeley
Sappi North America

Date Approved: 13th of January, 2016

ACKNOWLEDGEMENTS

First and foremost, I would like to thank my advisors Dr. Dennis Hess and Dr. Victor Breedveld, for their constant support of not only my work, but more importantly my ideas. There was never a point during my time at Georgia Tech where I did not feel that I could stop by their office and sort out my problems. I will forever be grateful of the knowledge and expertise that I have gained from their advising. I would also like to thank my committee members, Dr. Norman Marsolan, Dr. Amy Blakeley and Dr. David Bucknall for their help both during and after our committee meetings.

Thanks to the Hess and Breedveld group members, Dr. Sonam Sherpa, Dr. Tae Seop Choi, Dr. Emily Peterson, Dr. Kyung Hee Oh, Dr. Sricharan Yarlagadda, Won Tae Choi and Lu Jiang for listening to my problems, and lending a helping hand whenever I needed it. Special thanks to Dr. Lester Li for giving me a lot of helpful suggestions when I started doing research. I was very fortunate to have been the mentor of many talented, hardworking undergraduates. Hanyang Li, Justin Eisenberg and Kevin Park, thanks for putting up with me and helping me to develop as a leader.

I would like to thank SAPPI Fine Paper and RBI for financially support this project and also a lot of useful ideas and suggestion during our monthly meeting.

Finally, I would like to especially thank my family for their unwavering support of my desire to get a Ph.D: Mom and Dad, thanks for being the supportive parents that I needed to make it this far.

TABLE OF CONTENTS

LIST OF TABLES

LIST OF FIGURES

SUMMARY

Paper has traditionally been used for writing and printing, packaging and cleaning. Compared with products made with synthetic fibers, paper-based products offer many advantages such as low density, high flexibility, world-wide accessibility and good degradability. Due to these excellent properties, researchers are interested in further expanding the use of paper from its traditional roles to more advanced applications such as microfluidic devices and biological test strips. However, the intrinsic hydrophilicity and oleophilicity limit the potential applications of paper-based products. As a result, there is a continuous effort from both industry and academia to fabricate paper-based substrates with controlled wetting properties. However, although there is a plethora of existing methods to fabricate paper with a variety of modified wetting properties, most of these methods rely heavily on the use of fluorinated coating materials, which are often associated with significant environmental and health concerns. Therefore, investigation of methods to fabricate paper with controlled wetting properties using non-fluorinated chemicals is of significant interest. In this thesis, we utilize a variety of non-fluorinated coating materials to fabricate paper with controlled wetting properties including hydrophobic, amphiphobic and hydrophilic/oleophobic.

To fabricate paper with amphiphobic properties, a non-fluorinated polymer, poly (benzoxazine), was used. Benzoxazine monomer was applied to paper surfaces by either a dip coating or drop casting method. The coated paper samples were subsequently cured at different conditions to initiate the polymerization process. The oleophobicity of PBZ coated paper samples is closely related to both the degree of polymerization of PBZ and

the amount of PBZ on the paper. Paper samples with a loading of 10.6 mg/cm^2 of PBZ display prolonged resistance against oils after curing at 180 ^{o}C for 12 hours. However, the disadvantages of PBZ as coating material are also obvious: high loading and prolonged curing time means that this procedure has limited economical feasibility. Treated paper also loses some flexibility due to the high-temperature-curing.

To fabricate amphiphobic paper under milder conditions, a simple immersion coating method was developed to coat alkyltrichlorosilanes on paper surfaces under ambient conditions. Four different reagents were used in this study to investigate the effect of alkyl chain length on the wetting properties of alkyltrichlorosilane coated paper: methyltrichlorosilane (MTCS; -CH_3), butyltrichlorosilane (BTCS; -C_4H_9), dodecyltrichlorosilane (DTCS; -$C_{12}H_{25}$) and octadecyltrichlorosilane (OTCS; -$C_{18}H_{37}$). SEM analyses reveal that by systematically varying alkyl chain length, films with different surface morphologies could be generated on flat silicon wafer control samples and on cellulose-based paper samples. The variation in surface morphology leads to different wetting behavior, as determined by measuring static water and oil contact angles. Due to the nano- and micron- scale roughness on MTCS coated substrates, paper samples coated with MTCS display superhydrophobicity with a water contact angle of 152.2°, which is the highest water contact angle among these four alkyltrichlorosilanes. However, additional nano-scale roughness from an MTCS coating reduces the oil resistance of coated paper samples, while paper samples coated with long-chain alkyltrichlorosilanes have lower surface energy and lack nano-scale roughness. As a result, paper samples coated with OTCS display the highest resistance against oils (ethylene glycol contact angle, 125.5°; diiodomethane contact angle, 101.3°).

Hydrophilic-oleophobic surfaces have attracted significant attention recently due to their potential use in technologies ranging from oil-water separation to self-cleaning surfaces. Studies with alkyltrichlorosilane coated paper demonstrate for the first time that a simple, solution-based method can be used to fabricate oleophobic paper with tunable hydrophilicity using a non-fluorinated material, methyltrimethoxysilane (MTMS). Wetting control is achieved by paper surface modification using a thin film of hydrolyzed MTMS. Hydrophilicity is tuned by adjusting the sonication time during MTMS hydrolysis. ^{29}Si NMR and ATR-FTIR analyses reveal that the change in hydrophilicity results from varying the concentration of polar silanol groups in the MTMS solution and, ultimately, on the film surface. The modified paper displays wetting behavior ranging from superhydrophilic/oleophobic (immediate water absorption; motor oil contact angle, 64.2°±1.4°) to amphiphobic (water contact angle 85.2°±3.4°; motor oil contact angle 61.2°±2.5°) as a function of hydrolysis time. For all surface-modified samples, no absorption of motor oil is observed for several weeks, indicating stable oil resistance. Based upon results from SEM, optical profilometry, and air permeability, the intrinsic porosity of paper is also largely retained after coating.

Application of the fundamental knowledge gained from studies of MTMS coated paper, allowed the fabrication of amphiphobic wood and hydrophilic/oleophobic stainless steel mesh surfaces using hydrolyzed MTMS. The amphiphobic wood has potential applications as a packaging material that can repel both aqueous and oily fluids, while the hydrophilic/oleophobic stainless steel mesh can be used to separate oil/water mixtures.

CHAPTER 1

INTRODUCTION

Cellulose-based products have been traditionally used as writing media and packaging materials. Recently, paper has found further use in advanced applications such as microfluidics and biological test strips; these applications of paper based products are hindered by the intrinsic hydrophilicity and oleophilicity of cellulose fibers. As a result, interest has grown to impart paper with controlled wetting and adhesive properties. However, most of the existing methods heavily rely on fluorinated coating materials, which are often associated with severe environmental and health concerns. The primary aim of this thesis is to develop new solution-based methods to fabricate paper with controlled wetting properties by using non-fluorinated chemicals. To set the stage for studies to achieve this aim, background knowledge on surface energy and wetting is presented in the next couple of sections, before providing an outline for this thesis ast the end of this Chapter.

1.1 Surface Energy and Wetting

Surface energy quantifies the energy cost associated with the disruption of intermolecular bonds at the solid surface, [1] and therefore is a very important parameter for many industrial processes such as cleaning, drying and painting. [2] [3] Surface energy is an intrinsic property of a material, depending only on the magnitude of intermolecular forces of materials. Perfluorinated surfaces have long been known to have the lowest surface energies. [4] The most commonly used low surface energy material is

poly(tetrafluoroethylene) (PTFE), which has a surface energy of 18.1 mN/m. [5] For a surface with closely packed perfluorocarbon groups, the surface energy could be further reduced. For example, a surface energy as low as 6.7 mN/m was achieved through vapor deposition of $C_{20}F_{42}$ onto a glass substrate. [6] In this case, the axes of molecules were aligned perpendicular to the glass surface due to steric hindrance effects. As a result, closely packed trifluoromethyl groups are directed away from the surface. Because of this distinctive property of fluorocarbons, surface fluorination is widely used to reduce the surface energy of a variety of substrates.

Wetting is the ability of a liquid to maintain contact with a solid surface, resulting from intermolecular interactions when the two are brought together. The degree of wetting depends on the intrinsic properties of the individual materials: the solid surface energy and the liquid surface tension. The most common method to evaluate wetting behavior is contact angle measurements. Contact angle is defined as the angle, conventionally measured through the liquid phase, at which the solid surface meets the vapor/liquid interface. Contact angle quantifies the wetting behavior between a specific solid/liquid pair. Generally speaking, a high contact angle indicates that the solid has a low wettability with the specific liquid, and *vice versa*. The magnitude of the contact angle is determined by the solid surface energy, liquid surface tension and the balance of resulting adhesive forces at the solid-liquid interface on a flat surface. This relationship is given by Young's equation:

$$\cos\theta_Y = \frac{\gamma_s - \gamma_{SL}}{\gamma_L}$$

In this equation, θ_Y is the equilibrium contact angle, as measured on a flat surface, and therefore represents a thermodynamic equilibrium. γ_s is the solid surface energy, γ_L the

liquid surface tension and γ_{SL} the interfacial energy between two phases. According to Young's equation, a high contact angle, or low degree of wetting, can be most easily achieved with a high surface tension fluid on a solid with low surface energy.

A key limitation of Young's equation is that it only applies to perfectly flat, homogeneous, smooth surfaces. In reality, most solid surfaces are not perfectly flat and almost always have some degree of roughness. Therefore, understanding wetting behavior on rough surfaces is essential for designing and controlling wetting processes in general. When considering wetting behavior on a rough surface, one of the most important questions is whether the liquid is in full contact with the solid, thereby filling the roughness grooves, or if the liquid is suspended on top of the roughness features, leaving air pockets between the liquid and solid. The former situation is described by the Wenzel model, while the latter can be described using the Cassie-Baxter model. The Wenzel and Cassie-Baxter models are the two models most frequently employed to describe wetting behavior and contact angle on a rough surface. Both scenarios are depicted in Figure 1.1.

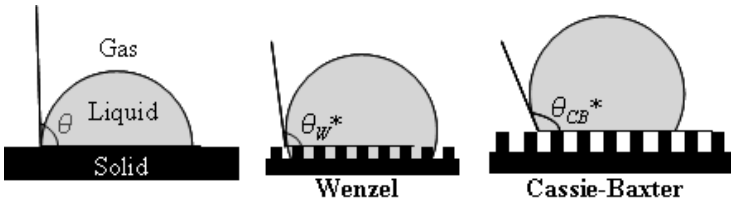

Figure 1.1: Illustration of different wetting states. From left to right: Equilibrium state, Wenzel state and Cassie-Baxter state. [7]

According to the Wenzel model for homogeneous wetting, the Wenzel apparent contact angle θ_W can be calculated from the equilibrium contact angle θ_Y and the roughness ratio *r*, which is defined as the ratio of the solid/liquid contact angle to its projected area (i.e. $r \geq 1$):

$$\cos\theta_W = r \cdot \cos\theta_Y$$

The Wenzel model shows that if the equilibrium contact angle is less than 90°, the apparent contact angle decreases with increasing roughness. On the other hand, if the equilibrium contact angle is greater than 90°, additional roughness further increases the apparent contact angle. [8]

The apparent contact angle θ_{CB} for a suspended droplet can be calculated by the Cassie-Baxter model as

$$\cos\theta_{CB} = f_s \cdot (1 + \cos\theta_Y) - 1$$

where f_s is the liquid-solid areal contact fraction. In contrast to the Wenzel state, the Cassie-Baxter relation allows the possibility of an apparent contact angle greater than 90° even with an equilibrium contact angle less than 90°. [9]

In addition to contact angle, another important parameter to characterize the wetting behavior is hysteresis. Contact angle hysteresis describes the adhesion of liquids to the substrate. This property is commonly quantified through contact angle hysteresis measurements, which determine the difference between advancing and receding contact angles of a liquid interface when moving across the surface. Another way to describe hysteresis is through roll-off angle measurements, which determine the angle between the sample surface and a horizontal plane at which a liquid drop starts to slide off the surface under the influence of gravity.

1.2 Surfaces with Controlled Wetting Properties

Generally speaking, surfaces with controlled wetting properties can be categorized into four types: amphiphilic surface, hydrophobic surface, amphiphobic surface and hydrophilic/oleophobic surface.

A hydrophobic surface is defined as having a water contact angle greater than 90°. On a flat substrate, hydrophobicity can be achieved by reducing the solid surface energy. For example, a flat PTFE sheet, with a surface energy of 18.1 mN/m, has a static water contact angle of 110^{o}. [10] By further reducing surface energy, a water contact angle of 119° can be observed on a surface with close hexagonal packing of $–CF_3$ groups, which is the highest water contact angle ever reported on a smooth surface to date. [11] In order to further increase the water contact angle, roughness needs to be generated on the flat substrate. A plethora of methods have been developed to fabricate substrates with hierarchical roughness. [12-14] By coating low surface energy materials on such substrates, surfaces with water contact angles greater than 150° can be fabricated. These surfaces, also known as superhydrophobic surfaces, are desirable for many industrial applications such as anti-fouling paints, self-cleaning windshields and some other biomedical applications. [14]

Compared to hydrophobic surfaces, design and fabrication of oleophobic surfaces are much more difficult. This is caused by significant differences between water and polar liquids in terms of surface tension. Water, due to its ability to form strong hydrogen bonding with neighboring molecules, has a much higher surface tension than non-polar oils. The surface tensions of some common fluids are shown in Table 1.1. Because of the difference in surface tension, water usually has a much higher contact angle than oils on

the same surface. Therefore, compared with hydrophobic surfaces, oleophobic surfaces normally require an even lower surface energy to achieve high contact angles. Consequently, most oleophobic materials reported in literature are fluoro-polymers or substrates with fluorinated materials as surface coatings. [15] [16] Even so, the equilibrium contact angles of oils seldom reach 90°. To achieve higher oil contact angles, specific micron-scale surface structures, often referred as "re-entrant" structures (*i.e.*, surfaces with concave topographical features), must be generated on the substrate. The schematic depiction of a re-entrant structure is shown in Figure 1.2. The re-entrant structure can be obtained either via special "undercut" structures as in Figure 1.2(B), or simply by using cylindrical fibers on the surface, as in 1.2(A). By combining such structures with a low-surface-energy coating, oleophobicity and superoleophobicity (as defined by a hexadecane contact angle > 150^{o}) have been successfully fabricated on different substrates such as silicon, aluminum, titanium, stainless steel, polymers and paper. [17-20]

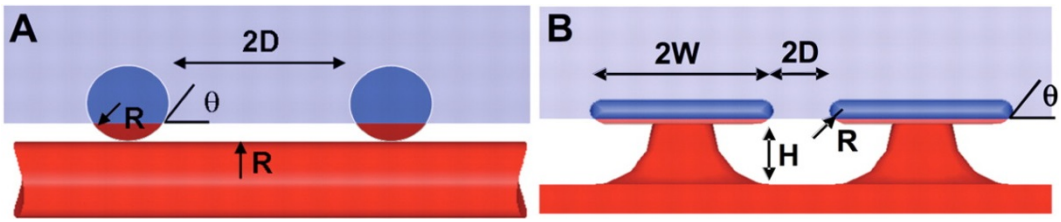

Figure 1.2: Two different examples of re-entrant structures. The blue part of the surface is wetted (in direct contact with liquid) while the red surface remains non-wetted.

Because water has a higher surface tension than most oils, oleophobic surfaces are generally hydrophobic as well. However, there are exceptions to this rule. Recently, interest has grown in surfaces that simultaneously display the unusual combination of hydrophilicity and oleophobicity. Such substrates have potential industrial applications, such as oil/water separation membranes, self-cleaning surfaces and anti-fog surfaces. [21-23] In order to decouple oleophobicity from hydrophobicity, chemical heterogeneity can be used to introduce favorable interactions with polar liquids (water), while maintaining unfavorable interactions with non-polar liquids (oil). This concept has been implemented with various coating materials such as polyelectrolyte-fluorinated surface complexes. On a flat substrate, oleophobic but hydrophilic surfaces have thus been fabricated with oil contact angles greater than 120^{o} while the water contact angle was less than 10^{o}. [21]

Table 1.1: Surface tension of some common testing fluids. R. P. test oil is a mixture of oleic acid and glycerol trioleate and is widely used industrially to measure oleophobicity because its composition is similar to oils in food.

Testing fluids	Surface tension (mN/m)
Water	72.8
Diiodomethane	50.8
Ethylene glycol	48.8
R. P. test oil	34.1
Motor oil	31.0
Hexadecane	27.5

1.3 Fabrication of Cellulose-Based Paper with Controlled Wetting Properties

Paper has traditionally been used for writing and printing, packaging and cleaning applications, most of which involve interactions with liquids during processing and/or use. The primary component of paper is cellulose, a linear condensation polymer consisting of D-glucose units joined together by β-1, 4-glycosidic bonds, as illustrated in Figure 1.3. Each glucose unit has three hydroxyl groups, which form inter- and intra-molecular hydrogen bonds. The hydrogen bonding provides strength to paper and also establishes its intrinsic hydrophilic and oleophilic character.

Compared with products made from synthetic fibers, paper-based products offer many advantages such as low density, high flexibility, world-wide accessibility and good biodegradability. Due to these excellent properties, researchers are interested in expanding the applications of paper from its traditional roles to more advanced possibilities. However, the intrinsic hydrophilicity and oleophilicity limit the potential applications of paper-based products. As a result, there is a continuous effort in both industry and academia to fabricate paper with controlled wetting properties.

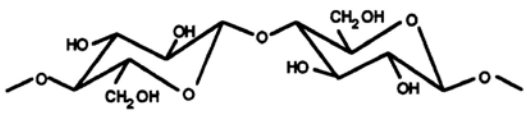

Figure 1.3: Molecular structure of cellulose [24]

Fabrication of Hydrophobic Paper

Fabrication of hydrophobic paper attracts great attention from industry due to its potential applications as packaging materials for water and wet groceries. The intrinsic hydrophilicity makes untreated paper unsuitable for containment of liquids with significant amounts of water. Even if the packaged product does not contain fluid, untreated paper still cannot be used as packaging material in moist environments (*e.g.*, humid climates and rainy weather). This is because the absorption of water into paper interferes with the hydrogen bonding between fibers, leading to weakening of bonds and thus compromising the overall strength of the paper product. [25] The decrease in strength of paper-based packaging material can then cause product damage. Furthermore, when used as advertising media, companies do not want the printed images on packaging to deteriorate when exposed to moisture. To solve this problem, the paper industry has been driven towards the design of hydrophobic paper. In academia, researchers are seeking novel applications for paper-based products such as paper-based microfluidic devices and paper-based membranes for water and oil separation, which also require fabrication of water resistant paper substrates.

One current technique that is widely used industrially to fabricate hydrophobic paper is referred to as “sizing”, which involves the addition of chemicals during the paper making process to fabricate water repellent paper. [25] Some commonly used sizing agents are alkyl succinic anhydride (ASA), alkylketene dimer (AKD) and rosin. [26, 27] All sizing agents share a similar chemical structure: they have hydrophilic functional groups that bond to the cellulose fiber, as well as hydrophobic moieties, which usually consist of long hydrocarbon chains, that are exposed on the surface of the treated fibers.

[27] A non-polar surface layer is thus formed on the substrate, which imparts hydrophobicity to the paper.

There are two different general methods for applying sizing agents to paper: internal sizing and surface sizing. Internal sizing is the process by which paper is made hydrophobic by adsorbing sizing colloids on the fibers before the formation of the paper sheet. This is typically done by adding a stabilized sizing suspension directly to the paper pulp, prior to introduction into the paper machine. [28] On the other hand, sizing agents can also be applied to the surface of the paper after it has been formed and (partially) dried with techniques like dip coating and drop casting. This method is called surface sizing. [29] Paper treated with sizing agents can display hydrophobicity with water contact angles greater than 110^{o}. [30] Compared with other techniques used in the paper industry to fabricate hydrophobic paper, such as waxing and polymer coating, the biggest advantage of sizing is that it only requires very small amounts of additives to overcome the inherent wettability of paper. Typical additional levels of the most efficient internal sizing agents lie in the range of 0.05 to 0.25%, based on the dry weight of paper. [25] However, the sizing of paper can only provide a moderate degree of water resistance, providing no protection against water vapor or complete submersion of the paper into water. [31]

Although paper sizing provides a facile and low cost method to fabricate hydrophobic paper, the water contact angle on sized paper seldom rises above 120^{o}. Although this moderate hydrophobicity is sufficient for many paper-based packaging materials, it is not sufficient for some novel applications of paper-based product such as microfluidic devices. For these applications, superhydrophobic surfaces with low

hysteresis are required. To achieve these aims, sub-micron and nano-scale roughness must be imparted to the fiber surfaces in addition to a favorable surface chemistry. This can be accomplished by several different surface morphology modification techniques.

One common technique to impart roughness on paper surfaces is by particle deposition. Nano- and sub-micron scale particles made of different materials were used in the fabrication of hydrophobic paper including silica, precipitated calcium carbonate (PCC) and titanium dioxide. [32-34] Among them, titanium dioxide (TiO_2) has attracted great attention from both academia and industry because it can not only impart roughness to paper surfaces, but also greatly improves the optical properties, such as brightness and opacity. However, due to the high price of TiO_2, its usage is limited to higher grade, value added products. Gao *et al.* demonstrated the use of TiO_2/epoxy resin (ER) thin films to fabricate hydrophobic surfaces on filter paper. [34] By using coupling agents, the amorphous titanium dioxide was bonded to the epoxy resin to create a TiO_2/ER mixture. Due to the high viscosity of the epoxy resin, TiO_2/ER could be applied to the filter paper surface with a simple immersion coating method. This process considerably enhanced the nano-scale roughness of the filter paper, as shown in Figure 1.4. To reduce the surface energy of treated filter paper, its surface chemistry was modified by octadecyltrichlorosilane (OTCS). The combination of nano-scale roughness and low surface energy renders the filter paper superhydrophobic with a maximum contact angle of 153 ± 1^{o}, but roll-off angles and hysteresis were not reported in this study.

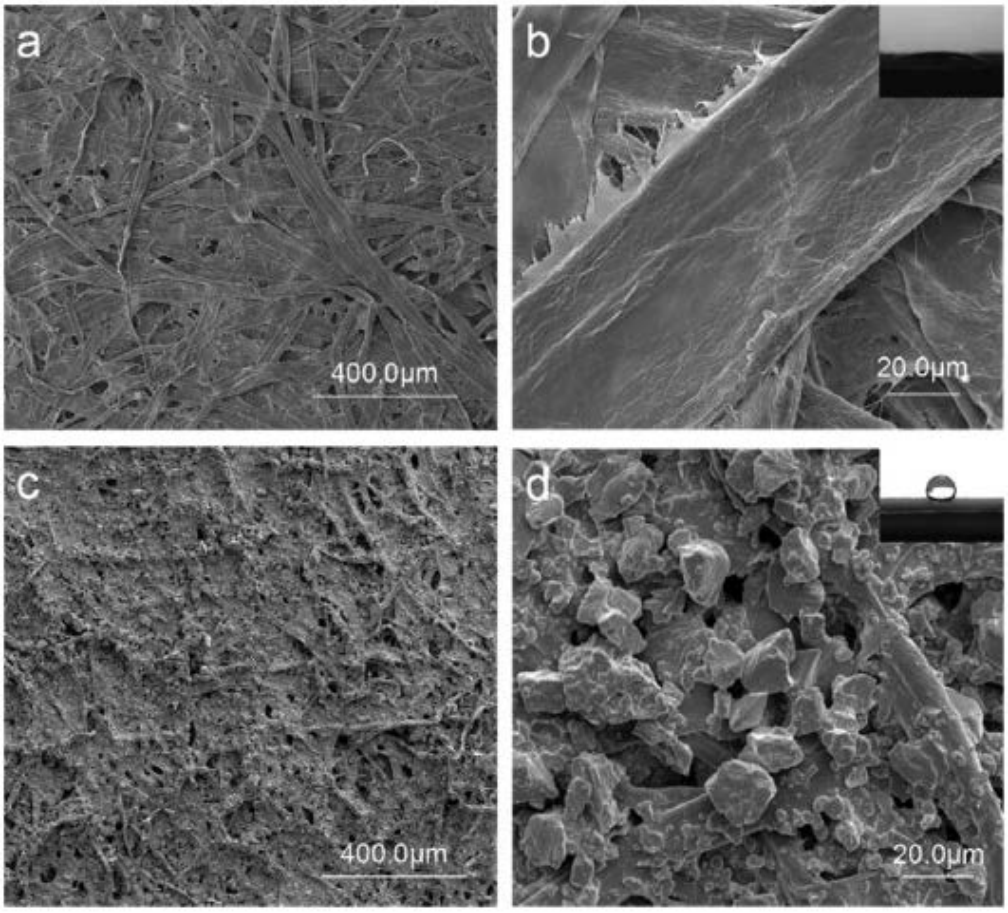

Figure 1.4: SEM images of a) the pristine filter paper and b) TiO_2/ER coated filter paper at low magnification. Complimentary high magnification SEM images are shown in c) and d). The insets of b) and d) are photographs of water droplets on the filter paper before and after treatment. [34]

Teisala *et al.* fabricated superhydrophobic paper with TiO_2 by using a different coating method: liquid flame spray (LFS). [35] LFS is a thermal spraying method for generating and depositing nanosized metal and metal oxide particles. In the LFS process the precursors are in liquid form, diluted in water or alcohol, and they are fed together with the combustion gases into a specially designed spray gun. Instantly after exiting the nozzle, the precursor solution is atomized into micron-sized droplets by the high-velocity gas flow. Liquid droplets evaporate in a hot and turbulent flame and subsequent reaction

of the precursor vapor leads to formation of nanoparticles of the desired material. In this study, by using titanium tetraisopropoxide (TTIP) as the precursor and H_2 and O_2 as combustion gases, TiO_2 nanoparticles were successfully deposited uniformly on paper surfacesBecause a carbonaceous layer is spontaneously formed on these particles, further surface chemistry modification was unnecessary. The authors found that the hydrophobicity of treated paper is highly dependent upon the concentration of the precursor solution: higher concentrations of the precursor solution led to a stable water contact angle greater than 150°, whereas on surfaces created at lower precursor concentrations, the water contact angle decreases slowly, as shown in Figure 1.5. However, strong droplet adhesion (high roll-off angle) was observed for all samples in this study.

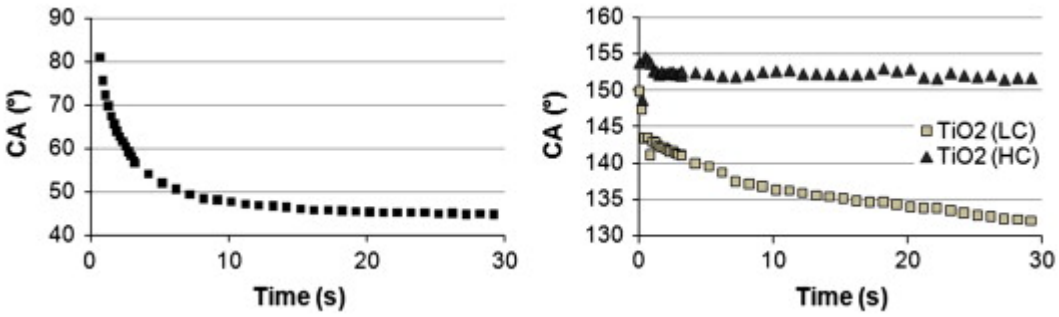

Figure 1.5: Water droplet spreading as a function on the untreated paper (left) and on the coated paper (right). Feed rates for TiO_2 low concentration (LC) and high concentration (HC) were 30 and 32 ml/min respectively. [35]

The use of nanoparticle coatings raises a question of the stability of the surface performance. Depending on the end-use application, various environmental factors together with friction, lubrication and chemical resistance influence the wear of a surface.

[36] Adhesion between nanoparticles and paper plays an important role in the durability of the hydrophobic surface. More importantly, poor adhesion of nanoparticles to a surface is a human health concern if the nanoparticles are introduced into air. Stepien *et al.* conducted a study to investigate the wear resistance of SiO_2 and TiO_2 nanoparticles coated paper samples. Nanoparticles were generated and applied to the paper substrate using LFS. The abrasion resistance of coated paper samples was evaluated using the Taber Abrader. Figure 1.6 shows a schematic for the abrasion. Surface topological changes of the samples were quantified by calculating surface roughness based on AFM measurements. It was found that the abrasion test significantly decreases the surface roughness values as a function of the number of abrading revolutions for both samples, as shown in Figure 1.7. Consequently, the hydrophobicity of both samples decreases with severe abrasionbecasue of removal of the nanoparticle coating on the paper surface.

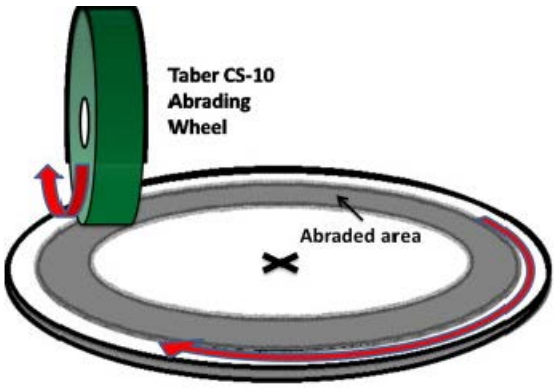

Figure 1.6: Schematic of a common set-up for abrasion testing. [36]

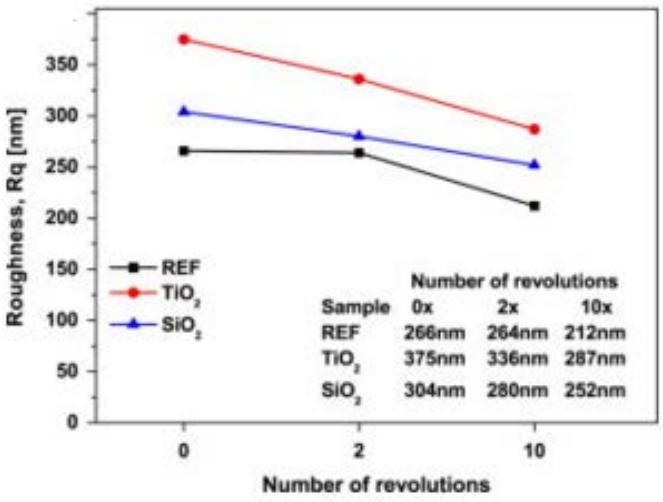

Figure 1.7: Changes in RMS roughness, R_q (nm) as a function of number of revolutions after abrasive testing [36]

Compared with particle deposition, where the strength of the bond between particles and the surface is of concern, selective etching has the advantage of maintaining the inherent mechanical stability of the substrate. Selective etching removes chemically less stable (i.e.more reactive) material, and generally enhances roughness. In one study, Balu *et al.* demonstrated the use of oxygen plasma etching to uncover nanoscale roughness on paper. [37] Cellulose contains both crystalline and amorphous regions. When exposed to an oxygen plasma, the amorphous cellulose is etched away at a higher rate than are crystalline regions. This process thus creates nanoscale roughness, as shown in Figure 1.8. After etching, the surface chemistry of treated paper was modified by deposition of 100 nm of fluorocarbon film by plasma enhanced chemical vapor deposition (PECVD) with pentafluoroethane (PFE) as the precursor gas. The coated paper displays superhydrophobicity with a roll-off angle less than 10^{o}.

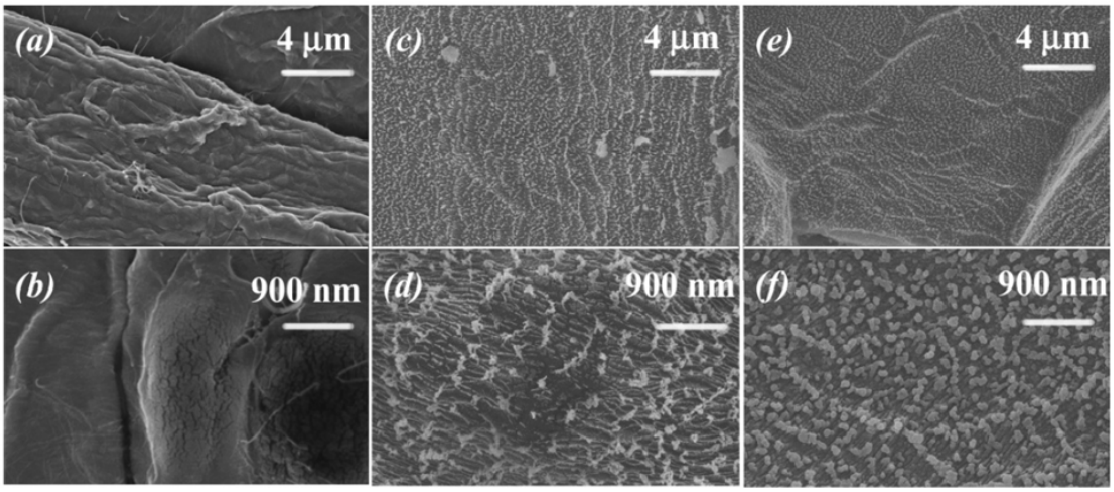

Figure 1.8: High magnification SEM images (5000x and 20,000x) of (a, b) untreated paper, (c, d) oxygen etched paper, and (e, f) oxygen etched and PFE-coated paper. [37]

Li *et al.* further demonstrated that by using selective oxygen plasma etching, superhydrophobic paper with low roll-off angle can be fabricated by applying a thin hydrophilic diamond-like-carbon (DLC) surface coating, [38] where the roll-off angle is correlated with etch time. After a relatively short etch, nano-scale structure was generated on DLC coated paper samples. As a result, treated paper samples display high water contact angle, but has strong adhesion of water droplets. Continued plasma etching of the paper substrates modified the micron-scale structure as well, partially etching away the larger fibers to create smaller diameter fibrils, thus enhancing the micron-scale roughness. After 60 minutes of etching, a hierarchical structure is created, which after deposition of DLC, yields low hysteresis superhydrophobic properties that are similar to paper substrates coated with fluorocarbon thin films, as shown in Figure 1.9.The significance of this work is that it demonstrates that low hysteresis superhydrophobic

paper can be fabricated even by using an inherently hydrophilic coating material, as long as the substrate possesses the appropriate hierarchical structure.

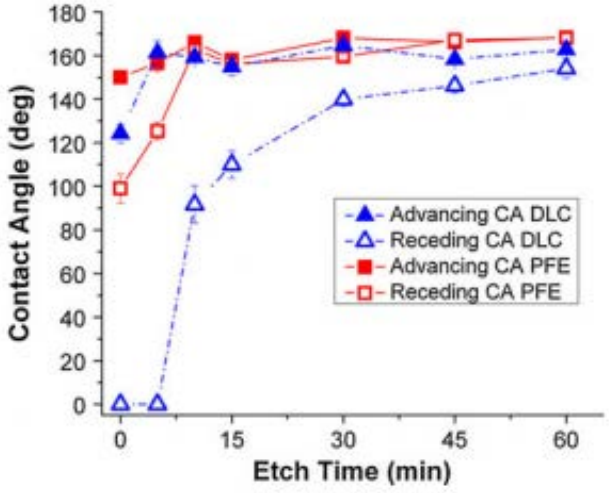

Figure 1.9: Advancing (solid symbols) and receding (open symbols) contact angle data for DLC (triangles) and PFE (squares) coated paper samples as a function of etch time in oxygen plasma. [38]

Fabrication of Amphiphobic Paper

As discussed in previous sections, surface roughness and surface energy are the two main factors controlling surface wetting properties. By deposition of low surface energy compounds onto roughened paper, hydrophobic or superhydrophobic paper can be fabricated. However, most of the superhydrophobic surfaces that are obtained this way are oleophilic and it remains challenging to enhance the anti-wetting property of the surface which repels liquids with surface tensions lower than water. Oil-repellent paper products that can be manufactured via scalable processes are of great interest for the paper industry, with applications in fluid and materials packaging. Furthermore, oleophobic paper can expand the use of paper products into other fields such as the

biomedical industry where disposable, bacteria-resistance surfaces and microfluidic devices can be envisioned. [39, 40]

In one study, Bongiovanni *et al.* reported photo-induced grafting of a highly fluorinated acrylic monomer onto cellulose substrates, which has a long perfluoropolyether chain. [41] To apply the monomer on the paper surface, paper samples were dipped into an acetone solution containing a fixed concentration of monomer and photo-initiator. Then the sample was irradiated on both sides under nitrogen with a medium pressure Hg lamp to start the photo-induced grafting process. The irradiation time was varied from 60 to 240 s. The sample was then solvent extracted with a Soxhlet apparatus and subsequently analyzed. Angle-resolved XPS was used to gather information on sample composition at different depths, ranging from 1.3 nm to 3 nm, depending on the take-off angle. The XPS result indicates that there is a high amount of fluorine at the paper surface after modification. In particular at the most external surface (~1.3 nm): the F/C ratios found are in the range of 1.24 and1.45, which is equal to that of the pure fluorinated acrylic monomer. By increasing the depth of the XPS probing, the concentration of the fluorine is clearly different: the F/C ratio decreases and the O/C ratio increases. This gradient indicates that the grafting is largely limited to the paper surface. The preferential segregation of perfluorinated chains at the treated paper surface successfully reduces the surface energy, as shown in Figure 1.10. Although dependent on the UV irradiation time, all samples display surface energies below 12 mN/m. This is much lower than some common fluorinated polymers, such as PTFE (20 mN/m). As a result, coated paper samples display good oil repellency with hexadecane contact angles ranging from 88° to 97° depending upon the grafting conditions.

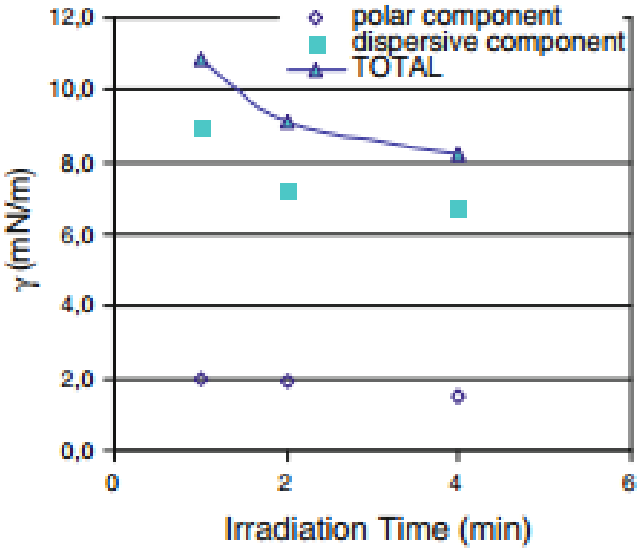

Figure 1.10: Surface energy of paper modified with fluorinated acrylic monomer as a function of irradiation time. [41]

Silanation is another method commonly used to apply fluorinated coatings on paper surfaces. Taking advantage of the hydroxyl-rich surface of cellulose, organosilanes with low surface energy organic groups have been used to make paper hydrophobic and amphiphobic following both gas-phase and solution immersion reactions. Glavan *et al.* reported the fabrication and properties of amphiphobic paper produced by silanation of paper with fluoroalkyltrichlorisilanes. [42] Gas-phase silanation is used in this study to render paper amphiphobic for the benefit that the procedure does not require pre- or post-treatment and the processing can be completed within minutes. To study the effect of chain length and fluorination of the organosilane on the wettability of paper, three fluoroalkyltrichlorosilanes with different fluorinated alkyl chain length were used in this study: (tridecafluorooctyl)trichlorosilane ($CF_3(CF_2)_5CH_2CH_2SiCl_3$) ($C_8^F$), (heptadecafluorodecyl)trichlorosilane ($CF_3(CF_2)_7CH_2CH_2SiCl_3$) ($C_{10}^F$) and (henicosadecafluorododecyl)trichlorosilane

($CF_3(CF_2)_9CH_2CH_2SiCl_3$) ($C_{12}^F$). C_{12}^F is the trichlorosilane with the longest fluorinated alkyl chain. To compare fluorinated and non-fluorinated coating materials with regards to liquid repellency, two alkyltrichlorosilanes were also used in this study: methyltrichlorosilane (CH_3SiCl_3) (C_1^H) and decyltrichlorosilane (CH_3 $(CH_2)_9SiCl_3$) (C_{10}^H). The silanation reaction was performed in a vacuum oven at 95^{o}C and 30 mbar using a solution of the organosilane (~10 mL of a ~30 mM solution in toluene) to supply an appropriate concentration of the silanating reagent in the vapor phase. The organosilane was allowed to react with the paper samples for 5 min. To investigate the effect of roughness of the underlying paper substrate, three different paper samples were used in this study: Whatman Gel Blot paper, Whatman #1 paper and Whatman #50 paper. As shown by the SEM images in Figure 1.11, Whatman #50 paper seemed the smoothest, followed by Whatman #1, while Whatman Gel Blot paper is the roughest. This observation is further confirmed by root mean square roughness as determined by optical profilometry. Contact angles of nine test liquids with surface tensions ranging from 16 to 83 mN/m were measured on all silanized paper samples, as shown in Figure 1.12. The result clearly indicates that although paper coated with non-fluorinated alkyl trichlorosilanes can resist wetting by liquids with surface tension greater than 54 mN/m, test liquids with lower surface tensions wick into the paper. On the other hand, for paper coated with fluoroalkyltrichlorosilanes, all samples were able to resist wetting by liquids with surface tensions as low as 27 mN/m (hexadecane). This result again reflects the lower surface energy of the paper fibers functionalized with fluorinated materials relative to those functionalized with alkyl groups. Although all paper samples coated with fluorinated trichlorosilanes display amphiphobicity, samples

coated with long fluorinated alkyl chain display higher oil contact angles. This is likely due to better surface coverage of long chain fluoroalkyltrichlrosilanes. However, further studies of the surface chemistry are required to confirm this hypothesis. Another important observation from this study is that the intrinsic roughness of paper can have significant impact on the amphiphobicity of coated paper: treated blot paper displays a much higher hexadecane contact angle than Whatman #1 or Whatman #50 filter paper. However, even for blotting paper coated with C_{12}^{F}, which is the sample with the highest oil repellency in this study, the hexadecane contact angle is still below 130^{o}.

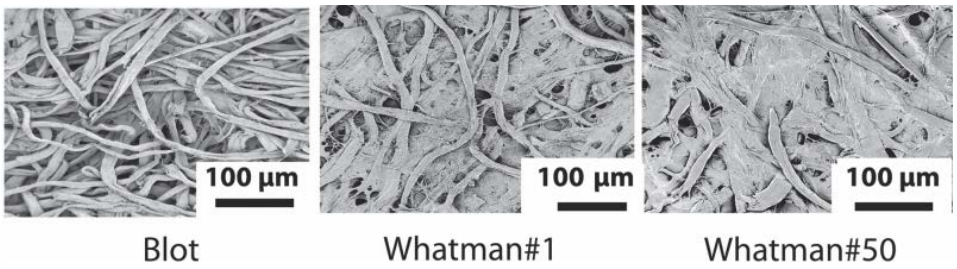

Figure 1.11: SEM images showing the topography of the different paper surfaces. [42]

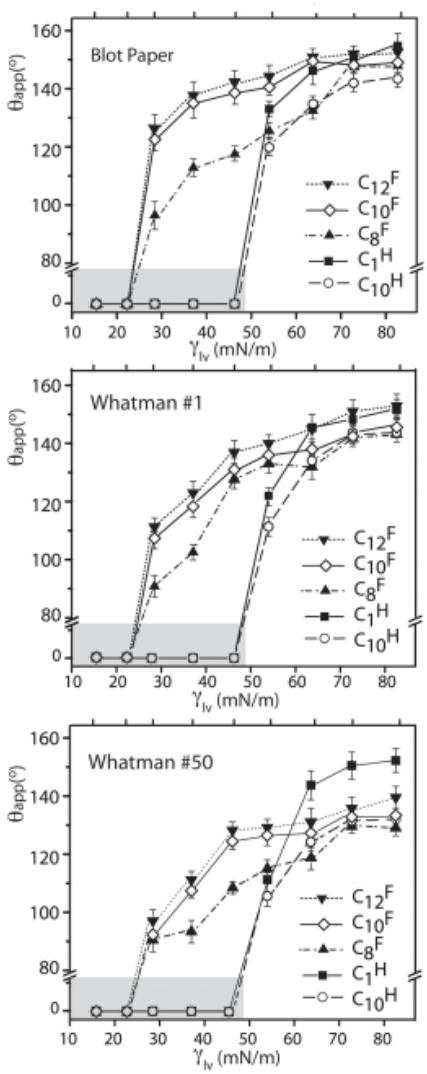

Figure 1.12: Contact angles for fluids with different surface tensions measured on coated paper samples. The grey area indicates liquids that spontaneously spread onto the substrate through capillary wicking. [42]

Glavan *et al.* demonstrated the importance of paper roughness in the fabrication of paper with amphiphobic properties. [42] In order to fabricate paper with even higher oil repellency, the paper surface morphology must be further adjusted. Li *et al.* reported an approach to the design and fabrication of superamphiphobic paper by systematically altering the average fiber size and inter-fiber spacing. [20] The optimum ratio between fiber size and spacing was calculated based on the framework provided by the Cassie-Baxter model. In order to model fiber-based substrates, modifications to the Cassie-Baxter equation have been made:

$$\cos\theta_{CB} = \frac{D(\pi - \theta_Y)}{L} \cdot \cos\theta_Y + \frac{D}{L} \cdot \sin\theta_Y - 1$$

According to the modified Cassie-Baxter equation, the apparent contact angle (θ_{CB}) is a function of the center-to-center distance between two fibers (L), the fiber diameter (D), and equilibrium contact angle (θ_Y). To fabricate paper with superamphiphobic properties, the *L/D* ratio must be much larger than that for traditional paper. Consequently, the fiber diameter must be reduced and the spacing between fibers must be increased to create superamphiphobic paper. Pulp refining was used to reduce the fiber diameter. During refining, fibrous pulp is ground between metal gears, thereby shearing (or "fibrillating") the individual fibers. An increase in refining intensity ultimately separates fibers into their elementary components, so-called fibrils, much like a braided rope can be deconstructed into many smaller diameter cords. As a result, increased refining intensity leads to smaller fiber diameter, as shown in Figure 1.13. To enhance the separation distance *L* between fibers and fibrils, a solvent exchange method was used, in which water was drained from the fibrous pulp and replaced by *sec*-butanol;

the pulp is then drained of the *sec*-butanol and dried without subsequent exposure to water. Organic solvents have been demonstrated to prevent hydrogen bonding between cellulosic fibers. [43] In this study, *sec*-butanol was employed to prevent the fibrils created during the refining process from binding together through hydrogen bonds, thereby significantly increasing sheet porosity. However, paper treated with *sec*-butanol also has a much lower mechanical strength due to the inhibition of interfiber hydrogen bonding. The treated paper was then exposed to an oxygen plasma to increase nano-scale roughness and subsequently coated with fluoropolymer. Contact angles of different test fluids were measured on samples that had been etched for different times, as shown in Figure 1.14. Without etching, deposition of a fluoropolymer layer is sufficient to render the paper superhydrophobic, but the sheets readily absorb oils. Paper etched for 10 min can repel all four test fluids. Etching for 30 min followed by fluoropolymer deposition yields a superamphiphobic surface which supports contact angles greater than 150° for all test fluids. Samples maintained high contact angles and repellency for at least 5 days. Development of superamphiphobic paper surfaces facilitate novel applications where water and oil absorption must be inhibited simultaneously for prolonged times.

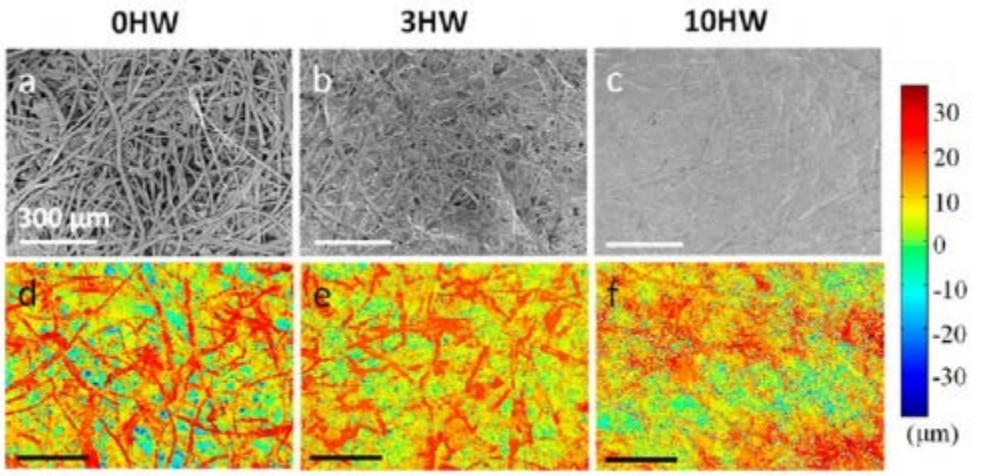

Figure 1.13: SEM images of unrefined paper, paper refined to 3000 revolutions and paper refined to 10,000 revolutions are shown in (a-c). Complementary profilometer images are presented in (d-f). All scale bars correspond to 300 µm. [20]

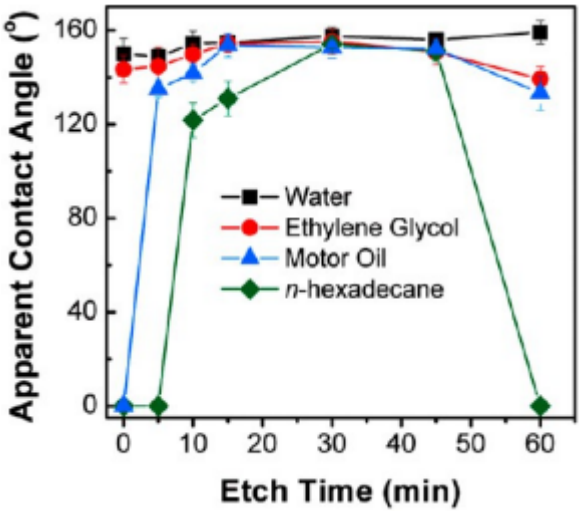

Figure 1.14: Contact angles of water, ethylene glycol, motor oil and *n*-hexadecane versus etch time for paper made with fibers refined to 10,000 revolutions by using solvent exchange processing. [20]

Fabrication of Hydrophilic/Oleophobic Paper

Paper that can simultaneously display hydrophilicity and oleophobicity, based on a favorable interaction with polar liquids and an unfavorable interaction with non-polar liquids, is of great interest in materials for applications such as oil/water separation membranes. [44] The underlying principle in designing hydrophilic-oleophobic surfaces is to utilize chemical heterogeneity. Hydrophilic and oleophobic functional groups are generally interspersed in these types of surfaces. Chemical groups with low surface energy contribute to oleophobicity, while polar surface moieties can exhibit sufficiently strong interactions with water molecules to yield hydrophilicity. This concept has been implemented with various coating material such as fluoroalkylated oligomeric silanes containing hydrophilic monomers [45], and segmented polyurethanes containing an assembly of polyoxyethylene, polydimethylsiloxane, and perfluororpolyether. These soft polymer blocks can transition into oleophobic, hydrophobic or hydrophilic surface behavior in response to the polarity of the contacting liquid. [46] Hydrophilic/oleophobic surfaces can also be obtained by complexation of cationic fluorinated surfactants on negatively charged films obtained by means of plasma assisted polymerization of acrylic acid or maleic anhydride. [23, 45, 47-49] However, the majority of hydrophilic/oleophobic surfaces have been fabricated on flat, non-porous substrates, or substrates with well-defined pore structures such as metal meshes and woven textiles. Creation of hydrophilic and oleophobic properties on substrates with a more random structure, such as paper or non-woven fabrics, has been rarely reported.

In one report, Molina *et al.* introduced a method to fabricate hydrophilic and oleophobic paper by using polyelectrolyte-fluorosurfactant complexes as coating

materials. [44] Polyelectrolytes can spontaneously interact with oppositely charged surfactants in aqueous solution to product polyelectrolyte-surfactant complexes according to a strict 1:1 stoichiometry required for overall charge balance. As a coating material, these complexes display a layered arrangement derived from demixing of the polar polyelectrolyte backbone and the hydrophobic surfactant tails. Conventionally, the entire polyelectrolyte-surfactant complex is prepared in solution, precipitated and then applied to a substrate. [49] However, in this report, a more direct approach is used comprising the coupling of ionic surfactants to pre-deposited polyelectrolyte plasma polymer surfaces, as shown in Figure 1.15. The plasma polymerization was performed using a dielectric barrier discharge (DBD) reactor operating at atmospheric pressure. Helium was used as the only carrier gas in this experiment with a flow rate of 5L/min. Paper substrates were introduced inside the reactor and 100 μL of acrylic acid solutions in water at different concentrations were placed over the substrates. Plasma polymerization was carried out for 10 min. After plasma assisted polymerization of acrylic acid solutions, samples were immediately immersed into a diluted cationic fluorosurfactant solution for 15 min. The treated samples were then rinsed with distilled water and dried for 24 hour under ambient conditions. Water and hexadecane contact angles were measured on coated paper samples, as shown in Figure 1.16. Results demonstrated that the acrylic acid plasma polymer surfaces can readily undergo complexation with the cationic fluorosurfactant solution. Since carboxylic acid groups at the surface of the plasma polymer layer will weakly ionize in water, a favorable electrostatic attraction between the ionized surface acid groups and oppositely charged fluorosurfactant ions occurs. Such interactions assist in orientating the charged surfactant head group toward the plasma polymer surface,

while leaving the fluorinated tail segment extended toward the air-solid interface, as indicated by the stable hexadecane contact angle on coated paper surfaces. On the other hand, due to the high affinity between water and the hydrophilic groups at the polymer-surfactant interface, water droplets can still wick into the coated paper samples.

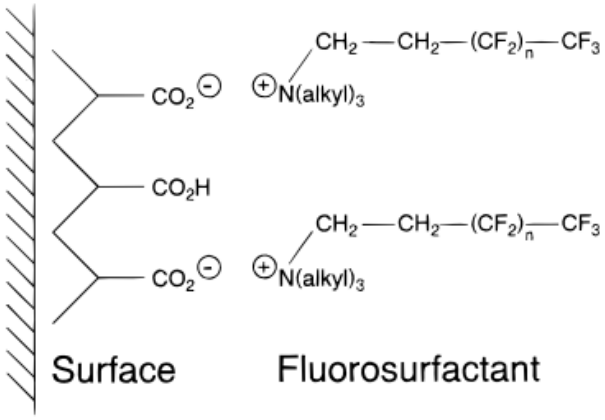

Figure 1.15: Complexation between the plasma polymer surface and cationic fluorosurfactant. [49]

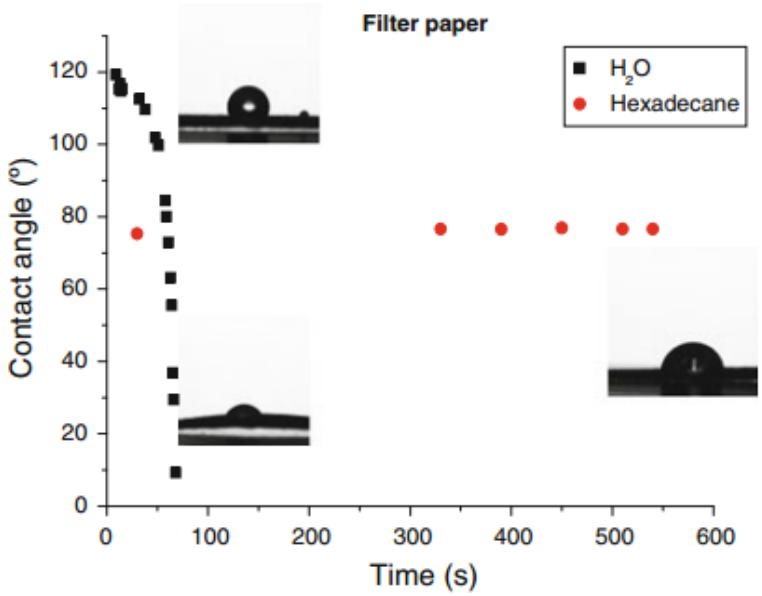

Figure 1.16: Contact angles as a function of time for hexadecane and water over filter paper after acrylic acid plasma assisted polymerization and fluorosurfactant complexation. [44]

1.4 Limitations of the Existing Methods

Due to the range of possible benefits of paper with controlled wetting properties, potential applications have received considerable interest from both industry and academia. Although there are a variety of existing methods to fabricate paper with different wetting properties, as discussed above, most of these methods rely heavily on the use of fluorinated coating materials, which are often associated with significant environmental and health concerns. [50-52] Because of the high strength of the carbon-fluorine bond, fluorocarbons cannot be degraded naturally in a short time and are therefore persistent in the environment. Low levels of the fluorinated compounds have contaminated nearly every corner of the food chain. [53] Research has shown that the compounds can cause cancer and disrupt sexual development in lab animals. [54]

Emerging epidemiological evidence suggests the compounds might cause or contribute to similar problems in human beings. [55] In addition to these issues, fluorinated materials are also expensive to manufacture and can be difficult to process. Because of these disadvantages, there is a global effort to reduce the use of fluorinated coating materials. However, developing non-fluorinated alternatives remains a great challenge: replacements may be straightforward in some applications, but not in others. For example, in paper products that only require water repellency, hydrocarbon waxes, different sizing agents and paraffin can be use as alternatives. But for the fabrication of oil repellent surfaces, fluorinated compounds are still required. Therefore, further research is required to fabricate paper with controlled wetting properties by implementation of non-fluorinated chemicals.

1.5 Thesis Outline

The goal of this thesis is to fabricate paper surfaces with controlled wetting properties on porous substrates by using non-fluorinated coating materials.

Chapter 2 focuses on the fabrication of amphiphobic paper using polybenzoxazine. The treated paper displays good oil resistance, but the processing requires economically unfavorable long cure times at relatively high temperatures, which could also compromise the mechanical strength of paper. *Chapter 3* investigates the properties of paper substrates coated with different alkyltrichlorosilanes. Alkyl chain length was found to have significant impact on the wetting properties of coated paper. *Chapter 4* describes the creation of oil repellent paper with methyltrimethoxysilane (MTMS). Hydrophilicity can be tuned by adjusting the sonication time during MTMS

hydrolysis. The modified paper surface displays wetting behavior ranging from hydrophilic/oleophobic to amphiphobic as a function of hydrolysis time. In *Chapter 5* it is shown that wood with amphiphobic properties can be fabricated by using the same MTMS coating material. *Chapter 6* further demonstrates the potential application of hydrophilic/oleophobic surface by coating MTMS on stainless steel meshes that can be used to separate oil and water mixtures. *Chapter 7* discusses the conclusions of this thesis along with recommendations for future research. *Appendix A* discusses the plasma-assisted modification of cellulose to achieve different desired, but non-traditional properties.

CHAPTER 2

FABRICATION OF AMPHIPHOBIC CELLULOSE-BASED PAPER USING POLYBENZOXAZINE AS COATING MATERIAL

2.1 Introduction

A potential candidate to achieve controlled wetting properties on porous substrates is polybenzoxazine (PBZ), a newly developed non-fluorinated polymer which is reported to have a surface energy as low as pure PTFE. [56]

Benzoxazine is a molecule where an oxazine ring, a hetero-cyclic six-membered ring with oxygen and nitrogen atoms, is attached to a benzene ring. Several benzoxazine structures exist depending upon the position of oxygen and nitrogen atoms. [57] Because the six-membered heterocycle has an irregular "chair-shaped" structure with some ring strain, benzoxazine can undergo a thermally accelerated, cationic ring-opening polymerization process to form the polymer PBZ. [58] Typical polymerization temperatures are in the range of 160 to 240^{o}C. [59, 60] A schematic of the polymerization process is shown in Figure 2.1.

Due to its high polarity and the ability to form hydrogen bond with water molecules, the hydroxyl group is the most common hydrophilic group. A unique characteristic of PBZ is that despite the presence of hydroxyl groups in in its structure, it displays a surface energy close to that of fluorinated materials, and even lower than it hydroxyl-free benzoxazine monomer. One explanation for this seemingly contradictory result is that the hydroxyl groups on PBZ have the ability to form a stable six membered

ring structure with the neighboring nitrogen atom through intramolecular hydrogen bonding. [61, 62] This strong interaction could impose an internal curvature on the molecule and thus change the polymer into a helical supramolecular structure. [63] As a result, the hydrophilic moieties could be protected on the interior of the folded structure, with hydrophobic groups being exposed to the outside environment; this type of assembly would be expected to lower the surface energy. [63] Because of its low surface energy properties, PBZ has been previously used to impart hydrophobicity and oleophobicity to different substrates such as steel [64], silica [65], polymer blend [66], and textiles. [67]

In this Chapter, a novel method to fabricate amphiphobic cellulose-based paper using PBZ is reported. Benzoxazine monomer was applied to the paper surface via dip coating and drop casting techniques. The coated paper samples were subsequently cured to start the polymerization process; cure time and temperature were varied. It is found the oleophobicity of PBZ coated paper samples is highly related to both the degree of polymerization of PBZ and the loading of PBZ. Paper samples with a loading of 10.6 mg/cm^2 of PBZ display prolonged resistance against oils after curing at 180℃ for 12 hours. The relation between polymerization degree and surface energy was interrogated using ATR-FTIR spectroscopy and contact angle measurements. Fluorinated materials are not used in this process, and the intrinsic porosity of paper is largely retained after the coating process, as judged from electron microscopy (SEM) images.

2.2 Experimental

Fabrication of PBZ Thin film

Benzoxazine monomer (BA-a) was kindly donated by Huntsman Chemical and used without further purification. BA-a is a yellow crystalline solid with a melting point in the range of 80-85^{o}C. The coating solution was prepared by dissolving benzoxazine monomer in anhydrous toluene (Sigma-Aldrich, 99.8%) at a concentration of 30 mg/mL. The stock solution was then filtered through a 25 mm syringe filter with 0.2 μm nylon membrane (VWR) to remove undissolved particles and impurities. Thin films were fabricated by spincoating 1 mL of solution on Si wafers at a speed of 650 rpm for 160 s. To initiate the polymerization process, benzoxazine thin films were cured at different temperatures for different lengths of time.

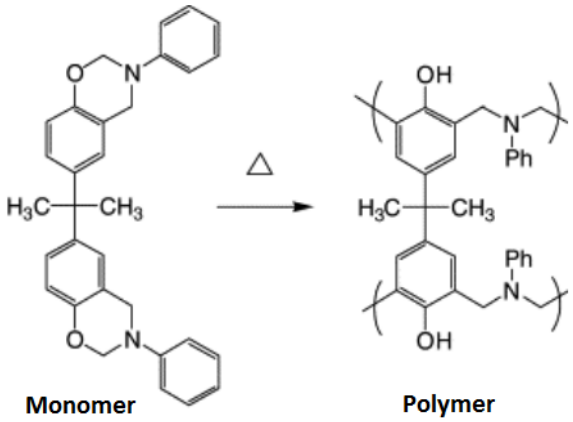

Figure 2.1: Polymerization process of benzoxazine (BA-a). [57]

Fabrication of PBZ Coated Paper

For this study, paper samples were prepared in house using northern bleached softwood Kraft fibers (NBSK) and a mixture of 15% bleached softwood / 85% bleached hardwood fibers (co-pulp). Paper samples were fabricated according to TAPPI standardized method T205 sp-02 using a 40/60 ratio (based on dry solids) of NBSK and co-pulp. After fabrication, benzoxazine monomer was applied on paper samples by using two different methods: dip coating and drop casting. For dip coating method, paper samples were dipped into the benzoxazine monomer solution for about 5 s and then dried under ambient conditions for 30 s. For the drop casting method, a specific volume of benzoxazine solution with known concentration was released onto the center of the paper samples. The solution then absorbed into the paper samples and spread out by capillary forces. Coated paper samples were also dried under ambient conditions. After coating, paper samples were subjected to curing at different temperatures for appropriate amounts of time.

Contact Angle Measurements

All static contact angle measurements were performed with an automated goniometer (ramé-hart, model 290, Succasunna, NJ). A 4 μL droplet of the selected fluid (DI water, diiodomethane (Sigma-Aldrich, reagent plus grade, 99%) or stained RP test oil (Ralston Purina)) was placed onto the substrate. Contact angles were determined by the standard goniometer software (Drop Image, version 2.6.1).

Lab-Scale 24 Hour Creased R. P. Oil Test

Lab-scale 24 hour creased RP2 test was conducted to test the long-term oil resistance of coated paper samples. A 1.5×1.5 cm^2 paper sample was creased along its center using a weighted roller. The creased sample was placed on grid paper and 0.4 g of white sand (SAPPI fine paper) was placed at the center of the sample. 25 μL of the stained RP test oil was then allowed to wet out into the sand. The prepared sample was then placed in a 60℃ oven for 24 hours. After heating, the areal fraction of any dyed sections of the grid was measured to determine the total percent staining. Staining of 2% or less is considered acceptable for many industrial applications.

Ellipsometry

Ellipsometric measurements were performed with a J.A. Woollam M-2000VI spectroscopic ellipsometer. The angle of incidence (as measured relative to the normal vector to the plane) was 70°. Measurements were carried out on three different spots on each sample. Thicknesses of the PBZ thin films were calculated from the ellipsometric parameters (Δ and Ψ) using WVASE32 software (version 3.632) following the transparent double-layer model.

SEM Imaging

Scanning Electron Microscopy (SEM) of uncoated and PBZ coated paper surfaces was perfomed using a Zeiss Ultra60 FE-SEM at an acceleration voltage of 5.0 keV. All samples subjected to scanning electron microscopy (SEM) imaging were sputter coated with Au/Pd to reduce accumulation of charge during measurement.

ATR-FTIR

Attenuated Total Reflectance-Fourier Transform Infrared Spectroscopy (ATR-FTIR) was carried out on a Nicolet IS-50 FTIR spectrometer (Thermo Scientific, Inc), operated in the ATR mode. The spectrometer was set to collect 128 scans at 4 cm^{-1} in the range from 4000 to 700 cm^{-1}.

2.3 Results and Discussion

Properties of PBZ Thin Films

PBZ thin films were made by spincoating benzoxazine monomer on cleaned Si wafers, followed by curing at different conditions. The thickness of the uncured PBZ thin film was 201.9 ± 1.8 nm as determined by ellipsometry.

The surface chemistry of benzoxazine thin films cured at different temperatures was characterized using ATR-FTIR. Spectra of five different samples were taken: benzoxazine monomer without any heat treatment, and benzoxazine cured at 60^{o}C for 1 hr, at 180^{o}C for 1 hr, at 180^{o}C for 12 hr and at 240^{o}C for 1 hr (Figure 2.2). The benzoxazine monomer has three characteristic peaks that can be monitored. Peaks centered at 1500 cm^{-1} and 950 cm^{-1} are due to absorption by the tri-substituted benzene ring and the peak at 1250 cm^{-1} is due to the aromatic ether stretching mode. All three peaks are prominent in spectra for the benzoxazine film without heat treatment and benzoxazine with 1 hour of curing at 60^{o}C. This result indicates that the polymerization process has not started after 1 hour at temperatures below 60^{o}C. On the other hand, for samples cured at 180^{o}C, the intensities of all three peaks are reduced significant, which clearly indicates that a ring-opening polymerization process has already started at this temperature. For samples cured at 240^{o}C for 1 hour or at 180^{o}C but for an extended

curing time of 12 hours, all three monomer peaks essentially disappeared. Also, these last two samples displayed two new strong absorption bands at ~2911 cm^{-1} and 2844 cm^{-1}, which are assigned to the C-H stretch of methylene groups in the polymer. These observations provide strong evidence that the polymerization process is essentially finished after 1 hour of curing at 240°C or 12 hours of curing at 180°C.

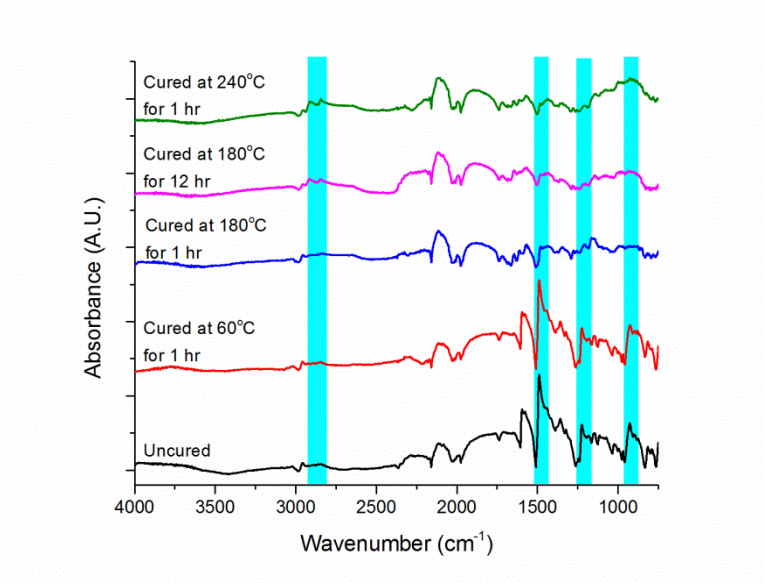

Figure 2.2: ATR-FTIR spectra of PBZ thin films cured at different conditions

To determine the change in wetting properties with respect to degree of polymerization, contact angles of three different fluids were determined on PBZ thin films cured at different conditions (Figure 2.3). Diiodomethane has been commonly used to characterize the oleophobicity because of its non-polar nature and moderate surface tension (50.8 mN/m). RP test oil is a mixture of oleic acid, glycerol trioleate and a red dye. RP test oil is widely used industrially to quantify oleophobicity because its composition is similar to oils in food. The surface tension of RP test oil was determined

to be 34.1 mN/m using the Owens-Wendt model. In addition to these two non-polar fluids, water was also used as a testing fluid in this study to represent polar fluids.

The results show that as the degree of polymerization increases, both water and oil contact angles increase as well on PBZ thin films. The fact that there is no significant difference in wetting behaviors between samples cured at 180^{o}C for 12 hours and 240^{o}C for 1 hour further highlights the fact that the surface chemistry is very similar between the two films, as was also indicated by spectroscopy. To compare surface energy of PBZ with fluorinated coating materials, a fluorocarbon thin film was fabricated using PECVD with pentafluoroethane (PFE) as the precursor gas. The thickness of the PFE thin film on the silicon wafer was 100 nm. Details about the properties PFE thin film and fabrication process can be found elsewhere. [37, 68] It was found that the water and oil contact angles on a PBZ thin film cured at 180^{o}C for 12 hours or at 240^{o}C for 1 hour are close to contact angles measured on PFE thin film. These results indicate that cured PBZ thin films exhibit a similar surface energy to that of fluorinated material.

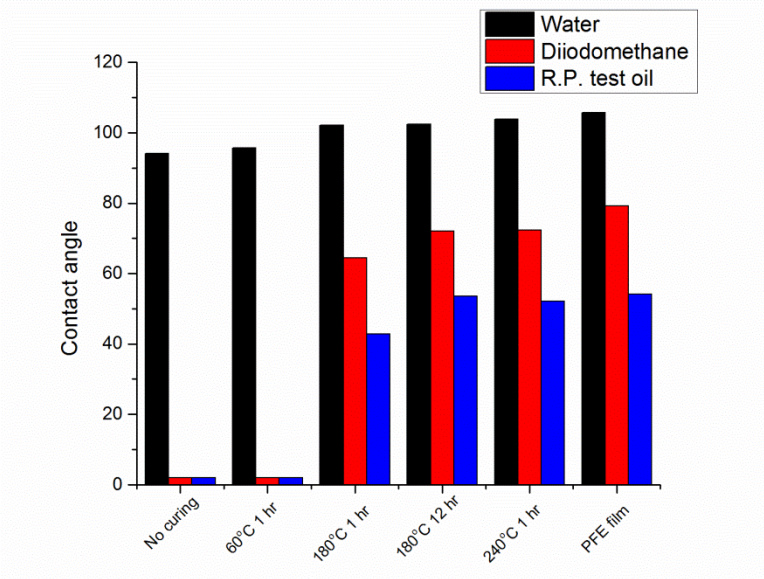

Figure 2.3: Water and oil contact angles measured on PBZ thin films cured at different conditions. Standard deviations of all measurements are below 2^{o}

Properties of PBZ Coated Paper Samples

To apply benzoxazine monomer to paper samples, a dip coating method was used at first because its fast coating rate and the facile one-step procedure. To optimize coating conditions, the paper samples were coated with benzoxazine solutions of different concentrations. After coating, all samples were cured in an oven at 60^{o}C for 1 hour. Water contact angles were measured on all coated samples (Table 2.1). It was found that paper samples coated with benzoxazine solution at a concentration of 7.5 mg/mL displays an initial water contact angle 103.1^{o}, but a slow absorption of water into the substrate was observed later. Paper samples coated with benzoxazine solution at a concentration of 15 mg/mL started to display stable water contact angle around 110^{o}. By further increasing the concentration, higher water contact angles were obtained until a maximum value was reached around 120^{o}. After that, further increases in solution concentration had very little

effect on water contact angles. It is also noteworthy to mention that the water contact angle on PBZ coated paper samples is higher than PBZ thin films, which is likely due to the fact that the micron-scale roughness from the underlying paper substrate helps to increase the contact angle for a non-wetting fluid. However, the coated paper samples with low-temperature curing do not show any resistance against oils: all samples absorb both diiodomethane and RP test oil immediately.

Table 2.1: Wetting behavior of coated paper samples dip coated with benzoxazine solution at different concentrations and cured for 1 hour at 60 °C. Italicized values indicate unstable contact angles, where absorption of water into the substrate was observed within 5 minutes. Standard deviations for all measurements are below 5^o.

Concentration (mg/mL)	Water contact angle
7.5	*103.1°*
15	111.3°
20	110.1°
25	119.3°
30	122.0°
60	118.9°
120	118.3°

To impart oil resistance to treated paper, the surface energy of the coating material needs to be further reduced and PBZ loading amounts must be increased. Based on our previous observation from PBZ thin films on silicon wafers, PBZ with a higher degree of polymerization displays lower surface energy, and hence higher oil contact

angles. To increase the polymerization degree of PBZ coated paper samples, the curing temperature was increased to 180^{o}C and the curing time was extended to 12 hours. The curing time and temperature were chosen to keep the thermal damage to the paper at acceptable levels; an even higher curing temperature like 240^{o}C is not suitable for paper substrates. Both ATR-FTIR and contact angle data on PBZ thin films indicate that benzoxazine cured at 180^{o}C for 12 hours is essentially equivalent to benzoxazine cured at 240^{o}C for 1 hour both with regards to chemical composition and surface energy.

In order to further increase PBZ loading on coated paper samples, drop casting was used instead of dip coating. This coating method enables precise control of the PBZ loading by controlling the volume and concentration of solution applied. Paper samples with different PBZ loadings were prepared using drop casting method. Coated paper samples were then cured at 180^{o}C for 12 hours. Oleophobicity was determined on different samples by measuring diiodomethane and RP test oil contact angles. Water contact angles were also determined for comparison (Figure 2.4). It was found that as PBZ loading increases, the oil resistance improved as well, while water contact angles remained essentially the same for all samples. At a loading of 5.3 mg/cm^2, coated paper samples start to display stable diiodomethane contact angles. By further increasing the loading to 10.6 mg/cm^2, coated paper display stable contact angle against RP test oil.

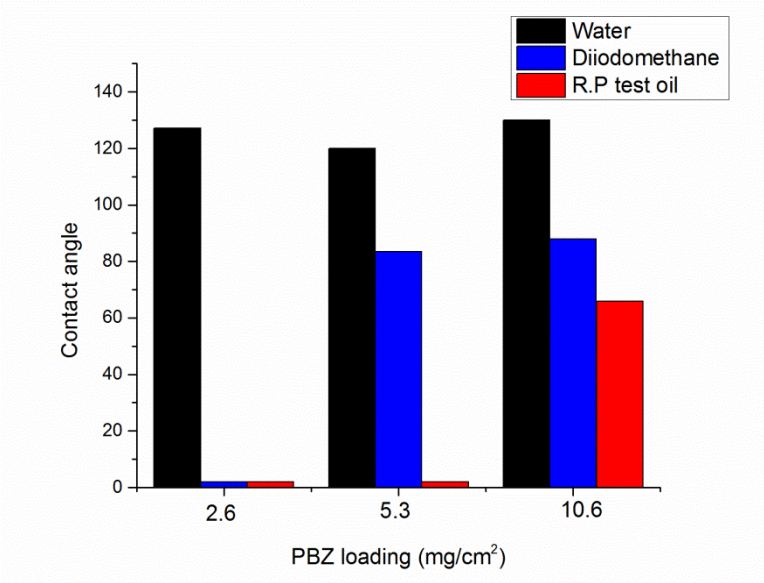

Figure 2.4: Water and oil contact angles measured on PBZ coated paper samples with different loading amount. All samples were cured at 180℃ for 12 hours. Standard deviations for all measurements were below 5^{o}

To determine if coated paper samples can display prolonged oil resistance, a lab-scale 24 hour RP test was conducted on paper with 10.6 mg/cm^2 loading of PBZ. The coated paper was creased in the middle before test. The purpose of this step is to ensure that coating layers will not be damaged by common folding operations. Also, instead of releasing RP test oil directly on coated paper sample, 0.4 g of sand was placed on top of paper sample and the RP test oil was released on sand. The RP test oil was then allowed to wick into the sand and uniformly wet the coated paper sample. The experiment was conducted at 60℃ to increase the permeation rate of oil into paper. After 24 hours, no stain was found on grid paper beneath coated paper samples, indicating that paper samples with 10.6 mg/cm^2 loading of PBZ can withstand RP oil at an elevated temperature for prolonged time.

In previous studies, liquid-repellent paper was fabricated by applying a pore-free barrier coating on top of the fiber surface. [69] The obvious disadvantage of this approach is the loss of intrinsic flexibility and air permeability. To determine if there is any significant change in surface morphology of coated paper due at our highest PBZ loading, SEM images were taken for two different samples: uncoated paper and PBZ coated paper samples with a loading of 10.6 mg/cm^2, which is the highest loading applied in the current study (Figure 2.5). No significant differences in surface morphology were found between uncoated and coated paper samples at low magnification: the porosity of uncoated paper is largely retained for PBZ coated paper. However, at high magnification, a thin coating layer can clearly be seen around each individual fiber for PBZ coated paper samples. This observation also agrees well with contact angle data: the fact that PBZ coated paper display a higher water contact angle than PBZ thin films on flat silicon wafers indicates that the natural roughness of paper is retained for paper with a high loading of PBZ.

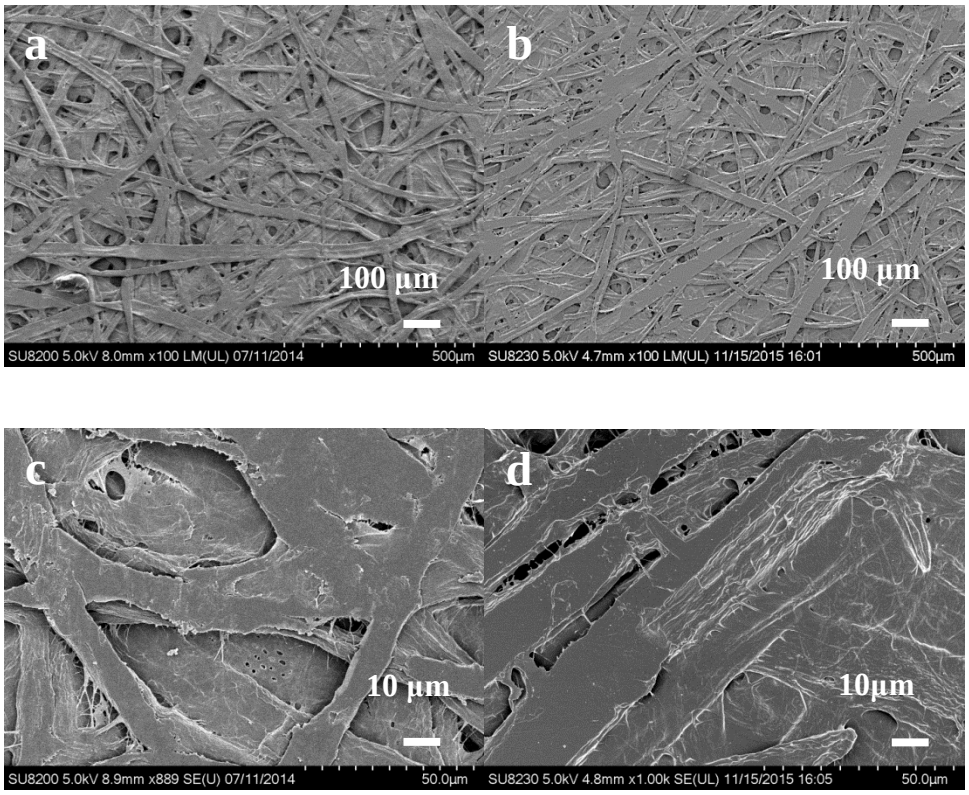

Figure 2.5: Low magnification SEM images of a) untreated paper sample and b) PBZ coated paper sample with a loading of 10.6 mg/cm^2, demonstrating that the porosity of native paper is largely retained after coating. Complementary high magnification SEM images are presented in (c-d).

2.4 Conclusion

This study has demonstrated a facile, one-step solution-based coating method to fabricate amphiphobic paper by using PBZ. Benzoxazine monomer solution was applied to paper samples using a drop casting method, followed by curing at elevated temperature. To fabricate oleophobic paper, a fairly high loading was required, in combination with prolonged curing time at high temperature. Coated paper displays stable diiodomethane and RP2 oil contact angles. PBZ coated paper with a loading of

10.6 mg/cm^2 also successfully passed the lab-scale 24 hour RP oil test, indicating that it has prolonged resistance against oil. Amphiphobic paper with prolonged oil resistance is of great interest for the paper industry, with applications in fluid and materials packaging, disposable lab-ware and self-cleaning surfaces

Compared with existing methods to fabricate amphiphobic paper, PBZ does not contain fluorine and is therefore more environmental friendly. The hydrophobicity and oil resistance of the PBZ coating is not due to over-coating of PBZ, and the porosity of native paper is largely retained after coating as indicated by SEM images. However, the disadvantages of this coating material and method are also obvious: high PBZ loading amounts and prolonged curing times means that this procedure is not very economically feasible. Treated paper also loses some flexibility due to the curing and high PBZ loading. Although some hypotheses and molecular modeling results have been proposed to explain the mechanism of the low surface energy of PBZ, the surface chemistry of PBZ is still poorly understood and requires more studies using surface sensitive techniques.

CHAPTER 3

EFFECT OF CHAIN LENGTH ON THE WETTING PROPERTIES OF ALKYLTRICHLOROSILANE COATED CELLULOSE-BASED PAPER

Material from this chapter was accepted for publication in *Cellulose* by Z. Tang, D. W. Hess and V. Breedveld

3.1 Introduction

Organosilane materials are of great interest for chemical surface modification because of the availability of these reagents with a wide range of chemical functionalities, their low cost, and the ease of covalent coupling chemistry to common functional groups on many substrates. [70] Among the larger class of organosilanes, specifically alkyltrichlorosilanes (trichlorosilane head group with a hydrocarbon tail group of variable length) have been widely used to functionalize a variety of inorganic and organic materials: silicon wafers [71], stainless steel [72], glass [73], silica [74, 75], alumina [76], cotton [77, 78], and paper. [79-81] Compared to other organosilanes, alkyltrichlorosilanes offer relatively fast covalent coupling reaction rates without requiring pre-hydrolysis steps, which are for example necessary for trialkoxysilanes. [82] The length of the hydrocarbon tail group in these reagents can be varied from a single methyl group to groups with more than 30 carbon atoms. When alkyltrichlorosilanes react with a hydroxyl-rich surface, the head group is hydrolyzed by trace amounts of water on the

surface (or in the solvent), and then grafted to the surface through a condensation reaction. As a result, a thin hydrocarbon layer is formed that generally reduces the surface energy of the substrate. Alkyltrichlorosilanes have many advantages compared to fluorinated coating materials, including lower environmental impact and immediate commercial availability.

The wetting properties of substrates with alkyltrichlorosilane coatings are highly dependent on both the intrinsic surface structure of the substrate and the structure imparted by coating material. The structure of the coatings is greatly affected by the relative rates of intermolecular silane-silane coupling and surface coupling reactions. [83] Furthermore, the relative rates of these reactions in comparison to mass transfer (i.e. diffusion coefficients) are an important consideration. For example, if surface reactions are dominant relative to silane-silane reactions, but slow compared to mass transfer, dense monolayers can be formed on the surface. With increasing silane-silane coupling rates, the coating layer thickness will increase [84] and, eventually, coupling reactions in the bulk may even result in the formation of small particulates; this is also referred to as "vertical polymerization". [85] If the proper balance is struck between these processes, alkyltrichlorosilane films can be formed that are covalently bonded to both the surface and to surrounding silane molecules; in this close-packed configuration, alkyl chains extend from the surface almost perpendicularly in a stretched all-trans configuration. [86]

Different types of the surface assembly structure can be obtained with slight changes in reaction conditions. Although parameters such as temperature [87], solvent [88], type of substrate and water content [89] can affect the assembly structure, one of the most important factors is the alkyl chain length. [90] For alkyltrichlorosilanes with long

alkyl chains, such as octadecyltrichlorosilane, surface reactions usually dominate; for short chain alkyltrichlorosilanes, such as methyltrichlorosilane, vertical polymerization becomes the primary process.

The relation between alkyl chain length and wetting properties has been studied previously on well-defined, non-porous substrates such as silicon wafers. [71, 83] It was found that alkyltrichlorosilanes with longer alkyl chains display higher water and diiodomethane contact angles. However, to our knowledge, such studies have not been performed on cellulose-based, porous materials, like paper, which are of great practical relevance. Because paper differs significantly from silicon in terms of surface morphology, porosity, density of surface hydroxyl groups, chemical heterogeneity and surface water content, it is unclear if these conclusions can be extended to alkyltrichlorosilane coated paper samples. Although a few studies exist on alkyltrichlorosilane coated cotton fibers [91, 92], these were focused on one particular alkyltrichlorosilane, such as octadecyltrichlorosilane. [93, 94] A systematic study is therefore needed to determine the effect of alkyl chain length on the wetting properties of cellulose-based paper coated with alkyltrichlorosilanes in order to assess the factors that control liquid interactions with and thus possible applications for treated paper.

In this Chapter, the effect of alkyl chain length on the wetting properties of coated paper samples is reported, and the chemical/morphological changes that impart such changes are discussed. Four alkyltrichlorosilanes with different chain lengths were coated on paper substrates following the same protocol: methyltrichlorosilane (MTCS, $-CH_3$), butyltrichlorosilane (BTCS, $-C_4H_9$), dodecyltrichlorosilane (DTCS, $-C_{12}H_{25}$) and octadecyltrichlorosilane (OTCS, $-C_{18}H_{37}$). By systematically varying the alkyl chain

length, coating layers with different structures were formed on paper. These differences in morphology affect the wetting behavior of coated paper samples. Due to the nano- and micron- scale roughness on methyltrichlorosilane coated substrates, paper coated with methyltrichlorosilane displays superhydrophobicity with the highest water contact angle ($>150^{o}$) among these four alkyltrichlorosilanes. However, the additional nano-scale roughness from methyltrichlorosilane coating also causes lower resistance against fluids with lower surface tension, while paper samples coated with long-chain alkyltrichlorosilanes have lower surface energy and lack nano-scale roughness. As a result, paper samples coated with octadecyltrichlorosilane display the highest resistance against oils. The relationship between alkyl chain length, surface chemistry, morphology and wetting properties was determined using ATR-FTIR, XPS and SEM, both on flat silicon wafers and on porous paper samples. Fluorinated materials are not used in this coating process, which renders the process and resulting coated paper more environmentally friendly.

3.2 Experimental

Fabrication of Alkyltrichlorosilane Thin Films on Si

Methyltrichlorosilane (MTCS), butyltrichlorosilane (BTCS), dodecyltrichlorosilane (DTCS) and octadecyltrichlorosilane (OTCS) were purchased from Gelest without further purification (deposition grade, 98%). The chemical structure of each alkyltrichlorosilane is shown in Figure 3.1. Coating solutions were prepared by adding 0.1 % (v/v) of alkyltrichlorosilane into anhydrous toluene (Sigma-Aldrich, 99.8%). Silicon wafers (P type 100 mm silicon wafer (100) P/E, Wafer World Inc.),

which served as flat control substrates for alkyltrichlorosilane thin films, were rinsed with acetone, methanol and isopropanol (BDH, ACS grade, 99%) and subsequently exposed to a low-pressure air plasma (Harrick Plasma, Plasma Cleaner PDC-32G, Ithaca, NY) for 5 minutes to remove solvent residue and ensure the presence of hydroxyl groups on the surface. Cleaned substrates were immersed in the alkyltrichlorosilane solutions for 3 hours. After coating, samples were again rinsed with acetone, methanol and isopropanol to remove any physisorbed coating materials. Coated substrates were then dried overnight under ambient conditions.

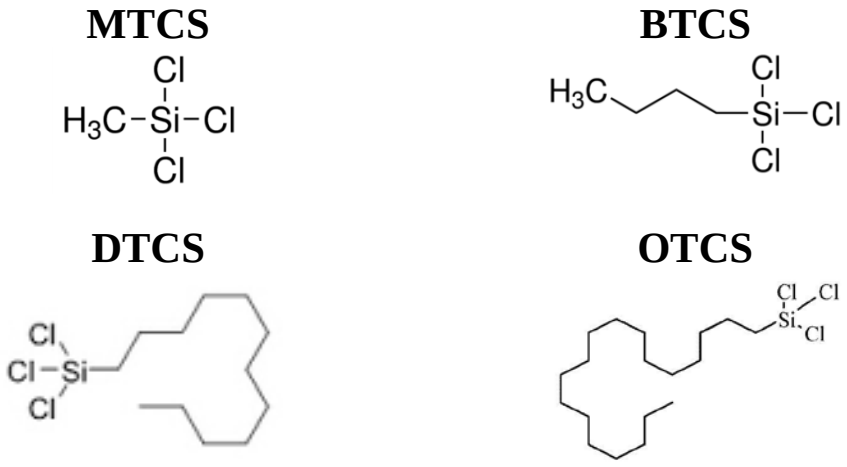

Figure 3.1: Molecular structures of four alkyltrichlorosilanes with different chain length

Fabrication of Alkyltrichlorosilane Coated Paper

For this study, paper samples were prepared in house using northern bleached softwood Kraft fibers (NBSK) and a mixture of 15% bleached softwood / 85% bleached hardwood fibers (co-pulp); paper samples were fabricated according to TAPPI standardized method T205 sp-02 using a 40/60 ratio (based on dry solids) of NBSK and

co-pulp. Paper samples were fabricated in this manner to eliminate the effects of additives and fillers that are commonly present in commercial paper. After fabrication, paper samples were immersed in alkyltrichlorosilane coating solutions for 3 hours. After coating, paper samples were blown dry using compressed nitrogen gas.

Contact Angle Measurements

All static contact angle measurements were performed with an automated goniometer (ramé-hart, model 290, Succasunna, NJ). A 4 μL droplet of the selected fluid (DI water, diiodomethane (Sigma-Aldrich, reagent plus grade, 99%), ethylene glycol (Sigma-Aldrich, anhydrous, 99.8%) or motor oil (SAE 10W-30, MotoTech)) was placed onto the substrate. Contact angles were measured immediately after the fluids were in contact with surfaces (less than 10 s).Contact angles were determined by the standard goniometer software (Drop Image, version 2.6.1).

Physical Characterization

Ellipsometric measurements were performed with a J. A. Woollam M-2000VI spectroscopic ellipsometer. The angle of incidence (from the normal to the plane) was 70°. Measurements were carried out at three different spots on each sample. Thicknesses of the alkyltrichlorosilane thin films were calculated from the ellipsometric parameters (Δ and Ψ) using WVASE32 software (version 3.632) following the transparent double-layer model.

Scanning Electron Microscopy (SEM) of uncoated and alkyltrichlorosilane coated paper surfaces and silicon wafers was performed using a Hitachi SU8230 FE-SEM at an acceleration voltage of 5.0 keV. All samples subjected to scanning electron microscopy

(SEM) imaging were sputter coated with Au/Pd to reduce accumulation of charge during measurement.

Chemical Characterization

X-ray photoelectron spectroscopy (XPS) analyses were conducted using a Thermo Electron Corporation K-Alpha XPS system with a microfocused monochromatic Al Kα X-ray source. The spot size of the instrument is 400 μm.

Attenuated Total Reflectance-Fourier Transform Infrared Spectroscopy (ATR-FTIR) was carried out on a Nicolet IS-50 FTIR spectrometer (Thermo Scientific, Inc), operated in the ATR mode. The spectrometer was set to collect 128 scans at 4 cm^{-1} in the range from 4000 to 900 cm^{-1}.

3.3 Results and Discussion

Properties of Alkyltrichlorosilane Thin Films

To investigate the effect of changes in surface chemistry as a function of alkyl chain length, four different alkyltrichlorosilanes were studied: methyltrichlorosilane (MTMS), butyltrichlorosilane (BTCS), dodecyltrichlorosilane (DTCS) and octadecyltrichlorosilane (OTCS). All of these have the same head group; the only difference between them is the alkyl chain length: MTCS has one methyl group attached to the head group, BTCS has a four-carbon-chain, DTCS a twelve-carbon-chain and OTCS an eighteen-carbon-chain. A silicon wafer was chosen as the initial model substrate for this study because it has a well-defined, flat surface and homogeneous chemical composition; effects of surface roughness and heterogeneity of the underlying substrate on wetting properties can therefore be excluded. For all samples, the coating

time was 180 minutes to ensure a high degree of alkyltrichlorosilane surface coverage.[95] Toluene was used as the solvent because high coverage densities can be consistently obtained using toluene. [88, 96]

Physical properties of alkyltrichlorosilane thin films

Silicon wafers coated with BTCS, DTCS and OTCS retained the clean, reflective appearance of uncoated silicon wafers, while MTCS coated wafers appeared non-reflective. These visual characteristics indicate that MTCS generates micrometer-scale roughness, while the other species generate coatings that remain smooth at the micrometer level. For BTCS, DTCS and OTCS, the film thickness could be determined accurately by ellipsometry and the results (Table 3.1) were in agreement with the visual observations: layer thickness was ~5 nm for all three materials. Due to the highly scattering, rough surface of the MTCS coated silicon wafer, the thickness of the MTCS film could not be determined via ellipsometry; instead, it was measured via cross-sectional SEM imaging (Table 3.1). The alkyltrichlorosilane thin films show a complex relationship between film thickness and alkyl chain length. First, the MTCS thin film is much thicker than the other three alkyltrichlorosilane thin films, which indicates that "vertical polymerization" of MTCS takes place on the substrate surface and, potentially, in the bulk. Compared to MTCS, the thicknesses of the other three alkyltrichlorosilane thin films were much thinner and very similar. The thicknesses of BTCS, DTCS and OTCS layers were at the nanometer length scale, but exceed single-molecule dimensions. The difference in film thickness clearly indicates that the MTCS film has a different surface structure compared to the other three alkyltrichlorosilanes.

Table 3.1: Alkyltrichlorosilane film thickness and degree of oligomerization

Alkyltrichlorosilane	Film thickness (nm)
MTCS	~700
BTCS	4.9 ± 0.4
DTCS	4.8 ± 0.3
OTCS	5.8 ± 0.3

To further investigate the surface morphology of different alkyltrichlorosilane thin films, SEM was used to characterize the samples (Figure 3.2). For silicon wafers coated with BTCS, DTCS and OTCS, a similar morphology was observed: a thin film without noticeable micro- or nanometer-scale structures. In contrast, the MTCS–coated silicon wafer displayed significant structure at these length scales: SEM images indicate the presence of a network of fibrillar elements.

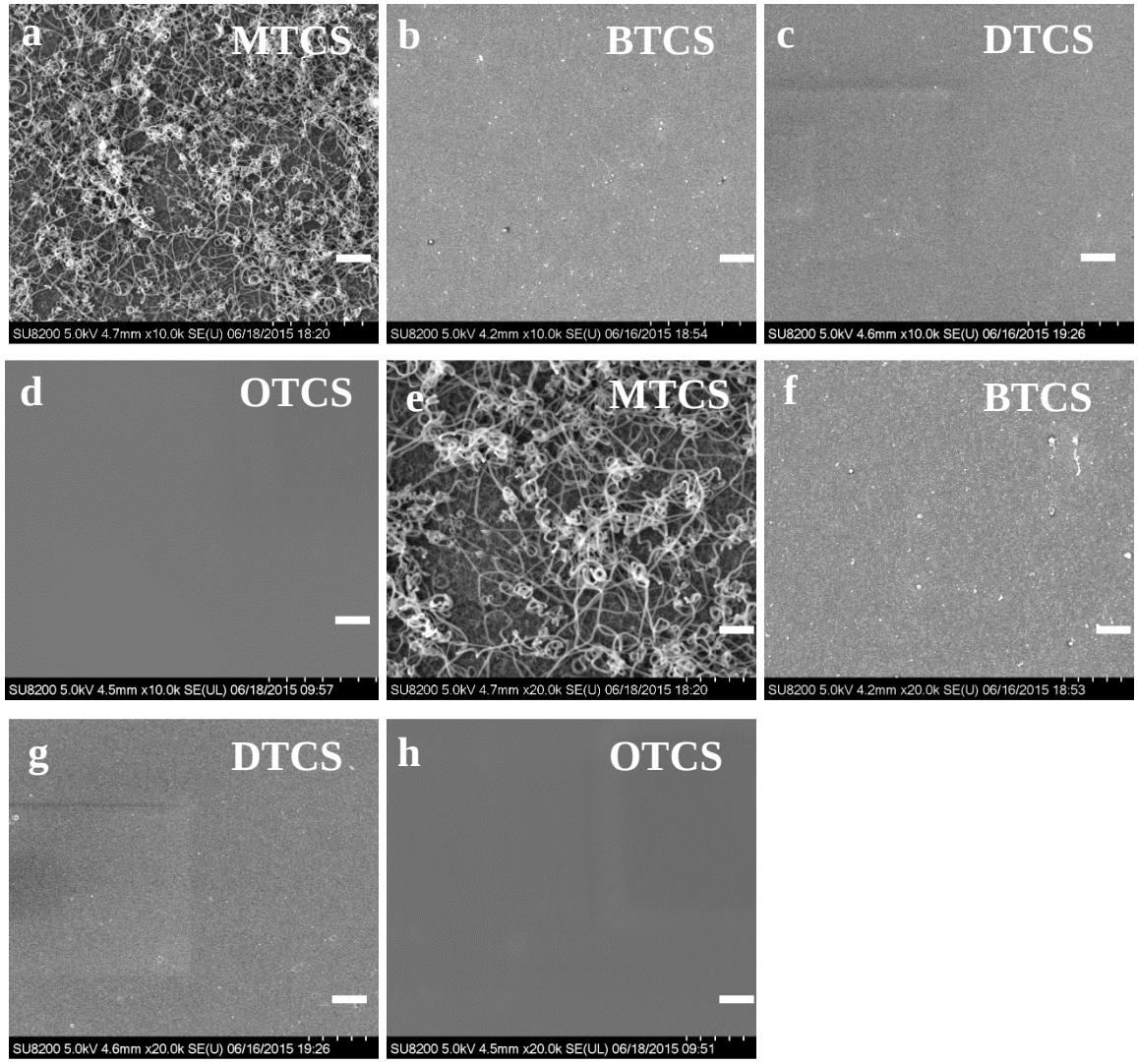

Figure 3.2: SEM images of a) MTCS b) BTCS c) DTCS and d) OTCS thin films. Scale bars represent 1 μm. Complementary high magnification images (scale bars 500 nm) are presented in (e-h)

We attribute this observation to the high reactivity of MTCS molecules relative to the other materials. Because of the short hydrocarbon chain, steric hindrance effects on polymerization are reduced, so that MTCS can more easily polymerize in the solvent or react with other MTCS molecules that are already grafted onto the silicon wafer through a vertical polymerization process. [83, 85] Both of these polymerization processes create

micro- and nanometer-scale structures on the surface, and introduce additional roughness on silicon surfaces. This unique morphology of MTCS film is consistent with previous reports [85] and has also been found on other short chain alkyltrichlorosilanes. [97] As the alkyl chain length increases, the reactivity of alkyltrichlorosilanes decreases due to greater steric hindrance. Consequently, surface coupling reactions become more dominant. As a result, BTCS, DTCS and OTCS films have a smaller degree of oligomerization and display a smooth morphology. This observation agrees well with film thickness measurements, and also explains why the MTCS film is much thicker than BTCS, DTCS and OTCS films.

Chemical properties of alkyltrichlorosilane thin films

To investigate changes in surface composition as a function of alky chain length, XPS analysis was performed on alkyltrichlorosilane thin films. A clean silicon wafer without coating was used as control sample (Figure 3.3). No chlorine was observed in any sample, indicating the virtually complete hydrolysis of silicon-chlorine bonds to yield silanol groups. For the control sample, oxygen and silicon were the two major elements detected, as expected; the small amount of carbon on the sample surface is likely due to contamination from air. Si wafers coated with all four alkyltrichlorosilanes display significant increases in carbon atomic percentage, indicating that alkyltrichlorosilanes were successfully coated on these substrates. For the MTCS coated Si wafer, the O: Si ratio is approximately 1.2. For fully condensed trichlorosilane compounds, one would expect a value of 1.5 (all three oxygen atoms shared by two Si atoms). In the high resolution Si XPS spectrum (Figure 3.4), the Si-O peak for MTCS is clearly shifted to lower binding energies relative to the oxide layer of the uncoated wafer, which is

consistent with a lower O: Si ratio. However, XPS data did not enable us to determine the detailed Si bonding structures in the MTCS coating. For the other three alkyltrichlorosilanes, the O: Si ratio is much smaller than 1.5. This can be explained by the fact that the film thicknesses of BTCS, DTCS and OTCS are smaller than the penetration depth of XPS (typically 5-10 nm); therefore, Si from the underlying wafer is detected in addition to the coating layer. As a result, the silicon atomic percentage increases compared to the MTCS layer, where the substrate is masked by the thicker coating. This argument is further supported by high resolution XPS spectra on Si, where the Si signal from both the underlying silicon substrate and coating layer were detected for BTCS, DTCS and OTCS coated Si wafer, while the signal for the MTCS coated Si wafer originated solely from the coating material itself (Figure 3.4). Among BTCS, DTCS and OTCS, carbon content increases with increasing alkyl chain length, which agrees with molecular composition and previous literature reports. [83] Oxygen content keeps almost constant for different samples, which is probably due to atmospheric adsorption.

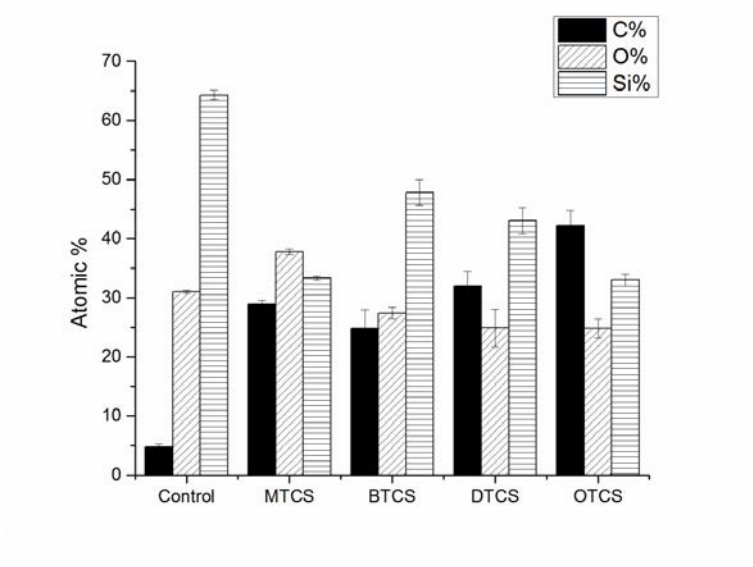

Figure 3.3: Relative atomic surface concentration of carbon, oxygen and silicon based on low resolution XPS of alkyltrichlorosilane thin films with different hydrocarbon chain length

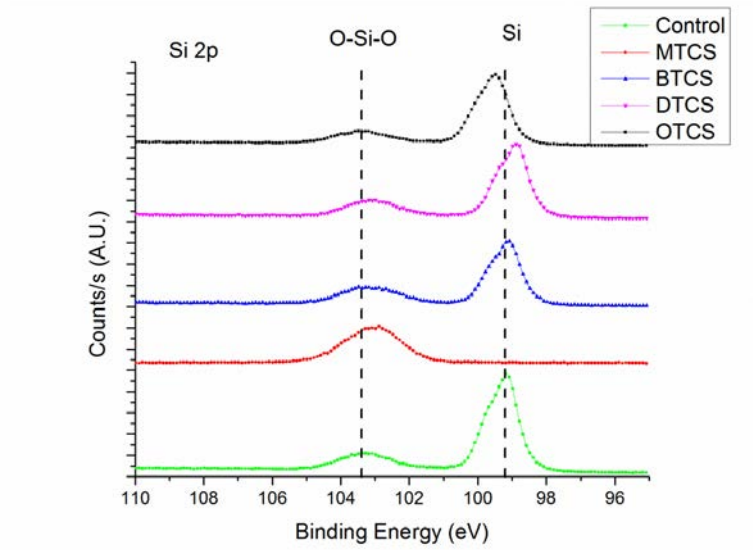

Figure 3.4: High resolution XPS data for Si 2p on silicon wafers coated with alkyltrichlorosilanes with different hydrocarbon chain length

To further understand the surface chemistry of the different alkyltrichlorosilane films, ATR-FTIR spectra were recorded for uncoated silicon wafers and silicon wafers coated with different alkyltrichlorosilanes (Figure 3.5). The spectrum of the silicon wafer

coated with MTCS shows strong peaks at 1270 cm^{-1}, which can be assigned to Si-CH_3 bonding [98], indicating that MTCS has been successfully grafted onto the substrate surface. The presence of methyl groups on the substrate surface is further confirmed by the peak at 2950 cm^{-1}, which is due to C-H bonding. The most significant difference between untreated Si wafers and MTCS coated Si wafers is the disappearance of the –OH peak at 3300 cm^{-1}. The spectra of BTCS, DTCS and OTCS are similar to that of the MTCS coating; the main difference is that the characteristic peaks are less intense due to decreased film thickness and the resulting signal loss. In summary, ATR-FTIR further confirms that all four alkyltrichlorosilanes were successfully grafted onto silicon wafers.

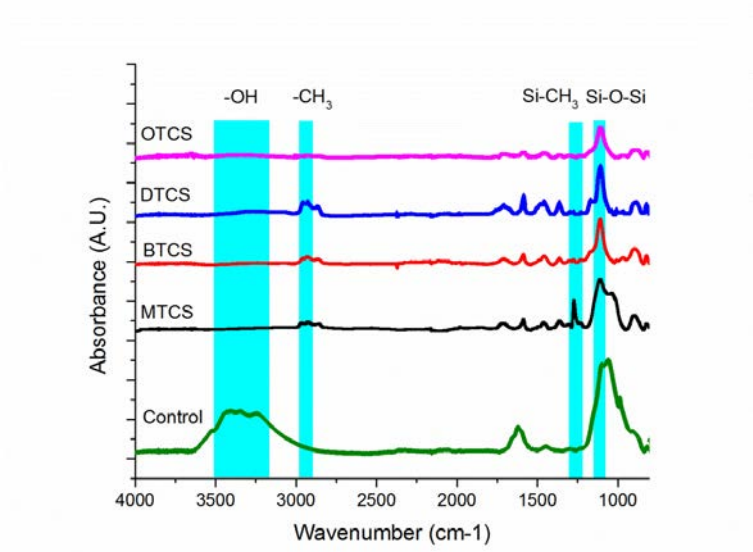

Figure 3.5: ATR-FTIR spectra of alkyltrichlorosilane thin films on Si

Wetting properties of alkyltrichlorosilane thin films

The characterization results presented above indicate that alkyltrichlorosilane coatings with different alkyl chain lengths exhibit significant differences in chemical and physical properties, which are expected to affect their wetting behavior. To test the wetting properties of different alkyltrichlorosilane films, contact angles were determined

for four different test fluids: water, diiodomethane, ethylene glycol and motor oil (Figure 3.6). These fluids were carefully selected to represent a broad distribution in both surface tension and liquid polarity (Table 3.2). For water and diiodomethane, a decrease in contact angle was observed when changing from MTCS to BTCS, followed by a gradual increase in the contact angle with alkyl chain length. On the other hand, for ethylene glycol and motor oil, contact angles increased monotonically with alkyl chain length. In summary, on a flat substrate, the MTCS film displays the highest water contact angle, while OTCS shows the highest oil contact angle.

Table 3.2: Properties of different testing fluids

Testing fluid	Surface tension (mN/m)	Polarity
Water	72.8	Polar
Diidomethane	50.2	Non-polar
Ethylene glycol	48.8	Polar
Motor oil	31.0	Non-polar

Since BTCS, DTCS and OTCS have smooth surface topologies, the consistent increase in contact angles clearly indicates a decrease in surface energy with increasing alkyl chain length. As alkyl chain length increases, the number of carbon atoms per alkyltrichlorosilane molecule increases, as well as the surface concentration of methyl and methylene groups, as indicated by XPS results. The higher carbon concentration lowers the surface energy and causes higher oil and water contact angles on Si substrates coated with long chain alkyltrichlorosilanes.

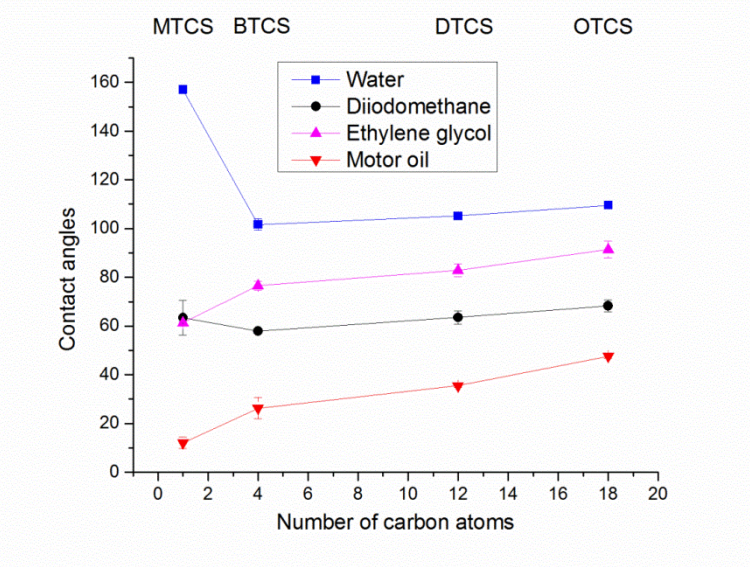

Figure 3.6: Water, diiodomethane, ethylene glycol and motor oil contact angles measured on alkyltrichlorosilane thin films coated on silicon wafers.

As pointed out previously, the wetting behavior of the MTCS films deviates from this trend. The equilibrium contact angle for flat MTCS films can be estimated by extrapolating the data for OTCS, DTCS and BTCS to the MTCS carbon length (C1). By comparison, the actual MTCS contact angles on Si substrates are unexpectedly low for ethylene glycol and motor oil, and surprisingly high for water; these observations can be attributed to surface morphology. To understand the MTCS wetting behavior, it is helpful to examine the Wenzel (Eq. 1) [7, 8] and Cassie-Baxter models (Eq. 2) [9], which are two classical frameworks to describe wetting properties of roughened surfaces. Droplets in the Wenzel wetting state are assumed to completely penetrate into the roughened surface structure, so that the contact area between liquid and substrates is enhanced:

$$cos\theta_A = r \cdot cos\theta_E \quad (1)$$

In Eq. 1, θ_A represents the apparent, measured contact angle; θ_E is the equilibrium contact angle, as measured on a perfectly flat surface; and r is the so-called roughness ratio, which is defined as the ratio of the true exposed area of the solid surface to its nominal area. For wetting fluids (equilibrium contact angle < 90°) roughness causes a decrease in apparent contact angle, while non-wetting fluids (θ_E > 90°) in the Wenzel state show an increased apparent contact angle. Droplets in the Cassie-Baxter state are assumed to suspend on the roughness grooves, thereby creating air-pockets between liquid and solid and decreasing the solid-liquid contact area:

$$\cos\theta_A = f_s \cdot (1 + \cos\theta_E) - 1 \quad (2)$$

In equation 2, f_s is the fractional liquid-solid contact area. Due to the reduced liquid-solid contact, droplets in the Cassie-Baxter state can display an apparent contact angle that is much higher than the equilibrium contact angle [99, 100].

The wetting behavior of low-surface-tension fluids (motor oil and ethylene glycol) on MTCS films can thus be explained using the Wenzel model: due to micro- and nanometer-scale structures the apparent contact angles are lower than would be expected for a flat MTCS substrate. On the other hand, the superhydrophobic behavior of MTCS films can be explained using the Cassie-Baxter model: the relatively high water contact angle on alkyltrichlorosilane thin films enables the suspension of water droplets on the micro- and nanometer-scale structures, leading to trapped air pockets and an apparent water contact angle greater than 150° on MTCS thin films. Diiodomethane is the only fluid in this study that does not clearly follow these model predictions: its estimated extrapolated equilibrium contact angle is less than 90°, but diiodomethane does not exhibit a significantly lower apparent contact angle on the roughened MTCS film. We

have no clear explanation for this observation, but note that diiodomethane is the least polar fluid and displayed a larger standard deviation on MTCS than any other coating/liquid combination in this study, indicating that subtle surface heterogeneities may play a role

Properties of Alkyltrichlorosilane Coated Paper

So far, the properties of alkyltrichlorosilanes with different alkyl chain length have been described on silicon wafers. Compared with silicon wafers, cellulose-based paper is a porous material with heterogeneous surface morphology. There are also significant differences between a silicon wafer and cellulose-based paper in terms of surface chemistry and surface water content. All of these factors can change the grafting process of alkyltrichlorosilanes on paper surfaces compared to silicon wafers, and hence affect the wetting behavior. To determine whether coated paper can display properties that are similar to coated silicon wafers, the same coating procedure was applied to fabricate alkyltrichlorosilane coated paper. An important first observation was that coated paper maintained both the visual appearance and mechanical flexibility of uncoated paper.

Morphology of alkyltrichlorosilane coated paper

Surface morphologies of paper samples coated with different alkyltrichlorosilanes were characterized via SEM (Figure 3.7). Alkyltrichlorosilane coated paper samples share critical morphological features to alkyltrichlorosilane coated silicon wafers. BTCS, DTCS and OTCS coated paper samples largely retain the morphology of untreated paper without noticeable nano-scale roughness on the surface of the cellulose fibers. This clearly indicates that even on a porous surface with heterogeneous morphology, covalent

attachment is still the dominant grafting process for long chain alkyltrichlorosilanes like BTCS, DTCS and OTCS. On the other hand, less dense or “fluffy” nano-scale structures can clearly be observed on MTCS coated paper samples. At high magnification, a web-like structure was seen wrapping around the cellulose fibers, similar to the structure previously observed on MTCS coated silicon wafers. The similarities in morphology between alkyltrichlorosilane coatings on silicon wafers and paper samples indicate that the grafting process is similar on different substrates, provided that reactive hydroxyl groups are present. This hypothesis will be further tested by chemical characterization of alkyltrichlorosilane coated paper samples.

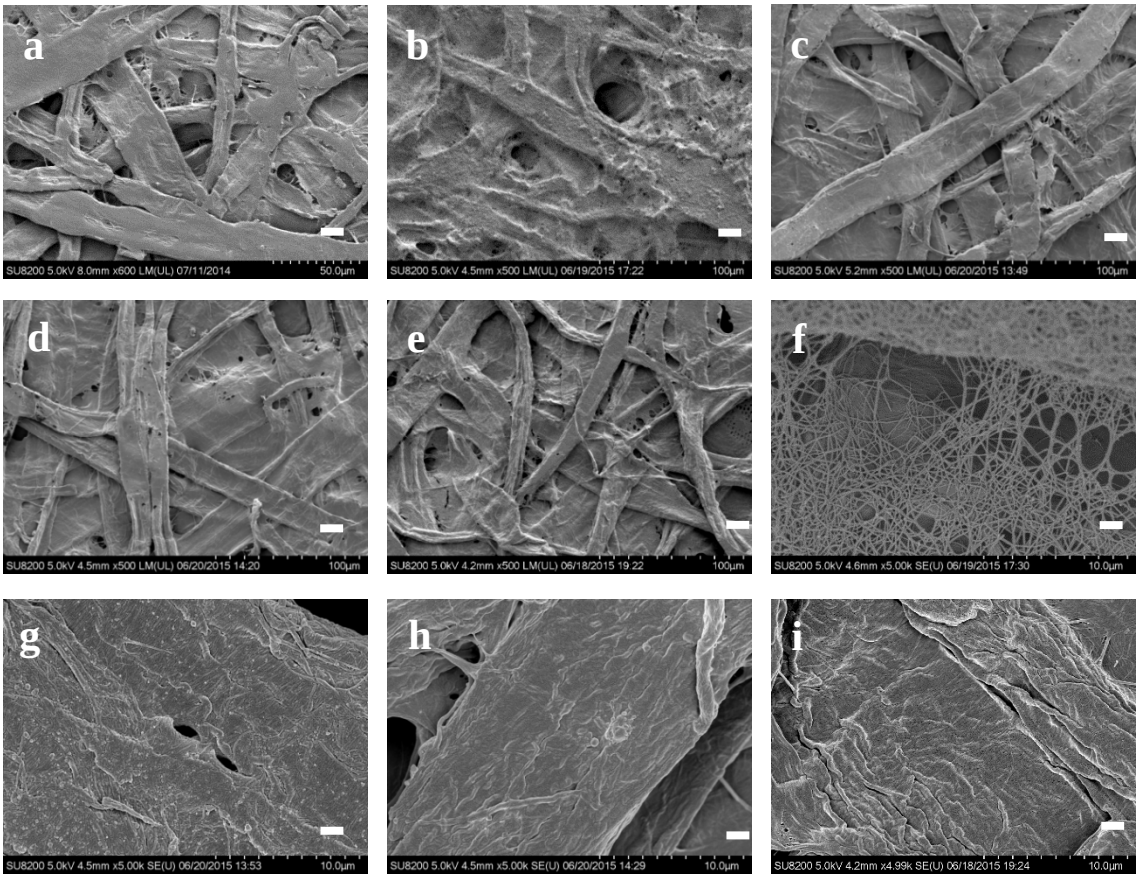

Figure 3.7: Low magnification SEM images of a) untreated paper sample and b) MTCS, c) BTCS, d) DTCS, and e) OTCS coated paper samples. Scale bars represent 10 μm. Complementary high magnification SEM images for MTCS, BTCS, DTCS and OTCS are presented in (f-i). Scale bars represent 1 μm.

Chemical properties of alkyltrichlorosilane coated paper

To determine the surface chemistry of alkyltrichlorosilane coated paper samples, XPS analysis was performed on all paper samples (Figure 3.8). Si was detected on all coated paper samples, but not on the control sample, indicating the presence of alkyltrichlorosilanes. High Si concentrations on paper samples coated with MTCS further confirm the presence of vertical polymerization. It is worth pointing out that the Si concentration on paper samples coated with BTCS is also significantly higher than that

on DTCS and OTCS coated paper. This observation can be explained by the fact that BTCS is expected to have a higher surface coverage on coated paper samples due to its shorter alkyl chain and lower steric hindrance. In addition, the carbon concentration on coated paper surfaces increases with alkyl chain length, which is consistent with the increased number of carbon atoms per alkyltrichlorosilane molecule as alkyl chain length increases.

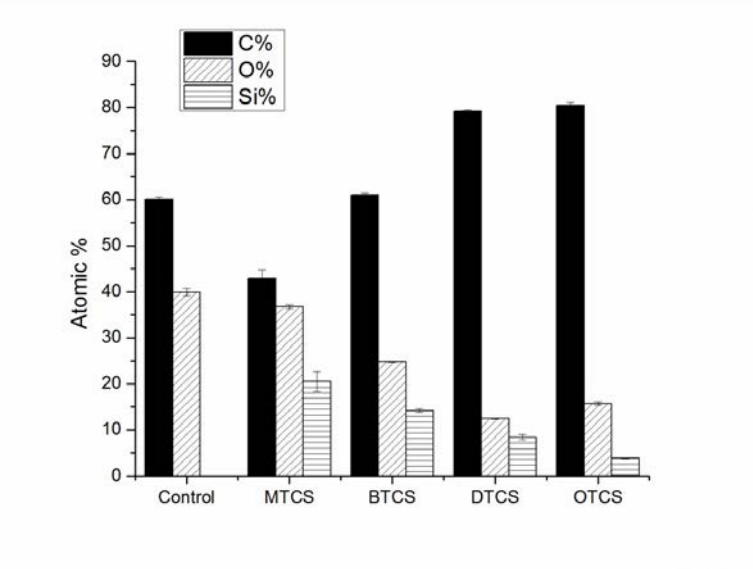

Figure 3.7: Relative atomic surface concentration of carbon, oxygen and silicon based on low resolution XPS of alkyltrichlorosilane coated paper samples

To further investigate the surface chemistry of coated paper samples, ATR-FTIR was also used. The spectra on the chemically heterogeneous paper samples are more difficult to interpret than for silicon wafers (Figure. 3.5), but the previous data greatly assisted with peak assignment and analysis (Figure 3.9). Unfortunately, the presence of Si-O-C groups, arising from the covalent attachment of alkyltrichlorosilane to cellulose,

cannot be detected by ATR-FTIR, because their typical position at ~1100 cm^{-1} was masked by the large and intense cellulose C-O stretching band that is centered at ~1064 cm^{-1}. However, the appearance of new peaks at 1270 cm^{-1}, assigned to the Si-CH_2 group, corroborated the presence of alkyltrichlorosilanes in all samples. The presence of alkyltrichlorosilane is further confirmed by two new strong absorption bands at ~2911 cm^{-1} and 2844 cm^{-1}, which are assigned to the C-H stretch of methylene groups in long hydrocarbon chains. Unlike the silicon substrate, due to the large number of hydroxyl groups in the bulk of coated paper samples, all samples display peaks at 3300 cm^{-1}.

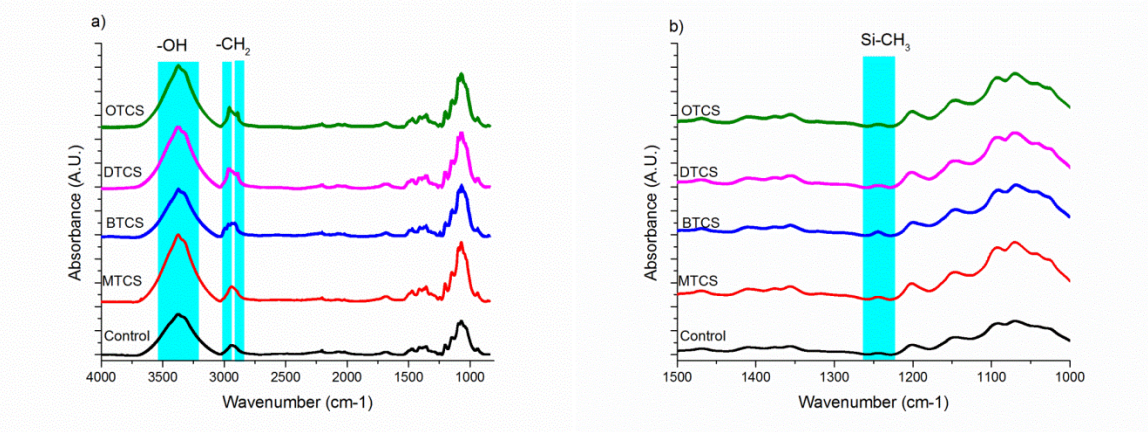

Figure 3.9: ATR-FTIR of paper samples coated with alkyltrichlorosilanes: a) overview from 1000 to 4000 cm^{-1}, and b) zoomed in at 1000 to 1500 cm^{-1}; control sample was uncoated paper.

Wetting properties of alkyltrichlorosilane coated paper

Previous results indicate that although paper and silicon wafers are two very different substrates, once coated with alkyltrichlorosilane these substrates are similar in both surface chemistry and morphology; the key distinction between the two is the

porosity of paper and associated micrometer-scale roughness. Knowledge of this characteristic greatly facilitates the interpretation and understanding of the wetting behavior of coated paper substrates. Contact angles were measured on the various paper samples using the same set of testing fluids employed for silicon wafers (Figure 3.10). Due to the intrinsic micrometer-scale roughness from the underlying porous paper surface, water contact angles on all coated paper samples increase compared to alkyltrichlorosilane films on flat silicon wafers, but the trend as a function of alkyl chain length is similar. For BTCS, DTCS and OTCS coated samples, water contact angle increases monotonically with alkyl chain length. Again, these observation likely results from the fact that even on a heterogeneous and porous substrate, alkyltrichlorosilanes with longer alkyl chains have a higher carbon concentration, and therefore lower surface energy; this conclusion is supported by the XPS results. For MTCS coated paper samples, due to the hierarchical two-scale roughness from the underlying paper surface (micrometer-scale) and the MTCS coating itself (micro- and nanometer-scale), a superhydrophobic surface (*i.e.* water contact angle >150°) was achieved. It should be noted that MTCS coated paper fabricated by the current solution-based method displays a much higher water contact angle than previously reported MTCS coated paper fabricated via vapor deposition (water contact angle ~ 130°). [81] Comparison of SEM images from our work to those of the prior study indicates that this difference can be attributed to the fact that the solution-based method generates a higher density of nano-scale structures than does the vapor deposition approach. According to the Wenzel equation, such an increase in surface roughness leads to a higher water contact angle.

Oil contact angles were also measured on the paper samples. All alkyltrichlorosilane coated paper samples display stable diiodomethane and ethylene glycol contact angles, indicating moderate resistance against fluids with lower surface tension. However, for fluids with even lower surface tension such as motor oil, none of the coated samples displayed stable contact angles. This result indicates that the surface energy of alkyltrichlorosilane coated paper is not sufficiently low to resist wetting and absorption by low surface tension fluids.

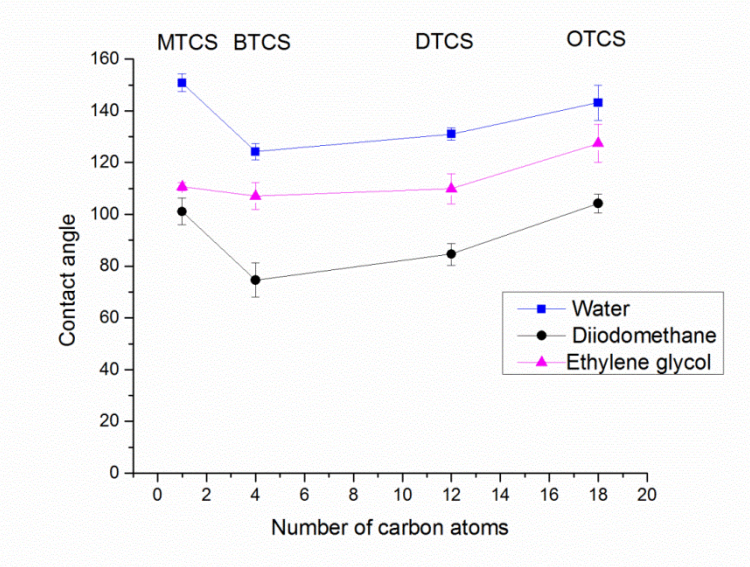

Figure 3.10: Water, diiodomethane and ethylene glycol contact angles measured on alkyltrichlorosilane coated paper samples.

3.4 Conclusion

The effect of chain length on the wetting properties of different alkyltrichlorosilanes was studied on both non-porous and porous substrates to elucidate the effects of surface chemistry and topology. Four different alkyltrichlorosilanes with

alkyl chain lengths varying from 1 to 18 were coated onto silicon wafers and paper samples through a simple, one-step solution-based coating method. On both substrates, for BTCS, DTCS and OTCS, surface coupling is the dominant attachment process, resulting in nanoscopically flat films; for MTCS, on the other hand, vertical polymerization (intermolecular silane coupling) is the dominant process, thus creating thick films with micro- and nanoscale roughness.

Among the three alkyltrichlorosilanes that do not create roughness (BTCS, DTCS, OTCS), OTCS displays the lowest surface energy and highest contact angles for all four testing fluids: water, diiodomethane, ethylene glycol and motor oil. The micro- and nanometer-scale roughness on MTCS coated substrates leads to higher water contact angles but lower oil contact angles than may be expected by extrapolating the results from the other materials. Although all coated paper samples display high water contact angles, MTCS coated paper is the only substrate to exhibit superhydrophobicity (contact angle greater than 150°). All coated paper samples also display moderate resistance against non-polar fluids such as diiodomethane and motor oil.

Compared with existing methods to fabricate hydrophobic/oleophobic paper surfaces, alkyltrichlorosilanes do not contain fluorine and are therefore more environmental friendly. The entire coating process is carried out by a solution-based method under ambient conditions. As a result, improved compatibility with current large-scale paper manufacturing processes relative to other coating methods such as vapor deposition is expected. The hydrophobicity and oil resistance is not due to overcoating of alkyltrichlorosilanes on paper surfaces; according to SEM images, the porosity of native

paper is largely retained after coating and low surface tension fluids such as motor oil and methanol can still easily penetrate the coated paper surface.

CHAPTER 4

FABRICATION OF OLEOPHOBIC PAPER WITH TUNABLE HYDROPHILICITY BY TREATMENT WITH NON-FLUORINATED CHEMICALS

This chapter has been published: Z.Tang, D. W. Hess and V. Breedveld, *Journal of Materials Chemistry A*, 2015, 3 (28) pp. 14651-14600

4.1 Introduction

Hydrophobic and amphiphobic surfaces have been studied in great depth over the past couple of decades for numerous potential applications. [73, 85, 101-106] Recently, interest has grown in surfaces that simultaneously display a more unusual combination of hydrophilicity and oleophobicity for potential use in industrial applications, like oil/water separation membranes [21], self-cleaning surfaces [22] and anti-fog surfaces.[23] However, due to the intrinsic difference in surface tension between water and oil, fabrication of such surfaces has proven to be much more challenging than hydrophobic or amphiphobic surfaces.

The wetting behavior of a liquid drop on a smooth, chemically homogeneous surface is governed by Young's equation, which predicts the magnitude of the observed contact angle based on a force balance that includes the solid surface energy, liquid surface tension and adhesive forces at the solid-liquid interface. According to Young's equation, on any given substrate, fluids with lower surface tension will always display

smaller contact angles than fluids with higher surface tension; similarly, any specific fluid will wet high-energy surfaces more easily than low-energy surfaces. On chemically homogeneous rough, structured substrates, Young's equation must be modified (e.g. Cassie-Baxter or Wenzel models [7, 9]) but these trends still hold.

Because of the high surface tension of water (~72 mN/m), water-repellent surfaces are easiest to achieve; hydrophobic (static water contact angle WCA > 90^{o}), and even superhydrophobic (WCA > 150^{o}) surfaces have been successfully developed on a plethora of inorganic and organic materials. [37, 107-112] Because oils generally have a much lower surface tension than water, most hydrophobic substrates are still oleophilic. In order to add oleophobicity and reach amphiphobicity (i.e. oleo- and hydro-phobic), it is necessary to combine low surface energy coating materials with carefully engineered surface structures; such properties have been created on various substrates.[17, 20, 113-115]

In order to overcome the limitation that oleophobic substrates are inherently hydrophobic, chemical heterogeneity can be used to introduce favorable interactions with polar liquids, while maintaining unfavorable interactions with nonpolar fluids.[44] Hydrophilic and oleophobic functional groups are generally interspersed along these types of surfaces. Chemical groups with low surface energy contribute to oleophobicity, while polar surface moieties can exhibit sufficiently strong interactions with water molecules to yield hydrophilicity. [116] This concept has been implemented with various coating materials, including polyelectrolyte-fluorinated surfactant complexes,[21, 49, 117] fluorinated polymer brushes [22, 23, 48, 49, 118], fluoroalkylated flip-flop-type silane

coupling agents [45], fluorinated block co-polymers [45] and blends of fluorinated and non-fluorinated polymers. [47]

The common characteristic among all existing hydrophilic and oleophobic coating materials is the presence of perfluorinated groups, which are associated with significant environmental and health concerns. [119] Currently, implementation of these materials is also limited by rather complicated coating methods and a fairly low degree of hydrophilicity that leads to slow wetting rates for water. [120] It is therefore desirable to identify alternatives to fluorinated materials for oleophobic/hydrophilic surfaces. One previously identified candidate is methyltrimethoxysilane (MTMS), an organosilane with one methyl group and three hydrolysable methoxy substituents. Taking advantage of the low surface energy properties of methyl side groups [121], MTMS has been used to impart hydrophobicity and oleophobicity to different substrates such as glass,[122] nanocellulose[123], wood [124-126], cotton [127-129] and paper. [130-134] Compared to most fluorinated materials, MTMS has many advantages: lower environmental impact, commercial availability, and compatibility with aqueous processing environments. It is known that hydrolysis is required before MTMS can be chemically bonded to substrates with hydroxyl groups; the impact of this hydrolysis process on the wetting behavior of coated substrates has not been reported.

Another important limitation of prior work is that the majority of hydrophilic/oleophobic surfaces have been fabricated on flat, non-porous surfaces such as silicon wafers [135], glass slides [136] and on substrates with well-defined porous structures such as stainless steel meshes [21] and hollow fiber membranes. [137] Creation of hydrophilic and oleophobic properties on substrates with more random structures, such

as regular cellulose-based paper, is much less common, in spite of the many practical advantages of paper [44, 119]: low density, low cost, high flexibility, abundance and biodegradability. Paper-based products with selective wetting for oil and water would be highly desirable for cost-effective oil-water separation, for example. Polyelectrolyte-fluorinated surfactant complexes have been previously utilized to create hydrophilic, oleophobic paper [44], but this method requires a complicated two-step process which inherently limits its wide application in industry and also requires use of fluorinated coating materials.

In this Chapter, a novel one-step method to fabricate paper with tunable wetting properties is reported and the chemical changes that impart such properties are described. By systematically changing the MTMS hydrolysis time prior to coating, different degrees of condensation were achieved, which allowed the paper surface chemistry to be controlled. Paper coated with these different MTMS precursor samples display water wetting behavior ranging from superhydrophilic (absorbs water immediately) to hydrophobic, while oleophobicity is maintained under all conditions. The relation between hydrolysis time, surface chemistry and wetting properties was interrogated using ATR-FTIR, XPS and ^{29}Si NMR, both on flat silicon wafers and on porous paper handsheets. Fluorinated materials are not required in this process, and the intrinsic porosity of paper is largely retained after the coating process based on results from SEM, profilometry and air permeability measurements. The entire coating process is conducted in an aqueous environment under ambient conditions, which renders it compatible with current paper manufacturing processes and offers a scalable, economical and environmentally benign approach to the modification of surfaces. [138-140]

4.2 Experimental

Handsheet Formation

For this study, northern bleached softwood Kraft fibers (NBSK) and a mixture of 15% bleached softwood / 85% bleached hardwood fibers (co-pulp) were used to fabricate handsheets; these pulps have already been refined to a consistency of 3.5%. Fabrication of handsheets began by mixing NBSK with the co-pulp in a 40/60 ratio based on dry solids. Handsheets were then formed following TAPPI standardized method T205 sp-02,[141] in which the pulp mixture is lowered in consistency and then drained under gravity through a mesh screen. The wet handsheets were removed from the mesh screen and subsequently pressed at 50 psi. Finally, handsheets were dried overnight under ambient conditions on a stainless steel plate.

MTMS Hydrolysis Procedure

Methyltrimethoxysilane (MTMS) was purchased from Sigma-Aldrich (deposition grade, > 98%). Without further purification, MTMS was mixed with 0.1 M hydrochloric acid (HCl, Fisher Chemicals, 37.3%) in a 4:1 v/v ratio. The mixture was then sonicated in an ice-bath for different lengths of time to induce hydrolysis.[134] Sonication was carried out using a Fisher Scientific ultrasonic cleaner (model FS20) at a power of 70 W and frequency of 42 kHz.

MTMS Coating Procedure

Silicon wafers (P type 100 mm silicon wafer (100) P/E, wafer world Inc.) and glass slides (VWR micro cover glass, 18x18mm), which served as flat substrates for MTMS films, were rinsed with acetone, methanol and isopropanol (BDH, ACS grade,

99%). Rinsed substrates were subsequently exposed to an air plasma for 5 minutes to remove any solvent residues and ensure the presence of hydroxyl groups on the surface. Cleaned substrates were immersed in the hydrolyzed MTMS solutions for 2 minutes. After coating, excess liquid was removed from the surface by touching the liquid with a piece of tissue paper (Kimwipe, Kimberly-Clark). Coated substrates were then dried at ambient conditions overnight. A similar coating process was invoked for paper substrates. Handsheets with a size of 1.5 x 1.5 cm^2 were immersed in the hydrolyzed MTMS solutions for 2 minutes. To prevent over-coating, residual fluids were again removed after coating by using tissue paper. Coated paper was also dried under ambient conditions overnight before performing characterizations.

Contact Angle Measurements

All static contact angle measurements were performed by using a Rame-Hart automated goniometer (model 290). A 4 μL droplet of the selected fluid (DI water, diiodomethane (Sigma-Aldrich, reagent plus grade, 99%) and motor oil (SAE 10W-30, MotoTech)) was placed onto MTMS coated substrates. Contact angles were determined by the standard software of the goniometer (Drop Image, version 2.6.1).

SEM Imaging

All samples subjected to scanning electron microscopy (SEM) imaging were sputter coated with Au/Pd to reduce accumulation of charges during measurement. Images were taken with a Hitachi SU8230 SEM at an acceleration voltage of 5.0 keV.

Surface Analysis

X-ray photoelectron spectroscopy (XPS) analyses were conducted using a Thermo Electron Corporation K-Alpha XPS system with a microfocused monochromatic Al Kα X-ray source. The spot size of the instrument is 400 μm.

FTIR Analysis

ATR-FTIR was carried out on a Nicolet IS-50 FTIR spectrometer (Thermo Scientific, Inc), operated in the ATR mode. The spectrometer was set to collect 32 scans at 4 cm^{-1} in the range from 4000 to 700 cm^{-1}.

NMR Analysis

^{29}Si NMR spectra were obtained for unhydrolyzed and hydrolyzed MTMS solutions on a Bruker Avance III 400 NMR spectrometer using a 5 mm broadband probe at 79.5 MHz. The ambient temperature (294K) was fixed during measurements. Deuterium oxide and deuterium chloride were used in lieu of DI water and HCl to prepare hydrolyzed samples. To obtain the control spectrum for unhydrolyzed MTMS, pure MTMS was mixed with methanol at a 4:1 ratio. Spectra were averaged over appropriate number of scans to enhance the signal-to-noise ratio. All chemical shifts were referenced to tetramethylsilane (TMS).

Air Permeability Analysis

Air permeability of paper samples was determined following standard TAPPI T 460 om-02 procedure. [142] Samples with a size of 5 x 5 cm^2 were placed under a

pressure differential of 1.22 kPa, and the time for 100 mL air to pass through paper was measured to determine the air permeability.

Profilometry

Measurements were conducted using a Wyko NT3200 Optical Profilometer. Arithmetic averages of the surface roughness (i.e. Ra values) were analyzed using the Vision32 software (Veeco Instruments Inc.). Roughness was calculated according to the ANSI B46.1 standard. [143]

4.3 Results and Discussion

Wetting Properties of MTMS Coated Paper

To investigate the effect of hydrolysis time on wetting behavior of porous substrates, handsheets (HSs) were coated with MTMS hydrolyzed between 0 (i.e. no hydrolysis) and 360 minutes. HSs are paper composed of only cellulose fiber, without chemical additives (e.g., fillers, brighteners). Compared to filter paper, for example, HSs are not designed to withstand prolonged exposure to fluids. Hydrolysis of MTMS was conducted in an acidic environment by mixing MTMS monomer with 0.1 M HCl at a 4:1 ratio by volume. The mixture was then sonicated for different lengths of time to initiate the hydrolysis process. Sonication was used to enhance mixing and prevent gelation of MTMS at this high concentration; the process was conducted in an ice bath to remove heat generated by the exothermic hydrolysis reaction and maintain constant sample temperature. The mixture became less transparent after 30 minutes of hydrolysis, indicating formation of small particulates in the solution. To coat the sample surface, a HS was immersed into the MTMS mixture for 2 minutes. To prevent overcoating of

MTMS (i.e. closure of all the substrate pores), excessive coating solution was removed from the HS surface with a piece of tissue paper immediately after coating. HSs were then dried under ambient conditions for 12 hours, after which they maintained the visual appearance of ordinary paper, including flexibility.

The wetting properties of coated HSs were determined through contact angle measurements (see Table 1). Water (surface tension 72.8 mN/m), diiodomethane (50.8 mN/m), ethylene glycol (48.0 mN/m) and motor oil (31.0 mN/m) were used as testing fluids that cover a wide range of fluid properties. Water and ethylene glycol are polar, while diiodomethane and motor oil are non-polar fluids. To evaluate the stability of oil contact angles, measurements were performed for 30 minutes after the droplet was placed on the substrate. For changes in contact angle less than 5^o, the contact angle was considered to be stable; larger changes indicated an unstable contact angle. However, due to the relatively fast evaporation of water under ambient conditions, this method cannot be applied to evaluate the stability of the water contact angle. Instead, a dyed water droplet was placed on the coated paper, and its stability was evaluated by visually checking for signs of water absorption into the paper.

As shown in Table 4.1, both uncoated HSs and HSs coated with unhydrolyzed MTMS absorb all fluids instantly. HSs coated with MTMS after 5 minutes of hydrolysis display a stable diiodomethane contact angle at 75^o and a stable motor oil contact angle at 65^o. However, the same sample absorbs water and ethylene glycol instantly. To our knowledge, this represents the first time that a hydrophilic/oleophobic surface has been fabricated on porous paper without the use of fluorinated materials. By further extending the hydrolysis time, the water repellency of coated HSs gradually increases, while oil

contact angles remain essentially the same. HSs coated after 60 minutes of hydrolysis still absorb water, but at a much slower rate, while HSs coated after 180 minutes or 360 minutes of MTMS hydrolysis display stable water contact angles of ~90^{o}. For ethylene glycol, on the other hand, all HS samples absorb the fluid, even at the longest hydrolysis time of 360 minutes. These results indicate that oleophobic paper with tunable hydrophilicity can be fabricated via a one-step coating process, using MTMS hydrolysis time as the controlling parameter. To explain this striking observation and determine the underlying mechanism, the chemistry of the MTMS solutions during the hydrolysis process and surface chemistry of the resulting coatings was investigated with various techniques, and the results of those studies are presented and discussed in the remainder of this paper.

Table 4.1: Wetting behaviors of handsheets (HSs) coated with MTMS after different hydrolysis times. "Absorbs" indicates instant (<3 sec) absorption of the fluid. "Unstable" indicates that the fluid is absorbed after some delay (>10 seconds); the number inside parentheses represents the contact angle immediately after the droplet was placed on these unstable samples. Stable contact angles indicate that the change in contact angle is less than 5^o within 30 minutes after drop placement.

MTMS Hydrolysis time (min)	Water	Ethylene glycol	Diiodo-methane	Motor oil	Wetting behavior
Uncoated	Absorbs	Absorbs	Absorbs	Absorbs	Hydrophilic/ Oleophilic
0 (control)	Absorbs	Absorbs	Absorbs	Absorbs	Hydrophilic/ Oleophilic
5	Absorbs	Absorbs	74.6 ± 0.7^o	64.7 ± 1.4^o	Hydrophilic/ Oleophobic
60	Unstable (77.4 ± 3.4^o)	Absorbs	72.1 ± 6.7^o	64.4 ± 2.1^o	Hydrophilic/ Oleophobic
180	85.2 ± 3.4^o	Absorbs	72.7 ± 2.0^o	61.2 ± 2.5^o	Amphiphobic
360	87.7 ± 4.7^o	Absorbs	68.1 ± 4.1^o	59.8 ± 1.3^o	Amphiphobic

MTMS Hydrolysis Process

As shown above, MTMS hydrolysis time is a critical variable that greatly affects wetting properties, in particular for water. During hydrolysis, the stepwise substitutions of the alkoxide ligands by hydroxyl groups produce the reactive monomers that are subsequently consumed in condensation reactions to form dimers and oligomers. When hydrolyzed MTMS is coated on a substrate surface, the oligomers form hydrogen bonds with the cellulose hydroxyl groups on the substrate. Finally, during drying, a permanent siloxane bond forms with concomitant loss of water. It is well-known that pH is an important parameter during the hydrolysis process; under acidic conditions, a fast hydrolysis reaction, followed by a slow condensation reaction, is observed. [144-147]

To examine the structural evolution of MTMS in both the early and late stages of hydrolysis, ^{29}Si NMR spectra were obtained for unhydrolyzed monomeric MTMS, and after 30 minutes and 180 minutes of hydrolysis (see Figure 4.1). Samples were scanned 256 times to ensure sufficient signal to noise ratio. Due to the long spin-lattice relaxation time of the silicon atoms, each spectrum took ~50 minutes to collect. Peak assignments were made following reports in literature. [123, 144, 145, 147] Signals with chemical shifts of -39.1 ppm, -47.6 pm, -57.2 ppm and -66.2 ppm can be assigned to MTMS monomer, dimer, linear oligomers and branched oligomers, respectively. Formation of cyclic species is also a common feature of MTMS hydrolysis under acidic conditions. Due to reduction of the Si-O-Si angle, these peaks are located further downfield relative to linear and branched species [145]: peaks at -56.5 ppm and -64.3 ppm are assigned to 4-membered ring and caged species, respectively. The disappearance of monomeric MTMS species after 30 minutes of hydrolysis indicates a fast process. In comparison,

condensation is relatively slow in the presence of acid. All forms of condensed species (dimers, linear oligomers and branched oligomers) are observed in MTMS hydrolyzed for 30 minutes. As the reaction continues, condensation becomes dominant. As a result, the signal from MTMS dimers disappears and more branched and caged oligomers are observed after 180 minutes. Because MTMS dimers and linear oligomers contain more silanol groups than branched oligomers, when coated on substrates, MTMS hydrolyzed for shorter periods of time is expected to display more polar silanol groups on the surface than MTMS with a prolonged hydrolysis. To test the validity of this hypothesis, the surface chemistry of MTMS coatings with different hydrolysis times was carefully characterized using XPS and ATR-FTIR.

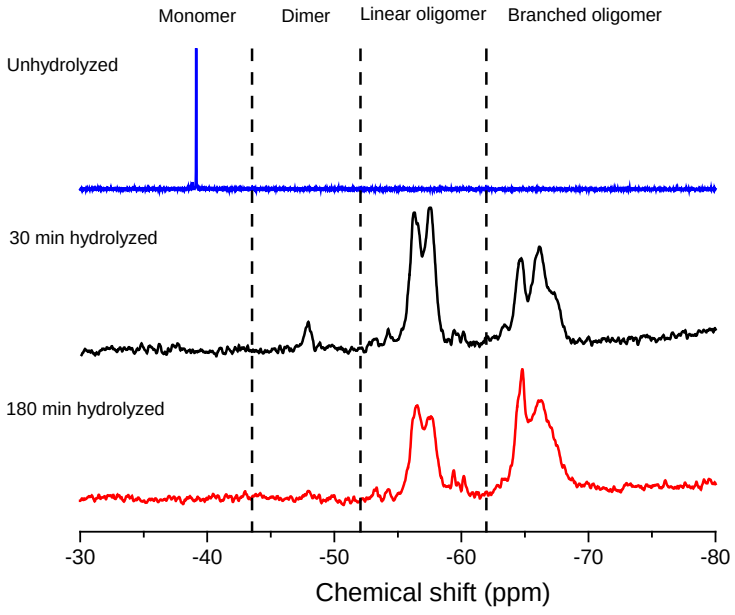

Figure 4.1: ^{29}Si NMR spectra after different hydrolysis times for acid catalyzed MTMS.

Surface Chemistry of MTMS Coatings

To investigate changes in surface composition as a function of hydrolysis time, XPS was performed on silicon wafers coated with MTMS. A silicon wafer was chosen as the substrate for this study because it has a well-defined, flat surface. The effects of surface roughness on wetting behavior can therefore be excluded. To apply the coating on silicon wafers, clean wafers were immersed in hydrolyzed MTMS solutions. After coating, excessive fluid was removed from the substrate with tissue paper. The coating time was 2 minutes for all samples. A clean silicon wafer without MTMS coating was used as control sample. As expected, carbon, oxygen and silicon were the only three elements detected on all samples. To further investigate changes in surface chemistry with hydrolysis time, high resolution XPS spectra were also taken. Figure 4.2 presents XPS spectral scans for MTMS films on silicon for different hydrolysis times. Before coating, Si (99.4 eV) and SiO_2 (103.2 eV) are present on the surface; these two peaks are preserved on the surface of the sample coated with unhydrolyzed MTMS, indicating that unhydrolyzed MTMS cannot form a continuous thin film on silicon within 2 minutes, which can be attributed to the fact that pure MTMS lacks silanol groups to form covalent bonds with Si-OH on the substrate surface. After 180 minutes of hydrolysis, the elemental Si peak disappears, and new peaks are observed around 102.8 eV, which correspond to $Si(CH3)O_{3/2}$. [148] This is strong evidence that the silicon surface is being fully covered by condensed MTMS species. A closer inspection of the XPS spectra reveals that as hydrolysis time increases, peaks around 103 eV gradually shift towards a lower binding energy. This shift is likely due to a change in MTMS species from dimers to linear polymers and branched polymers, as the condensation reaction progresses.

However, because of the subtle difference in XPS spectra between O-Si-O-H and O-Si-O-Si signatures [149], it is very difficult to extract quantitative information from this peak shift.

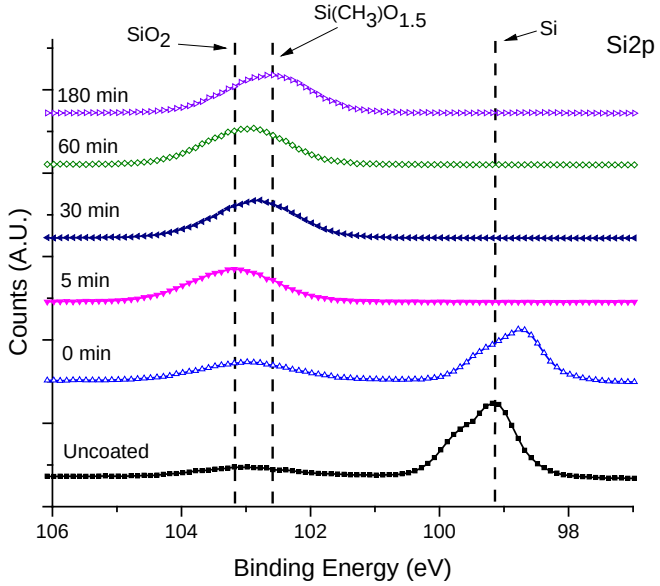

Figure 4.2: XPS data for Si 2p on silicon wafers coated with MTMS after different hydrolysis times. Peaks in the 95-110 eV range correspond to the $2p^{1/2}$ and $2p^{3/2}$ peaks.

To further investigate the surface chemistry on different MTMS films, ATR-FTIR spectra were taken on uncoated glass slides and glass slides coated with MTMS hydrolyzed from 0 to 360 minutes (Figure 4.3a). Glass slides were used as substrates in this set of experiments in lieu of silicon wafers to avoid overlap with broad Si-O-Si IR peaks from the underlying substrate. It is evident from Figure 3a that the spectrum for unhydrolyzed MTMS is similar to that of the uncoated substrate, which further confirms

that unhydrolyzed MTMS cannot graft onto glass slides during a short coating time. The spectrum for the glass slide coated with 5 minutes hydrolyzed MTMS shows strong peaks at 1100 cm^{-1}, which correspond to Si-O-Si bonds [150], indicating that MTMS has been successfully grafted onto the substrate surface following a short hydrolysis time. The peaks at 1270 cm^{-1} and 760 cm^{-1} can both be assigned to Si-CH_3 bonding. [98] The presence of methyl groups on the surface is further confirmed by the peak at 2950 cm^{-1}, which is due to C-H bonding. However, due to the relatively short hydrolysis time, large amounts of MTMS dimers and linear oligomers are still present in the mixture. Both of these species contain silanol groups, resulting in peaks at 890 cm^{-1} and 3300 cm^{-1} from Si-OH and O-H bonding, respectively. The presence of both methyl groups and hydroxyl groups on the substrate surface is the primary reason for the unique wetting properties of MTMS coated substrates, which is discussed in more detail below. As the hydrolysis time increases, MTMS dimers and linear polymers further react through condensation reactions and form branched oligomers. Consequently, peaks at 890 cm^{-1} and 3300 cm^{-1} gradually reduce in intensity, while the peaks corresponding to Si-O-Si and Si-CH_3 are preserved after prolonged hydrolysis. This result clearly proves that the concentration of hydroxyl groups on the substrate surface can be controlled by changing hydrolysis time of MTMS in an acidic environment. MTMS solutions with short hydrolysis time contain more dimers and linear oligomers, and are therefore rich in hydroxyl groups. As the condensation reaction continues, more branched oligomers are generated in the MTMS solution; as a result, hydroxyl groups on the substrate surface also gradually disappear.

In addition to the glass slides, the surface chemistry of uncoated and coated paper HSs was also characterized using ATR-FTIR (see Figure 4.3b). Although the spectra on the chemically more heterogeneous HS are more difficult to interpret, the data in Figure 4.3a greatly assist with peak assignment and analysis. It is clear that HSs coated with unhydrolyzed MTMS display a similar spectrum to that of the uncoated HS, again confirming the low surface reactivity of unhydrolyzed MTMS. Peaks corresponding to the Si-CH_3 bond (1270 cm^{-1}, 760 cm^{-1}) and methyl group (2950 cm^{-1}) are evident in the spectrum for HSs coated after 5 minutes or 180 minutes of MTMS hydrolysis. This result indicates that despite the rough surface of the porous HS, MTMS can successfully graft to hydroxyl groups on the HS surface following a short hydrolysis time. However, due to the large number of hydroxyl groups on native cellulose fibers, all samples display peaks at 3300 cm^{-1}. As a result, unlike the glass substrates, the density of hydroxyl groups on different HS samples cannot be directly compared based on ATR-FTIR.

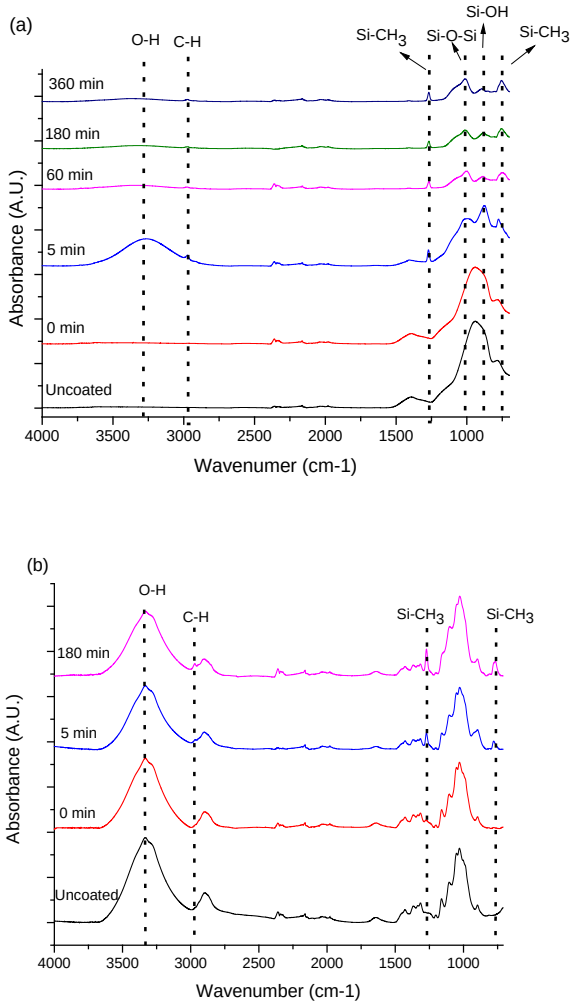

Figure 4.3: ATR-FTIR of (a) MTMS coated glass slides and (b) MTMS coated HSs after different MTMS hydrolysis times.

Wetting Properties of MTMS Films

Both surface chemistry and surface morphology can affect the wetting properties. To isolate the effects of surface chemistry, contact angles (CA) were measured on silicon wafers coated with MTMS after different hydrolysis times. The wetting behavior of MTMS films is summarized in Figure 4.4. Before coating, cleaned glass sides have a diiodomethane CA of $40.4^{o}\pm 0.6^{o}$ and a motor oil CA of $20.1^{o}\pm 2.3^{o}$. For silicon wafers

coated with unhydrolyzed MTMS, an increase in both diiodomethane and motor oil contact angles was observed. According to our NMR and FTIR data, this phenomenon is likely due to small amounts of unhydrolyzed MTMS monomer physisorbed onto the substrate. The introduction of methyl groups imparts oleophobicity to the surface due to their low surface energy. [121] For wafers coated with 5 minutes hydrolyzed MTMS, the diiodomethane and –most notably- motor oil contact angles increase further. Based on our previous ATR-FTIR observations, this result is due to the presence of a high concentration of methyl groups grafted to the substrate. Further increasing the hydrolysis time has little effect on the contact angles of non-polar fluids, indicating that the density of methyl groups on the surface does not change significantly with prolonged hydrolysis time.

Compared to non-polar fluids, water shows a very different wetting behavior as a function of MTMS hydrolysis time. The stability of the water contact angle was evaluated by observing the spreading dynamics of water droplets during the contact angle measurements. On the uncoated silicon wafer, due to the high density of hydroxyl groups on the surface, water wets the surface completely in less than 5 seconds (i.e. zero degree contact angle). For silicon wafers coated with unhydrolyzed MTMS, a stable water contact angle of 58.5^{o} was observed, again indicating the presence of physisorbed unhydrolyzed MTMS. However, complete wetting was observed on silicon wafers coated with MTMS hydrolyzed for 5 minutes. Because less than 5 seconds elapsed before water completely spread on the surface, a 0^{o} water contact angle is reported here. It should be pointed out that for other, fluorinated hydrophilic/oleophobic materials, it usually requires minutes before water contact angles drop to less than 20^{o}, while in our case

water wets the coated surface almost immediately. [45, 151, 152] Our NMR and ATR-FTIR results suggest that the hydrophilic behavior of the substrate coated with MTMS after a short hydrolysis time is due to the abundance of polar hydroxyl groups in hydrolyzed, but not fully condensed MTMS dimers or linear oligomers in the mixture. When coated on a silicon wafer, both methyl groups and hydroxyl groups are present on the substrate surface, as indicated by ATR-FTIR spectra. The contact angle of non-polar fluids is largely determined by the density of non-polar methyl groups on the substrate surface. On the other hand, water is very sensitive to the presence of hydroxyl groups. As our previous analysis indicates, as hydrolysis time increases, the condensation reaction becomes dominant, and the concentration of silanol groups slowly decreases. Indeed, for substrates coated with MTMS after 60 minutes hydrolysis, a much slower water wetting behavior was observed. For MTMS hydrolyzed for more than 180 minutes, stable water contact angles were found. As summarized in Figure 4.4, by tuning hydrolysis time, MTMS coated surfaces can be fabricated on a non-porous substrate with controlled wetting behavior against water but these surfaces maintain similar oil contact angles.

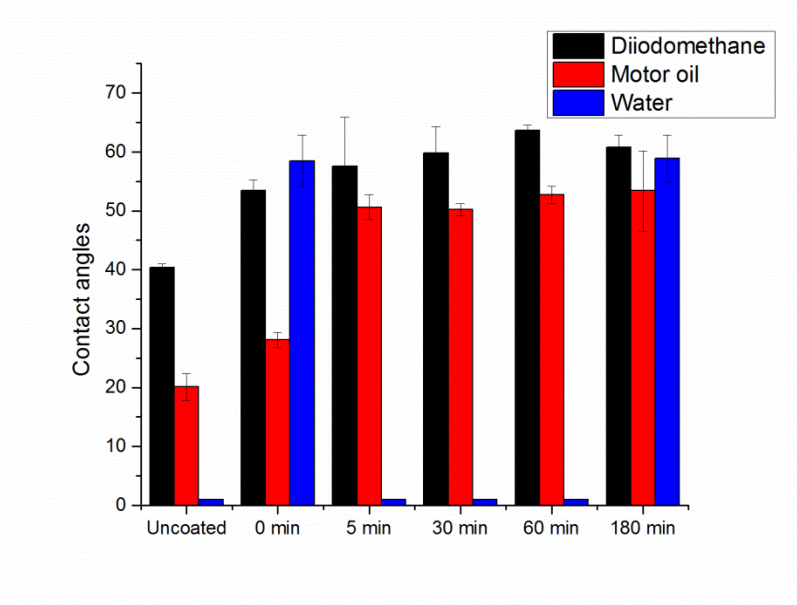

Figure 4.4: Contact angle measurement of water, diiodomethane and motor oil on silicon wafers coated with MTMS after different hydrolysis times.

To further illustrate the point that wetting on a MTMS coated substrate is not solely determined by surface energy, but also highly dependent on the polarity of fluids, ethylene glycol contact angles were measured on different samples. Ethylene glycol has a surface tension similar to that of diiodomethane, but it displays a completely different wetting behavior on MTMS coated silicon wafers. As is evident in Figure 4.5, ethylene glycol displays a wetting behavior that is similar to water. Because ethylene glycol has a much lower vapor pressure than water, it is possible to monitor changes in contact angle for 30 minutes without evaporation effects. An uncoated silicon wafer displays a 0^{o} ethylene glycol contact angle. A stable ethylene glycol contact angle of 46^{o} is observed on silicon wafers coated with unhydrolyzed MTMS. The contact angle is lower than that of water because ethylene glycol has a lower surface tension. For silicon wafers coated with hydrolyzed MTMS, a similar trend was observed as that for water: with an increase

in hydrolysis time, the resistance against wetting also increases. The main difference between water and ethylene glycol is that due to the lower surface tension of ethylene glycol, all samples display a lower wetting resistance against ethylene glycol than water; even after 360 minutes of hydrolysis, ethylene glycol spreads on the surface within 5 minutes.

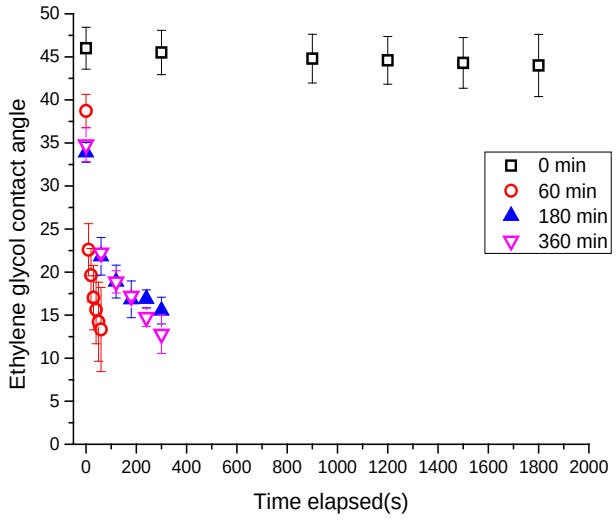

Figure 4.5: Contact angle measurements of ethylene glycol on silicon wafers coated with MTMS hydrolyzed for different times as a function of elapsed time after droplet placement.

Properties of MTMS Coated Paper

Based on the wetting properties and surface chemistry of MTMS thin films on flat substrates, the remarkable wetting properties of MTMS-coated paper HSs (Table 1) can now be explained. On a porous substrate, unhydrolyzed MTMS cannot form a coating that is sufficiently dense to support non-polar fluids; as a result, both uncoated HSs and HSs coated with unhydrolyzed MTMS display oleophilicity. The increased density of methyl groups after 5 minutes of hydrolysis imparts oil resistance to the paper. Similar to the wetting behavior of MTMS films on flat substrates, a further increase in hydrolysis time has no significant effect on oil contact angles. To determine if coated HSs can display prolonged oil resistance, a droplet of motor oil, which has a much lower surface tension than diiodomethane, was monitored over 12 hours (see Figure 4.6a). No oil stains were observed on the paper after 12 hours and the change in contact angle was less than 5^{o}. In fact, we have observed that droplets of motor oil can remain on HSs coated with hydrolyzed MTMS for several weeks without any signs of absorption.

The wetting behavior of polar fluids on MTMS coated HSs is also similar to silicon wafers (see Figure 4.6b). The hydrophilicity of HSs coated with unhydrolyzed MTMS is likely due to low grafting density. Due to the high concentration of hydroxyl groups, HSs coated with MTMS after 5 minutes hydrolysis absorbed water instantly. As the hydrolysis time increases, the concentration of silanol groups decreases. Consequently, HSs coated by MTMS after a prolonged hydrolysis time display higher resistance toward water. Analogous to the wetting properties of MTMS films on flat silicon wafers, none of the coated HS samples show resistance towards ethylene glycol

wetting. In fact, all coated HSs absorb ethylene glycol at a much faster rate than its spreading rate on MTMS coated wafers.

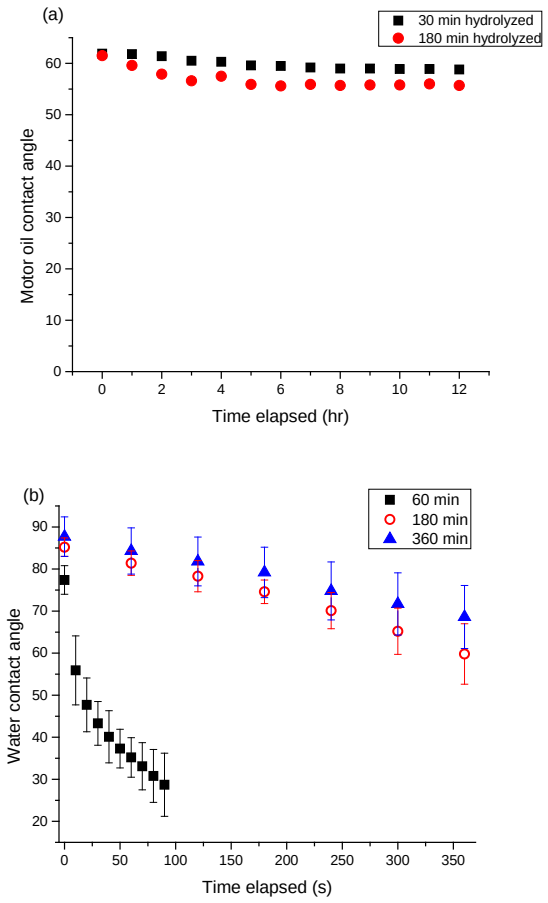

Figure 4.6: Contact angle measurements of (a) motor oil and (b) water on HSs coated with MTMS hydrolyzed for different times as a function of elapsed time.

In previous studies, liquid-repellent paper was fabricated by applying a pore-free barrier coating on top of the fiber surface. [69, 119, 153-156] The obvious disadvantage of this approach is the loss of intrinsic flexibility and air permeability. In the current study, overcoating was prevented by reducing the coating time to 2 minutes and removing excessive MTMS immediately after coating. To study the morphology of coated HSs, SEM and optical profilometry were used to characterize different samples (see Figure 4.7). At low magnification, the SEM images do not reveal a significant difference between coated and uncoated HSs: the porosity of uncoated paper is largely retained for MTMS coated HS. However, at high magnification, a thin coating layer can clearly be seen around each individual fiber for MTMS coated HSs. To study the topology before and after coating in more detail, roughness profiles were measured with an optical profilometer. Again, the difference between uncoated and coated HSs appears to be minimal, and all samples show similar micron-scale roughness. To further confirm the retention of sample porosity after coating, a droplet of dyed methanol was placed on each sample. With its much lower surface tension (22.5 mN/m), methanol immediately penetrated through all treated papers, leaving stains on paper substrates placed beneath the test paper, thus confirming that no continuous film has been formed on the coated paper surface.

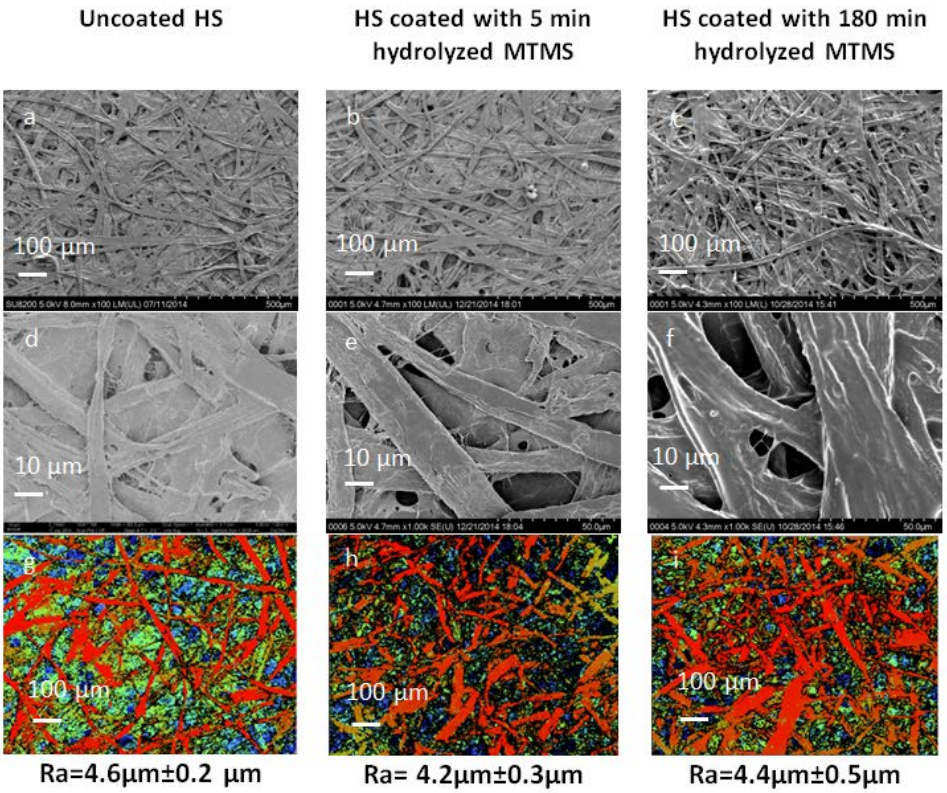

Figure 4.7: Low magnification SEM images of uncoated HSs, HSs coated with 5 min hydrolyzed MTMS and HSs coated with 180 min hydrolyzed MTMS are shown in (a-c), demonstrating that the porosity of native paper is largely retained after coating. Complementary high magnification SEM images are presented in (d-f). Profilometer images for each sample are also presented in (g-i)

To quantitatively determine any changes in air permeability after coating, Gurley air permeability tests were conducted according to TAPPI T-460 procedure on MTMS coated paper (see Table 4.2). The Gurley air permeability test is a common method used in the paper industry to evaluate air permeability of coated paper; it measures the time for 100 mL of air to pass through the paper under a pressure differential of 1.22 kPa. A decrease in air permeability was observed for samples coated with hydrolyzed MTMS, likely because the MTMS coatings partly cover small pores in the fibrous network,

resulting in lower porosity. However, it should be noted that a factor 6 increase in flow time is actually quite low compared to other fluid-repellent paper substrates with barrier coatings, which typically show decreased air permeability by factors of 100 to 10,000.[69] In our samples, the majority of pores are clearly retained after the coating process.

Table 4.2: Air permeability of HS coated with MTMS after different times

MTMS hydrolysis time (min)	Permeability (s)
Uncoated	25.8±1.0
0	23.9±1.0
5	120.7±2.4
60	131.7±1.8
180	144.7±1.0

4.4 Conclusions

We have developed a facile, one-step solution coating method to fabricate oleophobic paper substrates with tunable hydrophilicity using non-fluorinated coating material. The coating material was easily prepared by mixing pure methyltrimethoxysilane (MTMS) with 0.1 M hydrochloric acid at a 4:1 ratio, followed by sonication in an ice bath. The hydrophilicity of MTMS coatings can be tuned by simply adjusting hydrolysis time. Results from ^{29}Si NMR and ATR-FTIR provide evidence that

the change in hydrophilicity is caused by varying concentrations of polar silanol groups on the substrate surface. Consequently, coated surfaces display wetting behaviors ranging from hydrophilic/ oleophobic to amphiphobic as a function of hydrolysis time.

Compared with existing hydrophilic/ oleophobic surfaces, which are commonly fabricated on well-defined, flat substrates, MTMS coatings can easily be applied on more heterogeneous, porous substrates such as paper. Moreover, this material does not contain fluorine and is therefore more environmental friendly than those previously reported. The porous structure of paper is also largely retained after coating, which improves flexibility and air permeability relative to that of other grease-proof papers. The MTMS coating process is carried out in an aqueous environment under ambient conditions at a relatively fast rate. As a result, it is compatible with current large-scale paper manufacturing processes. Development of hydrophilic/oleophobic paper surfaces will facilitate important applications such as oil/water separation; further studies are underway to explore this in more detail. The amphiphobic paper has potential applications as packaging materials that can repel both aqueous and oily fluids, as a self-cleaning material, and as a material for disposable labware. This work also indicates that MTMS can be employed to functionalize other hydroxyl-group-rich surfaces.

CHAPTER 5

FABRICATION OF AMPHIPHOBIC SOFTWOOD AND HARDWOOD BY TREATMENT WITH NON-FLUORINATED CHEMICALS

Material from this chapter was submitted for publication in *Wood Science and Technology* by Z.Tang, D. W. Hess and V. Breedveld

5.1 Introduction

Wood, a naturally occurring polymer composite composed of cellulose, hemicellulose, lignin, and extractives, is the most versatile and widely used structural engineering material for indoor and outdoor applications. [157-159] Compared with synthetic materials, wood has an impressive range of attractive qualities, such as aesthetic appeal [160], low density [159], low thermal expansion [161], desirable mechanical strength [162-164] and world-wide availability. However, due to its intrinsic hydrophilicity and oleophilicity, unprotected wood is susceptible to dimensional instability [165], weathering [166-168], and biological degradation. [169-171] In recent years, growth of the wood products industry has been fueled by a significant expansion in the use of wood in outdoor applications. As a result, there is an evident need for enhancing the resistance of wood to weathering and natural degradation, increasing its durability as a substrate and extending the service life of wood. [172-174] One approach to improve durability is to reduce water absorption and oil contamination on the wood surface. [175]

Over the years, various methods have been developed to impart wood with controlled wetting properties, such as acetylation [176], silylation [124], covalent grafting of polymers [165], plasma enhanced chemical vapor deposition (PECVD) [177-179] and mild pyrolysis under an inert atmosphere. [180] The majority of these methods are used to impart only hydrophobicity to wood samples. [181-184] Compared with hydrophobic surfaces, fabrication of oleophobic surfaces has proven to be much more challenging. This is because non-polar liquids possess much lower surface tension than water, and therefore oil repellent surfaces require even lower surface energies than hydrophobic surfaces. [185] Another common characteristic among existing methods is the presence of fluorinated materials [178, 186], which are believed to be associated with significant environmental and health concerns. [187] Implementation of these materials is also limited by complicated coating methods and high cost. It is therefore desirable to identify alternatives to fluorinated materials as coating materials for wood. However, reports of facile approaches to fabricate wood with improved water and oil repellency using non-fluorinated coating materials are limited, and the existing literature focuses on water repellency.

Methyltrimethoxysilane (MTMS) is an organosilane species with one methyl group and three hydrolysable methoxy substituents. Taking advantage of the low surface energy properties of methyl side groups, MTMS has been used to impart hydrophobicity to different substrates such glass [188], nanocellulose [123], cotton [127], paper [130] and wood. [124-126] Compared to most fluorinated materials, MTMS has many advantages: lower environmental impact, commercial availability, and good compatibility with aqueous processing environments. It is known that a pre-hydrolysis step is required

before MTMS can be chemically bonded to substrates by forming covalent bonds with surface hydroxyl groups. In Chapter 4, we demonstrated that pre-hydrolyzed MTMS can be successfully coated on paper substrates utilizing the abundant surface hydroxyl groups on cellulose. By carefully controlling the pre-hydrolysis time, coated paper samples were created that display amphiphobicity, repelling both oil and water.[82] Because cellulose is also a major component of wood, it is reasonable to assume that amphiphobic wood can also be fabricated using MTMS.

However, unlike paper, which is almost entirely composed of cellulose, wood contains many other substances, including lignin as the second major component. [189] As a result, the concentration of hydroxyl groups on wood surfaces is much lower than on paper. The low concentration of surface hydroxyl groups will lead to a less efficient coating process for MTMS. A pre-treatment is therefore required to modify the wood surface chemistry before the coating process. Plasmas have been widely used to modify the surface chemistry of materials. Cold plasma treatments can induce physical and chemical changes to depths of a few micrometers without changing the bulk properties.[179] Cold oxygen plasmas have been previously employed to improve wood surface properties. It has been reported that oxygen plasma treated wood samples display higher surface polarity due to the formation of hydroxyl, carboxyl, aldehyde and other polar functional groups. [190-195] The increase in surface hydroxyl groups provides additional potential binding sites for pre-hydrolyzed MTMS. The increased surface polarity could also improve wettability on and penetration into the wood by an aqueous coating fluid. Compared with other chemical treatments, which are often costly and can result in leaching of toxic materials into the environment, plasma treatment offers

advantages such as more environmentally friendly reaction sequences and short processing times.

In this Chapter, a novel facile method to fabricate amphiphobic wood surfaces by using MTMS as a coating material is reported. The study was conducted on both hardwood and softwood to demonstrate wide applicability. Wood samples were treated with a cold oxygen plasma for a short amount of time before coating in order to activate the surface. After plasma treatment, wood samples were coated with pre-hydrolyzed MTMS following a solution-based method. For both hardwood and softwood, coated samples displayed hydrophobicity and prolonged resistance against oils. The surface chemistry was interrogated using ATR-FTIR and XPS. Fluorinated materials are not required in this process and the intrinsic appearance and roughness of wood was largely retained after the coating process. The entire coating process was conducted in an aqueous environment under ambient conditions, which offers a scalable, economical and environmentally benign approach to the modification of surfaces.

5.2 Experimental

Materials

Hardwood (Golden chinkapin, *Castanopsis chrysophylla*) and softwood (southern yellow pine) sliced veneer wood specimens were obtained from the Department of Natural Resource Ecology and Management at Iowa State University. The specimens were cut into thin slices of 50 mm x 15 mm x 0.8 mm and 15 mm x 15 mm x 1.0 mm, respectively, along the radial direction of the log. Before treatment, all samples were sanded with 120 grit sandpaper and cleaned with a nitrogen gas jet to eliminate

particulate residue from the wood surfaces. The purpose of sanding is to eliminate surface contamination as well as to create uniform, reproducible roughness on the wood surface. Silicon wafers (P type 100 mm silicon wafers (100) P/E; Wafer World Inc.), which served as flat control substrates for MTMS films, were rinsed with acetone, methanol, isopropanol (BDH, ACS grade, 99%) and then dried using nitrogen gas. Methyltrimethoxysilane (MTMS) was used as received from Sigma-Aldrich (deposition grade, $\geq$ 98%). Hydrochloric acid (HCl) was obtained from Fisher Chemicals. Oxygen (ultra-pure carrier grade, 99.996%) was purchased from Airgas Inc.

Oxygen Plasma Activation

A 2.5-inch parallel-plate rf (13.56 MHz) plasma reactor (Kurt J. Lesker, Jefferson Hills, PA) was used to activate sample surfaces prior to coating. Wood and silicon wafer samples were placed on the bottom grounded electrode and heated to 110^{o}C for all experiments using Omegalux CSH-101120 cartridge heaters (Omega Engineering Inc., Stamford, CT) and monitored by a platen temperature controller (Tek-Vac Industries Inc., Brentwood, NY). More detailed information about this reactor can be found elsewhere [38]. Before the surface activation treatment, the reactor system was evacuated to a base pressure of ~ 1.0 x 10^{-2} Torr. Oxygen plasma activation was performed at a working pressure of 0.5 Torr and an oxygen flow rate of 20 SCCM for 2 minutes. The applied rf power during activation was 120 W. After activation, the reactor system was back-filled to atmospheric pressure with nitrogen gas; samples were then removed from the reactor for the subsequent MTMS coating.

MTMS Hydrolysis Procedure

Hydrolysis of MTMS was performed by mixing MTMS with 0.1 M hydrochloric acid in a 4:1 v/v ratio. The mixture was then sonicated in an ice-bath for different lengths of time to induce hydrolysis. Sonication was carried out using a Fisher Scientific ultrasonic cleaner (model FS 20) at a power of 70 W and frequency of 42 kHz.

MTMS Coating Procedure

Activated silicon wafers were immersed in the hydrolyzed MTMS solutions for 2 minutes. After coating, excess liquid was removed from the surface by touching the liquid with a piece of tissue paper (Kimwipe, Kimberly-Clark). Coated silicon wafers were then dried at ambient conditions overnight. A similar coating process was invoked for wood substrates. To ensure high coverage of coating material, the coating time was varied from 5 min to 60 minutes. To prevent over-coating, residual fluids were again removed by using tissue paper. Coated wood samples were also dried under ambient conditions overnight before material characterization.

SEM Imaging

All samples subjected to scanning electron microscopy (SEM) imaging were sputter coated with Au/Pd to reduce charge accumulation during measurements. Images were taken with a Hitachi Su8230 SEM at an acceleration voltage of 5.0 keV.

Profilometry

Measurements were conducted using a LEXT OLS4100 Laser Scanning Confocal Microscope (LSCM) profilometer (Olympus Co., Japan) with a laser wavelength of 405

nm, a 20x objective and a scan area of 643 μm × 643 μm. Arithmetic averages of the surface roughness (i.e. Ra values) were analyzed using the OLS4100 software (version 3.1.5.9).

Contact Angle Measurements

All static contact angle measurements were performed with a Ramé-hart automated goniometer (Model 290). A 4 μL droplet of the selected fluid (DI water, diiodomethane (Sigma-Aldrich, reagent plus grade, 99%) and motor oil (SAE 10W-30, MotoTech)) was placed onto MTMS coated substrates. Photographic images of the liquid drop shape on the wood surface perpendicular to the grain direction were captured. Contact angles were determined from these images via the standard goniometer software (Drop Image, version 2.6.1).

Surface Analysis

X-ray photoelectron spectroscopy (XPS) analyses were conducted using a Thermo Electron Corporation K-Alpha XPS system with a microfocused monochromatic Al Kα X-ray source. The spot size of the instrument is 400 μm.

FTIR Analysis

ATR-FTIR was carried out on a Nicolet IS-50 FTIR spectrometer (Thermo Scientific), operated in the ATR mode. The spectrometer was set to collect 32 scans at 4 cm^{-1} in the range from 4000 to 700 cm^{-1}

5.3 Results and Discussion

Effect of Oxygen Plasma Activation

During the pre-hydrolysis step, alkoxide ligands of MTMS molecules are substituted with hydroxyl groups, producing the reactive monomers. The reactive monomers are subsequently consumed in condensation reactions to form dimers and oligomers. [82] When pre-hydrolyzed MTMS is coated onto the wood surface, oligomers can form hydrogen bonds with the cellulose hydroxyl groups on the wood. Finally, during drying, a permanent siloxane bond forms with loss of water. To increase the surface concentration of hydroxyl groups and enhance the adhesion between pre-hydrolyzed MTMS and wood, an oxygen plasma surface activation step was conducted.

XPS was performed to investigate changes in surface composition before and after the oxygen plasma treatment (Table 5.1). Carbon and oxygen are the only two elements detected on all samples, both before and after treatment. After oxygen plasma treatment, as expected, the O/C ratio increases significantly for both hardwood and softwood samples.

Table 5.1: XPS analysis of wood samples before and after oxygen plasma treatment

Wood sample	C%	O%	O/C
Untreated hardwood	78.7	21.3	0.27
Treated hardwood	63.4	36.5	0.58
Untreated softwood	81.7	18.3	0.22
Treated softwood	59.6	40.4	0.68

The high-resolution C1s spectra offer more detailed information about the change in surface chemistry before and after plasma treatment. Figure 5.1a shows the C1s signal originating from untreated softwood. The resolved signal shows three peaks, which correspond to carbons in three different oxidation states: C-C or C-H peak at 284.8 eV, C-O peak at 286.5 eV, and O-C-O or C=O peak at 287.8 eV. According to peak deconvolution, unoxidized carbon has the highest concentration on an untreated softwood surface (64.8%), followed by carbon with one oxygen bond (22.6%) and carbon with two oxygen bonds (12.6%). Due to oxidation of the wood surface during oxygen plasma treatment, the distribution of carbon species shifts significantly after plasma activation (Figure 5.1b): the concentrations of carbons with one and two oxygen bonds increase significantly (C-O: 47.6%; O-C-O/C=O: 25.9%). In contrast, the concentration of unoxidized carbon falls to less than half of its original value (26.5%). This change in C1s spectra indicates that wood exposed to an oxygen plasma displays more polar groups than

untreated wood. These additional polar groups can provide more binding sites for the subsequent MTMS coating process.

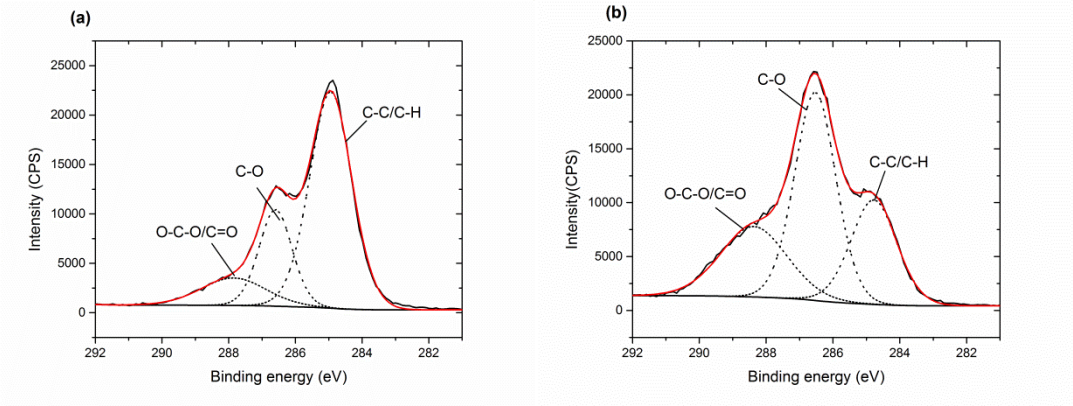

Figure 5.1: High resolution C1s spectra of a) untreated and b) oxygen plasma activated softwoods. Redline represents fitted spectra. Dotted lines represent individual deconvoluted peaks

In addition to surface chemistry modifications, long term exposure to an oxygen plasma can also increase surface roughness due to selective etching of the amorphous part of the cellulose. [179] To exclude the effects of surface roughness changes on wetting behavior, treatment time was limited to 2 minutes. To confirm that plasma activation does not modify the surface morphology, surface roughness of both hardwood and softwood were measured before and after treatment by using LSCM profilometry (Table 5.2). No statistically significant differences were observed between the various samples, which indicate that the brief plasma treatment only modifies the surface chemistry of wood samples.

Table 5.2: Arithmetic surface roughness of softwood and hardwood samples before and after oxygen plasma treatment

Samples	Arithmetic surface roughness (μm)
Untreated softwood	5.1±1.8
Plasma treated softwood	7.2±1.5
Untreated hardwood	4.7±0.4
Plasma treated hardwood	5.4±1.5

Characterization of MTMS Coated Wood Samples

After plasma treatment, both hardwood and softwood samples were coated with pre-hydrolyzed MTMS. Sonication was used during hydrolysis to enhance mixing and prevent gelation of MTMS; the process was conducted in an ice bath to remove heat generated by the exothermic hydrolysis reaction and maintain a constant temperature during the process. The hydrolysis time was maintained at 180 minutes in this study. During pre-hydrolysis, the stepwise reaction of the methoxide groups to hydroxyl groups produces the reactive monomers that are subsequently consumed in condensation reactions to form dimers and oligomers. Activated softwood and hardwood samples were then immersed in pre-hydrolyzed MTMS for 30 minutes.

To investigate changes in surface composition, XPS was performed on coated softwood and hardwood samples (Table 5.3). As expected, carbon, oxygen and silicon were the only three elements detected on all samples. Silicon was detected on both coated

softwood and hardwood samples, indicating that pre-hydrolyzed MTMS was successfully coated on wood surfaces. A high resolution XPS spectrum of C1s of coated softwood is also shown (Figure 5.2). The peak due to C-C or C-H at 284.8 eV is the primary signal detected for this sample, which is strong evidence that the polar functional groups on the activated wood surface are largely replaced by the methyl groups from the MTMS coating.

Table 5.3: XPS analysis of coated softwood and hardwood samples

	C%	O%	Si%
Coated softwood	31.7	37.6	30.7
Coated hardwood	34.3	35.7	28.9

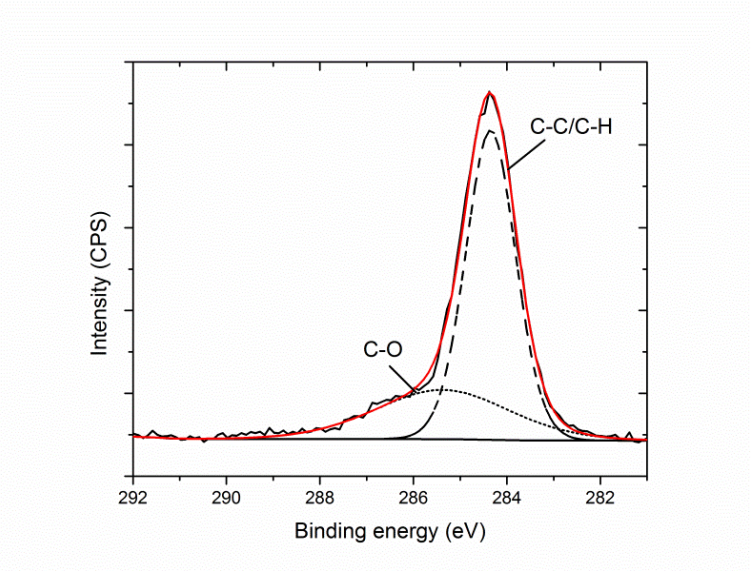

Figure 5.2: High resolution C1s spectrum of MTMS coated softwood. Redline represents fitted spectrum

To further understand the surface chemistry of MTMS coated wood samples, ATR-FTIR spectra were recorded for untreated wood samples, plasma activated wood samples and MTMS coated wood samples (Figure5.3). Because plasma treatment only modifies functional groups at the very surface of wood samples and because ATRR-FTIR is not particularly surface sensitive, the change in surface chemistry before and after plasma activation is not evident in the FTIR spectra. On the other hand, the spectra for both softwood and hardwood coated with pre-hydrolyzed MTMS show strong peaks at 1270 cm^{-1} and 760 cm^{-1}, which correspond to Si-CH_3 bonds, indicating that MTMS has been successfully grafted onto the substrate. The small peak at 890 cm^{-1} is assigned to silanol groups, which indicates that some MTMS oligomers coated on the wood were not yet fully condensed. This observation will be discussed in more detail in subsequent

sections. Due to the high concentration of hydroxyl groups on native cellulose fibers and methyl groups in lignin, all samples display peaks at 3300 cm^{-1} and 2950 cm^{-1}.

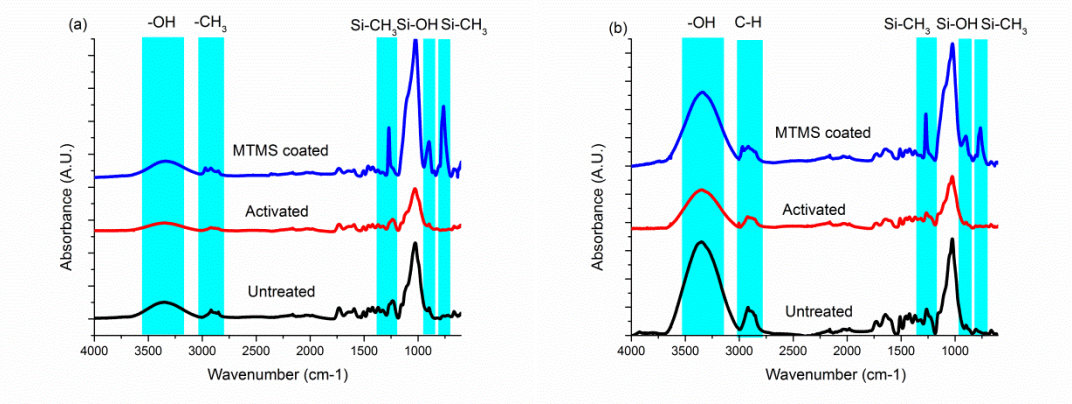

Figure 5.3: ATR-FTIR spectra of untreated, plasma activated and MTMS coated (a) hardwood (b) softwood samples

The morphology of the coated wood samples was investigated using SEM (Figure 5.4). These images indicate that the wood intrinsic roughness was not fully removed by the coating solution. Wood has a natural capacity for exchanging air and moisture with the outside environment by means of dimensional changes in response to changes in the relative humidity of the atmosphere. A suitable coating should not prevent this natural exchange with the environment. [196] To maintain the air permeability and also the visual appearance of wood veneer, any residual coating solution was removed immediately after coating by pressing the coated wood against tissue paper. At lower magnification, SEM images of both coated hardwood and softwood indicate that the wood's naturally occurring pores were not completely sealed by MTMS; the coated wood will therefore maintain at least part of its permeability. This observation is further

supported by the fact that some low surface tension fluids such as methanol can easily penetrate through the coated wood softwood and hardwood. Higher magnification images clearly reveal thin coating layers on the coated samples, which further confirms the presence of MTMS on the wood surface.

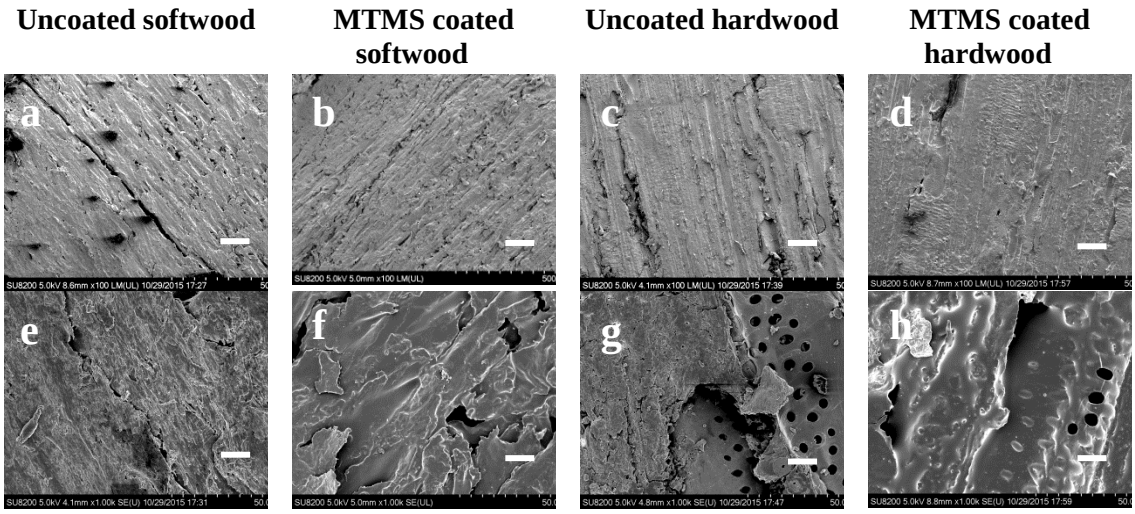

Figure 5.4: Low magnification SEM images of uncoated softwood (a), MTMS coated softwood (b), uncoated hardwood (c) and MTMS coated hardwood (d); complementary high magnification SEM images are presented in e-h. Scale bars represent 100 μm (top row) and 10 μm (bottom row).

Wetting Properties of MTMS Coated Wood

The characterization results presented above indicate that pre-hydrolyzed MTMS has been successfully coated on both softwood and hardwood. To test the wetting properties of coated wood samples, contact angles were determined for three different test fluids: water, diiodomethane and motor oil. These fluids were selected to represent a broad distribution in both surface tension and fluid polarity (Table 5.4). Untreated samples and plasma activated samples without coating were used as control samples in

this study. To highlight the importance of plasma activation, pre-hydrolyzed MTMS was also coated on inactivated wood samples following the same coating procedure (Figures 5.5 and 5.6).

As expected, untreated wood samples absorb water and oil immediately. Due to the increase in surface energy after plasma treatment, plasma activated wood samples also displays hydrophilicity and oleophilicity. For plasma activated and MTMS coated wood samples, stable water and oil contact angles were observed on both hardwood and softwood samples. This result suggests that the MTMS coating successfully imparts both hydrophobicity and oleophobicity to different wood samples. To our knowledge, this represents the first time that an amphiphobic surface has been reported on both hardwood and softwood samples without the use of fluorinated materials. The slight discrepancy in contact angle values between MTMS coated hardwood and softwood samples is probably due to the slight morphological differences between softwood and hardwood; surface topology plays a key role in wetting processes. This observation further confirms that MTMS coating does not overcoat the intrinsic wood surface structure. The intrinsic morphological heterogeneity of wood also causes relatively large standard deviations in contact angle measurements.

To determine the effect of plasma activation, contact angles of different fluids were also determined on MTMS coated wood samples without plasma activation. These samples show very different wetting behavior compared to activated samples. For both hardwood and softwood, coated samples display resistance against diiodomethane and motor oil, indicating oleophobicity; however, both samples slowly absorb water, indicating hydrophilicity. This phenomenon can be attributed to the fact that inactivated

wood samples possess insufficient surface hydroxyl groups to react with silanol groups from pre-hydrolyzed MTMS oligomers. As a result, along with methyl groups, some unreacted silanol groups from MTMS oligomers remain present on the surface. While methyl groups can impart oleophobicity to wood surfaces due to their low-surface-energy characteristics, water is very sensitive to the presence of polar silanol groups. This leads to the unique hydrophilic/oleophobic behavior of MTMS coated wood samples without plasma activation. On the other hand, for plasma activated wood samples, there are sufficient surface hydroxyl groups to react with silanol groups to form siloxane bonds. Consequently, only methyl groups are display on the coated wood surface, and these samples display both hydrophobicity and oleophobicity.

Table 5.4: Properties of different testing fluids

Testing fluid	Surface tension (mN/m)	Polarity
Water	72.8	Polar
Ethylene glycol	48.8	Polar
Motor oil	31.0	Non-polar

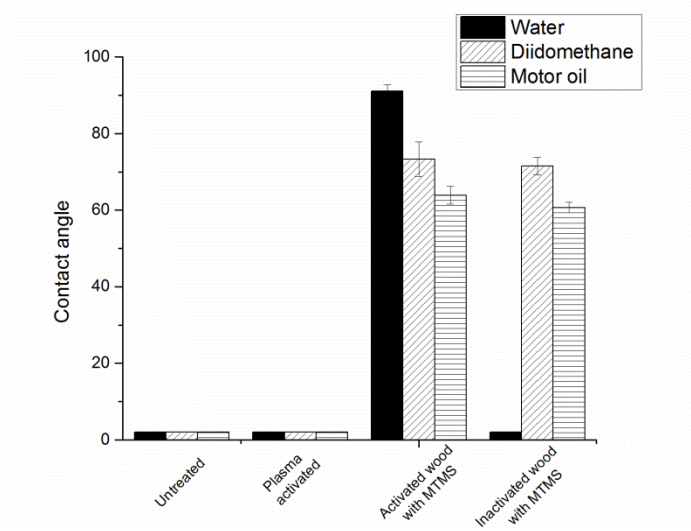

Figure 5.5: Wetting behavior of untreated softwood, plasma activated softwood, plasma activated softwood coated with pre-hydrolyzed MTMS and non-activated softwood coated with pre-hydrolyzed MTMS. For MTMS coated softwood samples, stable oil contact angles were observed for at least 12 hours, the longest duration of our continuous monitoring experiments.

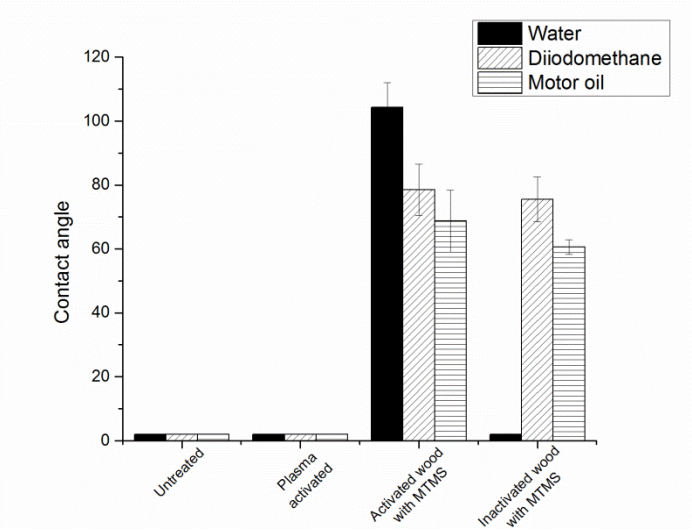

Figure 5.6: Wetting behavior of untreated hardwood, plasma activated hardwood, plasma activated hardwood coated with pre-hydrolyzed MTMS and non-activated hardwood coated with pre-hydrolyzed MTMS. For MTMS coated hardwood samples, stable oil contact angles were observed for at least 12 hours, the longest duration of our continuous monitoring experiments.

One common concern about oleophobic surfaces is the long-term resistance against fluids with low surface tension. To determine if coated wood samples can display prolonged oil resistance, a droplet of motor oil, which has a much lower surface tension than diiodomethane, was monitored over 12 hours on MTMS coated, plasma activated hardwood and softwood samples (Figure 5.7). The oil droplets were dyed with red coloring for better visual comparison; in particular, fluid absorption is difficult to detect without coloring. In these experiments, no oil stains were observed on the wood sample after 12 hours and the change in contact angle was less than 5^{o}. Although the longest in situ monitoring experiment in the goniometer lasted 12 hours, qualitative ex situ experiments have shown that droplets of motor oil can remain on MTMS coated wood samples for several months without any sign of absorption or staining.

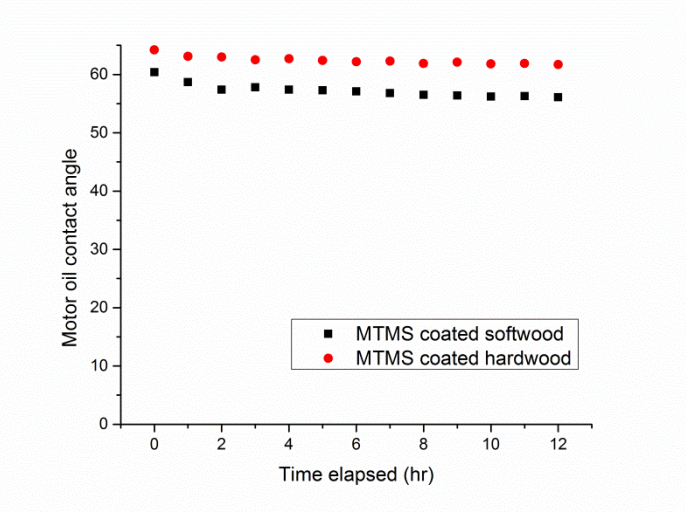

Figure5.7: Contact angle measurement of motor oil on activated hardwood and softwood samples coated with MTMS as a function of elapsed time

Effect of Pre-Hydrolysis Time

As we discussed in the previous section, pre-hydrolysis is a critical step for MTMS coating because it produces essential reactive MTMS dimers and oligomers for the subsequent grafting process by forming siloxane bonds with the hydroxyl groups on the wood surface. To examine the effect of pre-hydrolysis time on wetting properties of MTMS coated wood samples, MTMS pre-hydrolysis time was shortened to 5 minutes from 180 minutes, and then coated on both hardwood and softwood samples. All samples were plasma activated before coating in this study. Wetting properties were determined on both samples by using the same set of testing fluids (Table 5). For both hardwood and softwood, samples coated with 5 minutes pre-hydrolyzed MTMS absorbed water instantly, but displayed stable diiodomethane and motor oil contact angles, indicating that

pre-hydrolysis time has a significant effect on the wetting properties of MTMS coated wood samples.

It has been shown that the condensation reaction between MTMS dimers and oligomers is slow in acidic environments. As a result, MTMS solutions that are pre-hydrolyzed for short times contain more MTMS dimers and linear oligomers. [82] As the pre-hydrolysis time increases, MTMS dimers and linear oligomers slowly react with each other to form branched oligomers. Since MTMS dimers and linear oligomers contain more silanol groups than do branched oligomers, MTMS pre-hydrolyzed for short times has higher silanol concentration. Consequently, when applied to substrates, wood samples coated with MTMS after shorter pre-hydrolysis times have more polar silanol groups on their surface than after longer pre-hydrolysis times. The presence of polar (hydroxyl) and non-polar (methyl) groups leads to the unique hydrophilic and oleophobic behavior. A detailed discussion concerning this phenomenon can be found elsewhere for paper substrates. [82]

Table 5.5: Wetting behavior of plasma activated softwood and hardwood coated with MTMS hydrolyzed for 5 minutes

Samples	Water	Diiodomethane	Motor oil
Softwood	Absorbs	86.3±5.3°	62.4±3.8°
Hardwood	Absorbs	89.6±4.1°	63.5±4.6°

5.4 Conclusion

This study has demonstrated a facile, one-step solution coating method to fabricate amphiphobic wood, as well as wood that selectively absorbs water while repelling oil. The coating material was easily prepared by mixing pure methyltrimethoxysilane (MTMS) with 0.1 M hydrochloric acid at a 4:1 ratio, followed by sonication in an ice bath for different times. By immersing wood samples in the coating material, pre-hydrolyzed MTMS oligomers are coated onto the wood by forming siloxane bonds with surface hydroxyl groups through a condensation reaction. Because untreated wood surfaces have insufficient hydroxyl groups to react with pre-hydrolyzed MTMS, a surface activation step is required prior to the coating process; this is achieved by exposure to an oxygen plasma. The hydrophilicity of MTMS coatings can be tuned by simply adjusting the pre-hydrolysis time. Consequently, for wood samples coated with MTMS that was pre-hydrolyzed for a short amount of time, a unique selectively absorbing surface was observed: both hardwood and softwood samples absorb water but resist oil. On the other hand, MTMS with prolonged pre-hydrolysis time can be used to

impart amphiphobicity to both hardwood and softwood. After coating, both samples display hydrophobicity and prolonged resistance against oils for at least several months.

Compared with existing methods to fabricate amphiphobic wood surfaces, MTMS does not contain fluorine and the coatings are therefore more environmental friendly. The entire coating process is carried out by a solution-based method in an aqueous environment under ambient conditions. According to SEM images, the hydrophobicity and oil resistance of wood is not due to overcoating by MTMS. The porosity of native wood is largely retained after coating as indicated by the fact that low surface tension fluids such as methanol can still easily penetrate the coated wood surface. The amphiphobic wood has potential applications as packaging materials that can repel both aqueous and oily fluids. This method also has the potential to reduce wood degradation during the natural weathering process that occurs both outdoors and indoors. Further studies are underway to explore this in more detail.

CHAPTER 6

FABRICATION OF HYDROPHILIC/OLEOPHOBIC STAINLESS STEEL MESH FOR SEPARATION OF WATER/OIL MIXTURES

6.1 Introduction

The frequency of off-shore oil spillages and the emergence of fracking have raised attention to the separation of oil and water as an important environmental challenge. [47, 197] Efficient, cost-effective processes for oil-water separation are in great demand. Many technologies have been developed in this field such as oil skimmers, centrifugal water/oil separators and flocculation magnetic separation systems. [198-201] However, these methods suffer from various disadvantages such as expensive equipment, complex processing sequences and high cost.

One of the most commonly used methods to treat the oil-water mixture utilizes oil absorbent materials, because oleophilic materials can be created at lower cost and with simple processing methods. [202] Various oil absorbent materials can be used for this purpose: zeolites [203], organoclays [204], nonwoven synthetic fibers [205], or natural fibers. [206] However, the disadvantage of this approach is evident: these materials often also absorb water, thereby lowering their efficiency.[207] Furthermore, additional processing steps are required to remove the absorbed oils from these materials before they can be re-used, which makes them incompatible with continuous processing. Finally, although oil removal with absorptive materials is effective for rapidly removing the

majority of oil contamination, for example during oil spills, this approach is often insufficient to remove all contamination and generate clean water.

Hydrophobic/oleophilic membranes have been widely used for oil and water separation to overcome the limitations of absorbent materials. [208-210] Separation is based on selective oil wetting and permeation through the membrane. Compared with absorbent materials, hydrophobic/oleophilic membranes have higher separation efficiency and also improved compatibility with continuous systems. However, hydrophobic/oleophilic membranes are typically used in energy-intensive cross-flow filtration systems, because they are unsuitable for more economic, gravity-driven oil/water separation. [17] This is due to the higher density of water, causing it to settle below oil and thus be positioned in contact with the membrane, forming a barrier layer that prevents oil permeation. Another main disadvantage of hydrophobic/oleophilic membranes is that they are easily fouled by oil during separation, causing a drop in the separation efficiency, and not suitable for removal of all contaminants. [120] To solve these problems, hydrophilic/oleophobic membranes have been developed where the oil is repelled while water transports through the membrane, thus guaranteeing purity of the permeate water stream. [21, 135] Existing hydrophilic and oleophobic membranes rely heavily on fluorinated coating materials, which are often associated with significant environmental and health concerns. Also, implementation of these coating materials can be limited by rather complicated coating methods, which brings into question the economic feasibility for large-scale industrial applications. [82]

As discussed in Chapters 4 and 5, hydrophilic/oleophobic sybstrates (paper and wood, respectively) can be successfully fabricated using MTMS that was pre-hydrolyzed

for a short period of time. [82] However, the heterogeneous surface morphology and low mechanical strength of cellulose-based paper limits the utility of this material for oil/water separation applications. Due to the excellent mechanical strength and chemical resistance, coated stainless steel meshes are frequently used for oil and water separation. [211, 212] By reacting with the hydroxyl group from surface oxide layer, pre-hydrolyzed MTMS can be used to impart hydrophilicity/oleophobicity to stainless steel.

In this Chapter, a process to generate hydrophilic/oleophobic stainless steel meshes by a simple immersion coating method using pre-hydrolyzed MTMS is described. By using three stainless steel meshes with different geometric parameters, stainless steel mesh with high selectivity between water and oil has been fabricated. The hydrophilic/oleophobic stainless steel mesh can be used to separate motor oil/water mixtures with high efficiency. Compared with existing methods, MTMS coated stainless steel mesh offers a more scalable, economic and environmental benign approach to the separation of water and oil mixture.

6.2 Experimental

Materials

Stainless steel 316 plates (20 cm x 30 cm x 0.05 cm) were purchased from Maudlin Products and cut into samples with a dimension of 2.5 cm x 1.5 cm x 0.05 cm using a waterjet cutter. SS meshes 100 x 100, 200 x 200 and 400 x 400 were purchased from McMaster. Geometric parameters of different SS meshes were shown in Table 6.1. SS meshes were cut into 1.5 cm x 1.5 cm squares or circular disks with a diameter of 2 cm before treatment Methyltrimethoxysilane (MTMS) was used as received from Sigma-

Aldrich (deposition grade, ≥ 98%). Hydrochloric acid (HCl) was obtained from Fisher Chemicals. Acetone, methanol and isopropanol (BDH, ACS grade, 99%) were purchased from Sigma-Aldrich without further purification.

Table 6.1: Geometric parameters of SS mesh 100, 200 and 400. Opening size (L) is the distance between two adjacent wires.

Mesh	Wire diameter (D) (mm)	Opening size (L) (mm)
100	0.11	0.14
200	0.05	0.07
400	0.02	0.04

MTMS Hydrolysis Procedure

Hydrolysis of MTMS was performed by mixing MTMS with 0.1 M hydrochloric acid in a 4:1 v/v ratio. [82] The mixture was then sonicated in an ice-bath for different lengths of time to induce hydrolysis. Sonication was carried out using a Fisher Scientific ultrasonic cleaner (model FS 20) at a power of 70 W and frequency of 42 kHz.

MTMS Coating Procedure

Stainless steel plates and meshes were rinsed with acetone, methanol, isopropanol and then dried using nitrogen gas. Cleaned stainless substrates were immersed in the hydrolyzed MTMS solutions for 2 minutes. After coating, excess liquid was removed from the surface by touching the liquid with a piece of tissue paper (Kimwipe, Kimberly-Clark). Coated stainless steel samples were then dried at ambient conditions overnight.

SEM Imaging

Scanning electron microscopy (SEM) images were taken with a Hitachi SU8230 SEM at an acceleration voltage of 5.0 keV.

Contact Angle Measurement

All static contact angle measurements were performed by using a Rame-hart automated goniometer (model 290). A 4 μL droplet of the selected fluid (DI water, diiodomethane (Sigma-Aldrich, reagent plus grade, 99%) and motor oil (SAE 10W-30, MotoTech)) was placed onto MTMS coated substrate. For better visual comparison, motor oil was dyed with Oil Red O (Sigma-Aldrich). Contact angles were determined by the droplet images by the standard goniometer software (Drop Image, version 2. 6. 1).

Oil/water Separation Experiment

The oil/water separation experiment was performed by using a filter holder (VWR) and MTMS coated stainless steel mesh. The oil wand water mixture was created by mixing 1 mL of water with 1 mL of motor oil. Motor oil was dyed with Red O (Sigma-Aldrich) for better visual comparison.

6.3 Results and Discussion

Wetting Properties of MTMS Coated Stainless Steel Plate (SS plate)

It is well-known that a pre-hydrolysis step is required before MTMS can be chemically bonded to substrates with hydroxyl groups, and the length of pre-hydrolysis time can significantly affect the wetting behavior of MTMS coated surfaces. [23] In this study, SS plates were coated with MTMS solutions prepared at two different hydrolysis

times: 5 and 180 min. Pre-hydrolyzed MTMS was applied to cleaned SS plates following a simple immersion-coating method. A SS plate was chosen as the initial model substrate for this study because it has a well-defined, flat surface; effects of surface roughness and porosity of the underlying substrate on wetting properties can therefore be excluded. To determine if the pre-hydrolyzed MTMS has been successfully coated on the SS plate, water, diiodomethane and motor oil contact angles were determined on all MTMS coated samples. The wetting property of an uncoated SS plate was determined for comparison (Table 6.1). Uncoated SS plates display a somewhat hydrophobic surface with low diiodomethane and motor oil contact angles. On the other hand, a SS plate coated with 5 min hydrolyzed MTMS is strongly hydrophilic with a water contact angle less than 5°. Compared with the uncoated SS plate, it also displays much higher diiodomethane and motor oil contact angles. The significant change in wetting behavior is a strong indicator that pre-hydrolyzed MTMS has been coated successfully on the SS plate. The SS plate coated with 180 min hydrolyzed MTMS has similar diiodomethane and motor oil contact angles to 5 min hydrolyzed MTMS. The major difference between the two samples is water contact angle: A SS plate coated with 180 min hydrolyzed MTMS displays a much higher water contact angle than does a SS plate coated with 5 min hydrolyzed MTMS. This behavior was previously observed on MTMS coated silicon wafers: the water wetting property of MTMS coating can be tuned from hydrophilic to hydrophobic by adjusting the hydrolysis time, while the oleophobicity is maintained at all conditions. The detailed mechanisms can be found in Chapter 4. [24]

Table 6.2: Wetting properties of uncoated and MTMS coated stainless steel plates. The standard deviations of all measurements are below 5°

Sample	Water	Diiodomethane	Motor oil
Untreated	87.9°	43.1°	22.0°
5 min hydrolyzed MTMS	<5°	73.3°	65.9°
180 min hydrolyzed MTMS	76.6°	79.0°	69.4°

Wetting Properties of MTMS Coated Stainless Steel Mesh (SS mesh)

Results from previous section indicate that MTMS pre-hydrolyzed for 5 min can be used to impart hydrophilicity/oleophobicity to stainless steel-based substrates. This unique property can be utilized to separate water and oil mixtures. To realize this aim, SS mesh was used as the substrate in this study. To determine if the SS meshes coated with 5 min pre-hydrolyzed MTMS could have sufficient selectivity for this application, theoretical contact angles were first calculated on SS meshes with different porosities. (Table 6.1).

Due to the intrinsic micron-scale roughness of SS mesh, the apparent oil contact angles measured on coated SS mesh will be different from the contact angle measured on coated SS plate. The apparent contact angles on coated SS meshes can be calculated by the modified Cassie-Baxter equation (1): [20]

$$\cos\theta_{app} = \frac{D(\pi-\theta_e)}{L}\cdot\cos\theta_e + \frac{D}{L}\cdot\sin\theta_e - 1 \quad (1)$$

This equation demonstrates that the apparent contact angle (θ_{app}) is a function of the center-to-center distance between two SS wires (L), the wire diameter (D) and the equilibrium contact angle (θ_e). In this study, contact angles measured on coated SS plates were used as equilibrium contact angles. Based on this equation, apparent contact angles of different fluids on SS meshes were calculated (Figure 6.1a). The equation predicts a high selectivity between water and oil for all three meshes: all coated meshes should display extreme hydrophilicity, while also displaying strong oil repellency. Due to the additional micron-scale roughness from SS meshes, the predicted apparent oil contact angles on all three SS meshes are greater than 100^{o}, which are much higher than oil contact angles measured on the SS plate. According to the Cassie-Baxter model, Mesh 400 is predicted to display slightly higher oil contact angles than the other two meshes, but the difference is not very significant.

Calculations indicate that all three MTMS coated SS meshes should have good oil/water selectivity. To verify this prediction, SS mesh 100, 200 and 400 were coated with 5 min pre-hydrolyzed MTMS. Water, diiodomethane and motor oil contact angles were determined for these coated meshes (Figure 6.1b). Coated mesh 200 and mesh 400 display good selectivity between water and oil, as predicted by the modified Cassie-Baxter equation. However, for coated SS mesh 100, an unstable motor oil contact angle was observed. This is likely due to the fact that mesh 100 has the largest wire-wire spacing among the SS meshes. Previous work reported that the micron-scale structure with large spacing will be unable to suspend the liquid, and therefore cannot support a composite interface as required by the Cassie-Baxter model. [213] Furthermore, although water can easily pass through both coated mesh 200 and 400, permeation of water

droplets was delayed for about 15 sec on mesh 400; on mesh 200, the water passed though the mesh almost instantaneously. As a result, coated mesh 200 has a slightly better selectivity compared to mesh 400. Therefore, SS mesh 200 coated with 5 min pre-hydrolyzed MTMS was used for the following oil/water separation study. The delayed permeation of water droplets on mesh 400 is most likely due to its lower porosity compared to mesh 200. However, a further study is required to fully understand this phenomenon.

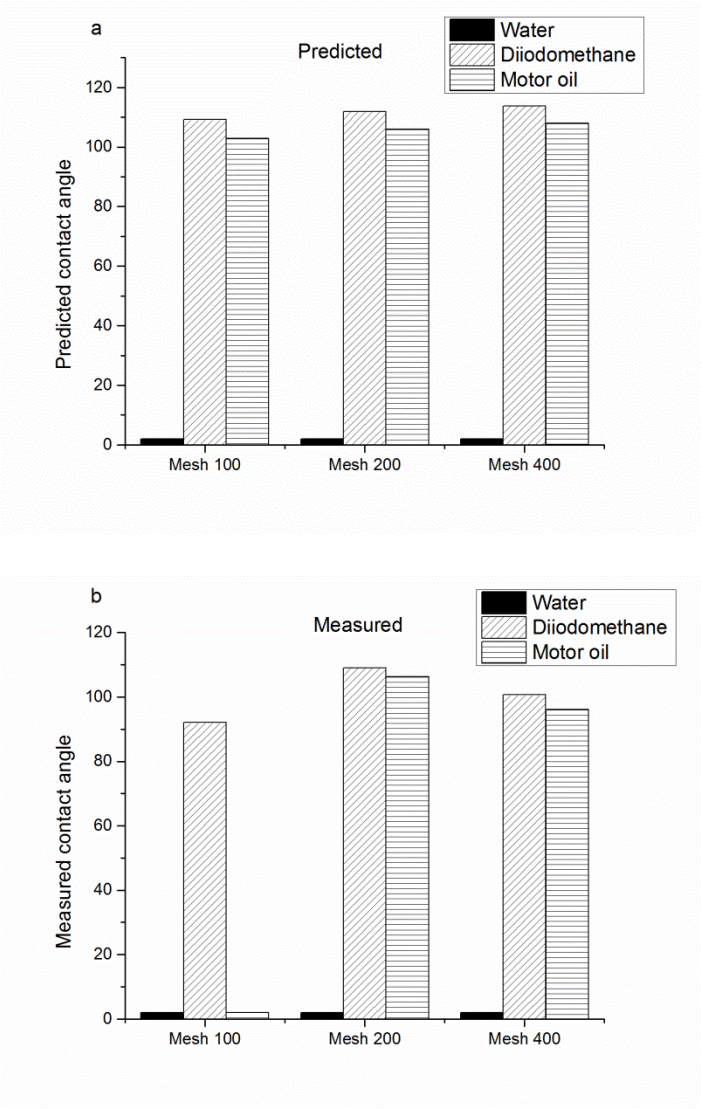

Figure 6.1: a) Predicted and b) measured wetting behavior of different SS meshes coated with 5 min pre-hydrolyzed MTMS

Oil and Water Mixture Separation Experiment

A filtration apparatus was used for oil/water separation experiments. SS mesh 200 coated with 5 min pre-hydrolyzed MTMS was placed between a glass filter holder and a glass funnel. Two PTFE O-rings were placed below and above the coated SS mesh to establish an effective seal. The unit was then clamped together to minimize fluid leakage (Figure 6.3a). In order to test the sealing integrity of this configuration, pure motor oil (dyed with red color) was introduced. For a moderate amount of motor oil, the system worked well; the motor oil remained on the top part of the setup without leakage for at least 10 minutes (figure 3b). However, with larger oil volume, the motor oil starts to leak from the edges of the metal mesh into the filtrate due to the increased pressure head. Future improvements are needed to prevent the fluid leaks

To demonstrate the capability of MTMS coated SS mesh to separate oil and water, the mixture of water and oil was poured into the separation apparatus. The mixture was created by mixing 2 mL of water and 2 mL of motor oil (dyed with red color). Due to the good selectivity between water and oil, water passed through the coated SS mesh freely while the oil was blocked on the top part of the unit. Water in the filtrate was colorless and visually did not contain dyed motor oil, indicating good separation efficiency.

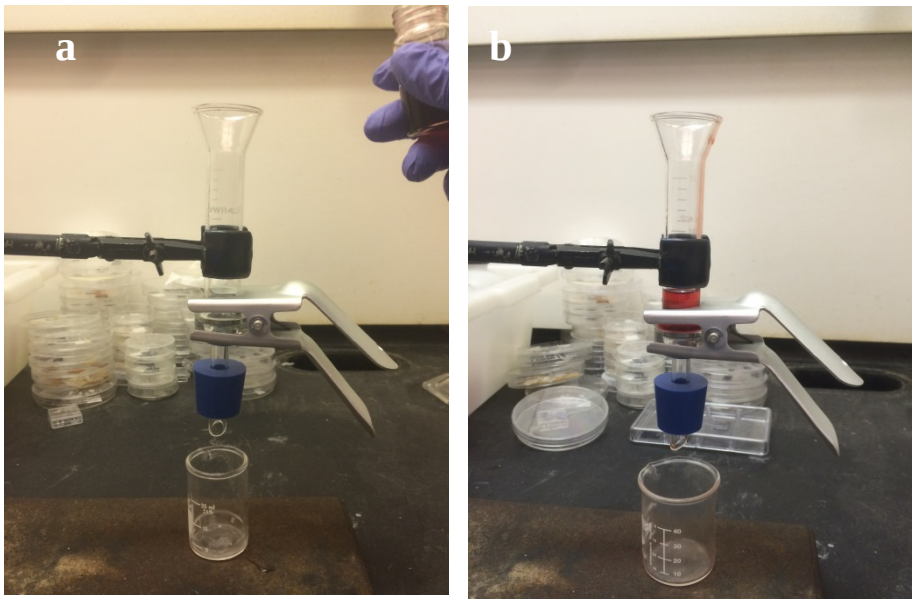

Figure 6.2: a) Apparatus for water/motor oil separation experiments. Coated SS mesh 200 was inserted between the filter holder and the glass funnel. b) Pure motor oil (dyed red) was poured into the separation unit. The strong oil repellency of the MTMS coating prevents motor oil from penetrating through the SS mesh 200.

6.4 Conclusions

Stainless steel mesh with hydrophilic/oleophobic wetting properties was successfully fabricated with a facile, one-step coating method using non-fluorinated coating material. The coating material was prepared by mixing pure methyltrimethoxysilane (MTMS) with 0.1 M hydrochloric acid at a 4:1 ratio, followed by sonication in an ice bath. The hydrophilicity of MTMS coatings can be tuned by adjusting pre-hydrolysis time. For a short pre-hydrolysis time, coated stainless steel meshes display extreme hydrophilicity with high resistance against motor oil and diiodomethane. The wetting property is also related to the porosity of metal meshes

according to modified Cassie-Baxter equation. Metal meshes with larger openings display unstable oil contact angles, while the metal meshes with smaller openings can resist oils for a prolonged period of time.

Stainless metal meshes coated with MTMS pre-hydrolyzed for a short amount of time displays good oil/water selectivity. As a result, coated metal meshes can be used to separate oil/water mixtures with high efficiency. Compared with existing approaches to separate water/oil mixtures based on selective water permeation, pre-hydrolyzed MTMS does not contain fluorine and is therefore more environmental friendly. The MTMS coating process is carried out in an aqueous environment under ambient conditions at a relatively fast rate, which offers compatibility with current industrial manufacturing processes. The application of hydrophilic/oleophobic metal meshes can also potentially extend to separation of oil/water emulsions. However, improved sealing in the separation apparatus is required prior to further experiments to establish quantitative separation efficiency.

CHAPTER 7

CONCLUSIONS AND FUTURE WORK

Paper with controlled wetting properties has attracted much attention recently due to potential applications in novel fields such as biomedical test strips or oil/water separation membranes. As a result, a variety of technologies have been developed to fabricate paper with different wetting properties. However, hurdles remain; most of the existing methods heavily rely on low surface energy, fluorinated coating materials, which can cause severe environmental and health issues. To resolve this problem, this thesis focuses on developing new methods to fabricate paper with different wetting properties by treatment with non-fluorinated chemicals.

A novel method to fabricate amphiphobic paper using a low non-fluorinated polymer, polybenzoxazine (PBZ) was developed. Despite the present of hydroxyl groups in its structure, PBZ is reported to have a surface energy close to many fluorinated materials. One explanation to this seemingly contradictory observation is that the hydroxyl groups on PBZ have the ability to form intramolecular bonds with neighboring nitrogen atoms. This strong intramolecular bonding imposes an internal structure on the molecule. As a result, hydrogen bonding is protected on the inside of the structure while the hydrocarbon side chains are exposed to the surface and lower the surface energy. To apply PBZ onto paper surfaces, paper was first coated with benzoxazine monomer by using either a dip coating or drop casting method. The coated paper was then cured at high temperature to initiate the polymerization process. The coated paper successfully displayed amphiphobicity after curing at 180^{o}C for 12 hours. On the other hand, the

disadvantages of this method are also obvious: the high loading amount and prolonged curing time limits the economical feasibility of this process. Furthermore, treated paper loses flexibility due to the high curing temperature. In spite of these drawbacks, this study revealed that hydrocarbon materials without fluorinated moieties can indeed be applied as coatings to cellulose-based paper surfaces to impart hydrophobicity and oleophobicity; these observations thus formed the foundation of this thesis.

To further investigate the wetting properties of paper coated with non-fluorinated coatings, alkyltrichlorosilanes were applied to paper surfaces. Compared with PBZ coatings, which require high temperature curing, the entire coating process of alkyltrichlorosilanes was carried out via a solution-based method under ambient conditions. As a result, this process is more compatible with current large-scale paper manufacturing processes.

The effect of alkyl chain length on the wetting properties of alkyltrichlorosilane coated cellulose-based paper was reported for four different reagents: methyltrichlorosilane (MTCS; $-CH_3$), butyltrichlorosilane (BTCS; $-C_4H_9$), dodecyltrichlorosilane (DTCS; $-C_{12}H_{25}$) and octadecyltrichlorosilane (OTCS; $-C_{18}H_{37}$). SEM analysis reveals that by systematically varying alkyl chain length, films with different surface morphologies can be generated on flat silicon wafer control samples and on cellulose-based paper samples. The variation in surface morphology leads to different wetting behavior, as determined by measuring static water and oil contact angles. Due to the nano- and micron- scale roughness on MTCS coated substrates, paper samples coated with MTCS displayed superhydrophobicity with a water contact angle of 152.2^{o}, which was the highest water contact angle among these four alkyltrichlorosilanes. However,

additional nano-scale roughness from the MTCS coating reduces the oil resistance of coated paper samples, while paper samples coated with long-chain alkyltrichlorosilanes have lower surface energy and also lack nano-scale roughness. As a result, paper samples coated with OTCS displayed the highest resistance against oils (ethylene glycol contact angle, 125.5^{o}; diiodomethane contact angle, 101.3^{o}).

Although alkyltrichlorosilane coated paper can display resistance to some low surface tension fluids (*e.g.*, ethylene glycol and diiodomethane, it cannot repel oils with even lower surface tension such as motor oil. To further increase the oleophobicity of coated paper, methyltrimethoxysilane (MTMS) was used as the coating material. To overcome the relatively low reactivity of methoxy groups, a pre-hydrolysis step is required before MTMS can be chemically bonded to paper surfaces. Pre-hydrolyzed MTMS was subsequently coated on paper using a solution-based protocol similar to the alkyltrichlorosilane coating process. By systematically changing the MTMS hydrolysis time prior to coating, different degrees of condensation were achieved, which provides control over the paper surface chemistry. Paper coated with these different MTMS precursor samples displayed water wetting behavior ranging from superhydrophilic (absorbs water immediately) to hydrophobic, while oleophobicity was maintained under all conditions. For all MTMS coated paper samples, no absorption of motor oil was observed for several weeks, indicating stable oil resistance. These results indicate that MTMS can be employed to functionalize other hydroxyl-group-rich surfaces such as wood and metal.

Amphiphobic wood was successfully fabricated by using MTMS pre-hydrolyzed for prolonged times. Unlike paper, which is almost entirely composed of cellulose, wood

contains many other substances. As a result, the concentration of hydroxyl groups on wood surfaces is much lower than on paper, which leads to a less efficient coating process for MTMS. To resolve this issue, wood samples were pre-treated with a cold oxygen plasma before coating in order to activate the surface. After plasma treatment, wood samples were coated with pre-hydrolyzed MTMS. For both hardwood and softwood, coated samples displayed hydrophobicity and prolonged resistance against oils. The amphiphobic wood has potential applications as construction materials that can repel both aqueous and oily fluids. This method also has the potential to reduce wood degradation during the natural weathering process that occurs both outdoors and indoors.

Finally, hydrophilic/oleophobic stainless steel meshes were fabricated by employing MTMS. The wetting properties of coated stainless steel mesh were highly dependent on the porosity of metal meshes, as predicted by the modified Cassie-Baxter equation. With the correct porosity, stainless steel mesh coated with MTMS pre-hydrolyzed for short times displayed good oil/water selectivity, and could be used to separate oil/water mixtures with high efficiency.

7.1 Future Work and Recommendations

While significant work has been completed to functionalize paper substrates and create surfaces with different wetting properties by treatment with non-fluorinated chemicals, this thesis also provides inspiration and direction for future work.

Although the amphiphobic paper created in this study using pre-hydrolyzed MTMS as a coating material displayed strong resistance towards motor oil, it cannot resist fluids with even lower surface tensions, such as *n*-hexadecane. To create paper with

enhanced amphiphobicity using non-fluorinated coating materials, two approaches can be considered: the paper can be coated with non-fluorinated materials with even lower surface energy, or the surface morphology of paper substrates can be modified to increase the apparent contact angle. In this thesis, Chapter 3 has shown that the alkyl chain length can have a significant effect on the wetting behavior of paper coated with alkyltrichlorosilane: alkyltrichlorosilanes with longer alkyl chains display a lower surface energy and higher resistance towards fluids with lower surface tensions. In principle, this trend can be further extended to trimethoxysilane, in that a trimethoxysilane with longer alkyl chains can display even lower surface energy compared to MTMS. However, alkyl silanes with longer hydrocarbon chains are also often associated with reduced reactivity, which may lead to longer coating time and less surface coverage. As a result, a more systematic study is required before any conclusions can be reached. For the latter approach, it has been long known to our research group that oxygen plasmas can selectively etch away the amorphous part of cellulose, thereby increasing the surface roughness of paper substrates and hence the apparent contact angle. [20] Most of these studies were conducted using fluorinated coating materials, which have lower surface energy than MTMS. It is still unclear if plasma etching can promote the oil resistance of paper treated with non-fluorinated chemicals. More detailed research can be conducted to investigate the effect of etching on the oil repellency of MTMS coated paper. It is also important to mention that the current immersion-coating processes present challenges in maintaining the nano-scale roughness created by etching due to the thicker coating layer. New coating techniques may be required to preserve the roughness after coating.

As discussed, the process of fabricating amphiphobic paper by treatment with MTMS can be further improved by using different coating methods. Although the current immersion coating method is straightforward, it requires a second step to remove the excess coating material, which creates waste, and therefore is not very attractive economically. Alternatively, a spray coating technique can be developed to apply the pre-hydrolyzed MTMS to paper substrates, which enables improved loading control. Spray coating is also appropriate for the paper industry, because it can be easily integrated into current manufacturing process.

Additionally, the amphiphobic wood studies detailed in Chapter 5 may have the potential to reduce wood degradation both outdoors and indoors. Some preliminary experiments have already indicated that in a natural environment, MTMS coated amphiphobic wood may have lower degradation rates than uncoated wood. However, a detailed, quantitative investigation is still required to establish the degradation rate of coated and uncoated wood under a controlled environment to confirm this conclusion.

The work conducted using MTMS to create hydrophilic/oleophobic stainless steel mesh also has a promising future. The hydrophilic/oleophobic mesh has the potential to separate oil/water emulsions, which has applications in fields such as waste water treatment. However, more investigations are required before the hydrophilic/oleophobic mesh can be put into practical use. First of all, it is still unclear whether or not the surfactant can interfere with the surface chemistry of MTMS. Therefore, the stability of MTMS coated SS meshes should be tested with different surfactants. The separation of water/oil emulsions is also highly dependent on the oil droplet size: if the oil droplet size is too small, current micrometer meshes will not be suitable. Membranes with smaller

pore size may be required in this scenario. Furthermore, the pH of the oil/water mixtures or emulsions can also be adjusted to study the long- term stability of hydrophilic/oleophobic metal meshes in harsh chemical environments.

APPENDIX A

CELLULOSE-BASED MATERIALS: PLASMA MODIFICATION

This Appendix has been accepted for publication: Z.Tang, V. Breedveld and D. W. Hess, Chapter in *Encyclopedia of Plasma Technology*, to be published in 2016

In this Chapter, we describe the plasma-assisted modification of cellulose to achieve desired, but non-traditional properties. Modification takes place due to three processes that can occur as a result of plasma exposure using specific gases or vapors: (1) modification of the surface structure and properties of cellulose-based materials due to ion, electron and photon impingement; (2) generation of free radicals for molecular grafting and cross-linking; (3) plasma enhanced chemical vapor deposition (PECVD) to form thin films. For clarity and organizational purposes, these three processes are treated separately and discussed in different sections, which highlight the plasma conditions that are invoked to generate specific effects on cellulose-based substrates and mechanistic considerations for each process. However, it is important to recognize that these processes do not occur independently. Rather, due to the complexity and highly reactive nature of plasmas, these processes often occur simultaneously and synergistically. For example, surface modification is always accompanied by radical generation and PECVD often causes surface etching. Nevertheless, control of process/plasma parameters typically allows the establishment of a dominant mechanism, e.g., etching vs. polymerization vs. grafting. Therefore, this review considers primarily the dominant

processes for particular applications, but also points out the various effects that contribute to the final material properties.

A.1 Background

Cellulose is the most abundant organic polymer on earth.[214, 215] It is the major component of wood, cotton, hemp and jute. Cellulose is a linear condensation polymer consisting of D-glucose units joined together by β-1,4-glycosidic bonds (Figure A.1). [216] Each glucose unit has three hydroxyl groups; these groups form inter-and intra-molecular hydrogen bonds, which give strength to cellulose-based material and establish hydrophilic character. [217] Compared with synthetic polymers, cellulose has a number of advantages, including low density, low cost, high tensile strength and bio-renewability, which make cellulose environmentally friendly. [218-221] Due to these unique properties, there has been a growing interest to extend the range of cellulose applications by modifying its properties, for example through plasma treatment.

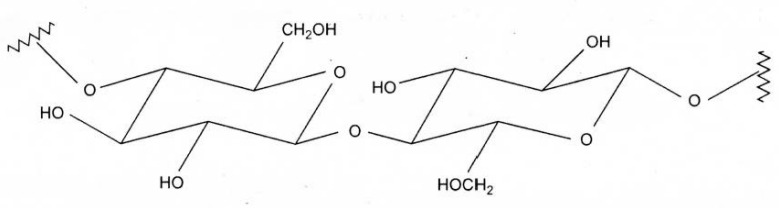

Figure A.1: Molecular structure of cellulose

Cellulose fibers are more chemically inhomogeneous than man-made fibers. In fact, cellulose is never found naturally in its pure form. Cotton fibers are probably the purest natural source; cotton seldom contains more than ~5% of other substances, including absorbed water. More commonly, in wood, plant stalks, and leaves, cellulose is associated with other substances such as lignin and hemicellulose, both in considerable amounts. [24] In the pulping industry, chemical processes are commonly applied to increase the concentration of cellulose by dissolving impurities with a strong base. As a result, paper is usually composed of cellulose fibers with high purity.

Plasmas that are used for thin film processing and surface modification are partially ionized gases that consist of electrons, negatively and positively charged particles, and neutral atoms and molecules in ground and excited states. [222, 223] Compared with conventional (thermal) chemical processes, plasma modification of cellulose offers numerous advantages. The short penetration depth of ions and electrons that impinge on surfaces limits modification to the surface region (normally <10 nm under low plasma power conditions) while leaving bulk properties of cellulose unchanged. [224] However, it should be noted that photons can penetrate polymeric materials and cause bond breaking within the bulk cellulose material. In addition, long-lived reactive neutral moieties (radicals) can diffuse into the fiber network and cause chemical modification of the cellulose structure beneath the surface layer. Plasma treatment does not require large amounts of water or solvents, and is therefore considered more economical and environmentally friendly relative to solution processing. [225] Plasma processes are also versatile in that selection of the appropriate gases can result in material etching, film deposition, or chemical bond alteration. Moreover, plasma

treatments can be used to treat large substrates (widths up to several meters, and even roll-to-roll processing), which offers high throughput process opportunities for industrial applications. The low temperature (non-thermal) plasmas used for thin film processes are particularly useful for cellulose modification because of the inherent heat sensitivity of cellulose-based materials. Due to the wide variety of chemical processes that potentially occur in a plasma, cellulosic materials can be modified or treated to achieve a range of functionalities, including surface cleaning, free-radical grafting, wettability enhancement, improved compatibility with other hydrophobic polymers, and establishment of hydrophobicity/oleophobicity. It is important to realize that plasma treatment of cellulose can affect the surface chemistry well after direct exposure has been terminated. Like other organic polymers [226], cellulose-based materials can trap free radicals that are generated during plasma exposure. These plasma generated free radicals are highly reactive; upon exposure to air (oxygen and water vapor) they oxidize and hydrolyze, thereby forming oxygenated chemical moieties that can alter the chemical and physical properties of cellulose.

A.2 Plasma Induced Surface Modification

Plasmas are used to modify the surface chemistry and morphology of cellulose-based materials by invoking non-polymerizable gases such as noble gases [227] , nitrogen [228], hydrogen [229] and oxygen [230]. These non-polymerizable gases can be further divided into two categories: non-reactive gases like argon, and reactive gases such as oxygen.

Although the energetic species created in a non-reactive plasma by their nature cannot react directly with the substrate surface, they do impart kinetic energy to the surface atoms and molecules. During this momentum transfer, the impinging ions may break chemical bonds, thereby producing low molecular weight fragments that are intrinsically volatile.[231] Thus, plasmas generated using non-reactive gases can etch or ablate cellulose-based materials.[232] Due to the ability of polymeric or cellulosic materials to trap or stabilize free radicals, polar groups (e.g., hydroxyl-, ether-, and ketone-moieties) may also form as a result of exposure of the treated samples to air. [227] In contrast, reactive gas plasmas interact with cellulosic substrates in a different manner. The reactive ions, atoms, and molecular fragments readily react with surface atoms/molecules to generate volatile products and thereby remove or etch material. Moreover, reactive plasmas can also cause chemical modification of the substrate through direct incorporation of polar groups on the surface. [233]

One application of plasma-induced surface modification is to enhance the wettability of cellulose-based materials, for example to increase the dyeability or printability of cotton and paper. [229, 234] This effect can be achieved by either chemical or physical modification. In the case of physical modification, wettability can be increased by simply increasing the porosity and pore sizes of the substrate via etching (ablation), or by removing weakly attached hydrophobic impurities from the fiber surface, which may be accomplished using either a reactive plasma or a non-reactive plasma. [235, 236] Specifically for the case of chemical (reactive) modification, substrate wettability is increased by the introduction of water compatible functional groups onto the cellulose surface; these moieties include –COOH, -OH and $–NH_2$,

depending upon the feed gas used. [237, 238] Although the most common way to determine wettability is through contact angle measurements, in many cases it is not possible to evaluate wettability directly from contact angle data due to the irregular surface structure of cellulose-based materials such as paper substrates and cotton yarns. Therefore, the wettability is often determined indirectly through measurements of liquid absorption time and wicking height. Wicking height is measured by suspending a small piece of fabric vertically above the liquid surface such that the horizontal bottom edge is immersed just below the surface of the liquid. Spontaneous upward wicking then occurs due to capillary forces that are a function of the surface energy. The height of the liquid rise above the reservoir level after a certain time interval is then recorded as a measure of wettability. [237] The liquid often contains a dye to enhance the contrast between wetted and non-wetted regions of the fabric.

Argon is one of the most frequently used non-reactive plasmas to modify surface properties of cellulose-based materials such as cotton, jute and paper. In most cases, argon plasmas are created in a low pressure environment, [227, 232, 235, 239] but it is also possible to generate an argon plasma at atmospheric pressure using dielectric-barrier-discharges (DBD). [240] In all cases, dramatic changes in the surface morphology of cellulose have been identified via scanning electron microscopy (SEM) imaging. The smooth surface of cellulose fibers becomes roughened and fragmented after only one minute of plasma exposure [240]; prolonged treatment time causes further degradation/modification of the fiber structure. Kolarova et al.[232] quantified this morphological change by measuring the fiber width before and after treatment with confocal microscopy. After only 10 s of exposure, the fiber width dropped from ~13.5

μm to ~8.8 μm. The significant change in morphology clearly indicated that argon plasmas are capable of etching cellulose-based materials at significant rates. However, the surface chemistry was also changed, as indicated by X-ray photoelectron spectroscopy (XPS). Sahin [227] reported a decrease in oxygen/carbon atomic ratio (O/C) with increasing plasma exposure time and power on bleached kraft paper. The untreated paper had an O/C ratio of 0.85, which agreed well with the value for untreated cellulose. After argon plasma exposure for 10 minutes at 500 W, the O/C ratio quickly dropped to 0.57. This result is likely due to the generation of oxygen rich volatile species such as carbon dioxide during the treatment or due to desorption of water from the substrate. Analysis of the carbon C_{1s} XPS spectrum indicated that small concentrations of polar groups such as carboxylate were also found on treated samples. These new functional groups, which did not exist on untreated samples, were believed to be formed by the reaction of long-lived free radicals with air (oxygen or water vapor) after plasma treatment. In contrast, Kokarova et al. [232] reported an increase in O/C ratio for cotton after argon plasma exposure. However, natural cotton fibers are not pure cellulose. Impurities such as pectins and waxes also adhere to the surface of cotton fibers; the presence of these impurities was confirmed by XPS data. The O/C ratio for untreated cotton was 0.33, far below the theoretical value of pure cellulose (0.83). This seemingly contradictory observation (relative to the paper study) can be explained by the removal of carbon-rich impurities from the fiber surface due to argon plasma etching. In general, argon plasma treatment of a pure cellulose substrate results in substantial etching, a decrease in O/C ratio and very limited ability to add polar groups to the substrate surface.

The use of readily accessible air as a plasma gas source primarily applies to atmospheric pressure plasmas such as corona discharges or dielectric-barrier-discharges (DBD), [234, 241-243] although it can also be used as a processing gas in low pressure plasmas. [244, 245] The primary application of air plasma exposure for cellulose-based materials is to enhance wettability. Atmospheric pressure plasmas do not require a vacuum system and are therefore somewhat simpler in design. However, they require large (~10 L/minute) inert gas flows, usually He. In addition, atmospheric pressure plasmas are readily configured for continuous processes, although low pressure plasmas are also amenable to such approaches. Karahan et al. [234] studied the wetting behavior of cotton fibers treated with air plasmas at atmospheric pressure using a DBD system. The water contact angle of cotton fabric dropped from 108^{o} on the untreated substrate to 0^{0}, which indicates complete wetting, in less than 40 seconds. XPS analyses also showed a large increase in O/C ratio from 0.208 to 0.364 after the treatment. To investigate the mechanism of the O/C ratio, Ward et al. [246] conducted similar studies on cotton using an air plasma at low pressure. Multiple internal reflectance infrared spectra on the cotton indicated the presence of carbonyl groups after plasma treatment, which confirms that the increase in O/C ratio is at least in part due to incorporation of polar groups as a result of oxygen and water vapor contained in air.

The most extensively used reactive plasma for modification of cellulose-based materials is an oxygen plasma. Oxygen plasmas have been used primarily to enhance substrate wettability, [229, 247-249] but can also be used to generate desired surface structures. [37] Carlsson et al. [229] reported the treatment of filter paper using oxygen plasmas at low pressure. Compared with other cellulose-based materials, filter paper is a

relatively “clean” material, which is usually made of pure cellulose fibers; indeed, XPS confirmed that filter paper has an O/C ratio near that of pure cellulose. Carlsson et al. found that despite the high substrate purity, the O/C ratio increased slightly from 0.75 to 0.83 after plasma treatment, which clearly indicated the incorporation of oxygenated species onto the substrate surface. Compared with an argon plasma, the oxygen plasma showed a much enhanced ability to oxidize the surface. Wong et al. [248] performed a more comprehensive comparison between argon and oxygen plasmas with respect to both chemical and physical modifications of linen fibers. The chemical composition on the surface of linen fibers was characterized before and after the treatment using XPS. Higher degrees of incorporation of polar groups were detected with oxygen plasmas than with argon plasmas. It was also found that oxygen plasma produced a much faster weight loss rate than argon plasma (Figure A.2), which indicated that oxygen plasmas display more effective etching compared with an argon plasma. The combined effects of chemical and physical modification significantly increased the wettability of linen fabrics. The difference between argon and oxygen plasmas can be mostly ascribed to the fact that the argon plasma mainly produces physical material removal (ablation) while oxygen plasmas produce chemical etching as a result of creation and subsequent desorption of volatile species. Furthermore, the reactive species in the oxygen plasma also create polar groups on the substrate surface.

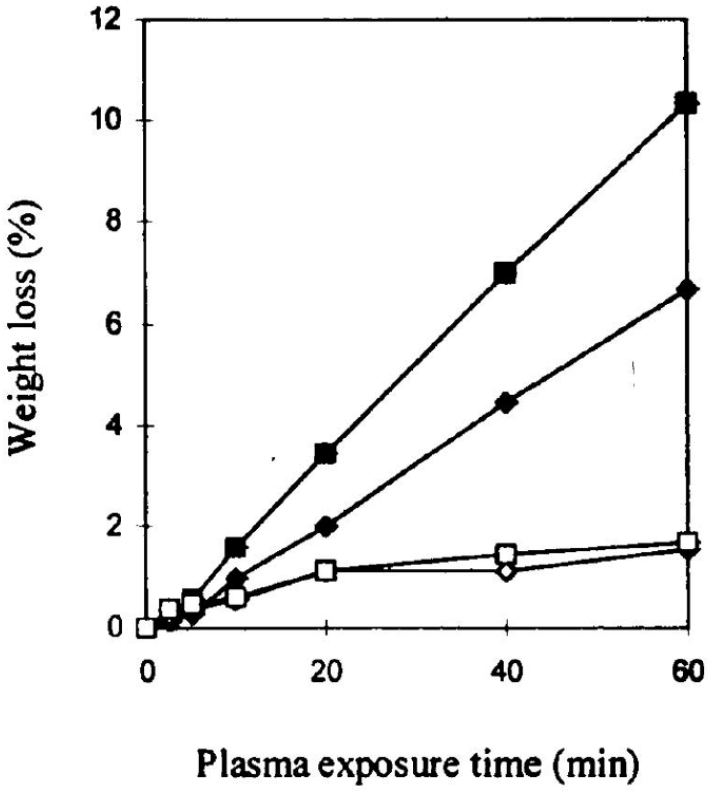

Figure A.2: Fractional weight loss of linen fibers when exposed to pure oxygen and pure argon plasma treatment: (◆) oxygen plasma 100 W, (◇) argon plasma 100W, (■) oxygen plasma 200W, (□) argon plasma 200W

By taking advantage of the higher etch rate of amorphous cellulose domains relative to crystalline domains, Balu et al. [37] used an oxygen plasma to selectively etch cellulose fibers and thus increase surface roughness on the nanoscale. The etching process was conducted in a low oxygen pressure, high plasma power environment in order to enhance the cellulose etch rate and promote domain selective etching. Etching proceeds by reaction of oxygen species with cellulose to form water vapor, CO and CO_2, thereby removing material from the surface. To verify the effect of plasma etching, SEM images (Figure A.3) were obtained for samples before and after plasma treatment. The "cotton-like" surface in the original image can be attributed to the amorphous cellulose

layer on the fibers. After oxygen etching, the fibers display a roughened surface with nanoscale crystalline protrusions that are exposed because the oxygen plasma selectively etches away the amorphous parts of fiber at much higher rates. The same technique can also be employed to tune the nanoscale roughness of wood. [250] Unlike paper, wood is composed of several chemical components, primarily cellulose, hemicellulose, extractives and lignin. Xie et al. [179] demonstrated that the inherent chemical heterogeneity of wood permits differences in etching rates among the wood components to be realized, thereby generating surface roughness by oxygen plasma etching. The increase in nanoscale roughness after etching was confirmed by Laser Scanning Confocal Microscope (LSCM) profilometry.

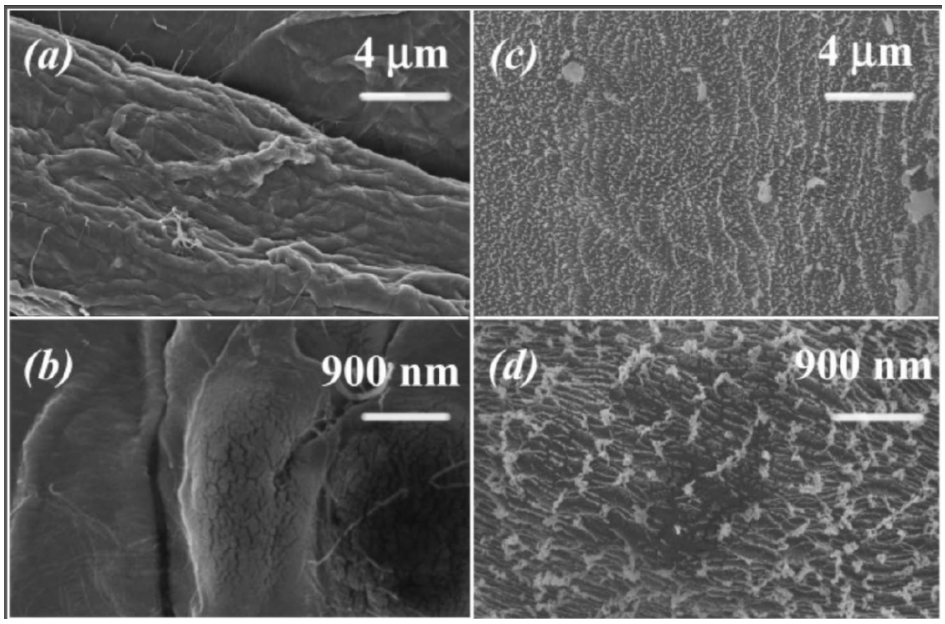

Figure A.3: High magnification SEM images of (a, b) paper fiber untreated, (c, d) paper fiber etched with pure oxygen plasma for 30 minutes.

Plasmas generated with other reactive gases, such as hydrogen [229] or tetrafluoromethane (TFM) [251] can also be used to modify surface properties of cellulose-based material. Hydrogen plasmas were reported to have the opposite effect on filter paper compared with oxygen plasmas. A hydrogen plasma treatment reduced the O/C ratio from 0.75 to 0.25 on substrate surfaces after prolonged exposure. Specifically, XPS demonstrated that the amount of carbon bonded to hydroxyl groups decreases sharply from 72% to 28% of the total peak intensity, and unoxidized carbon increases significantly from 17% to 60% after plasma treatment. These data strongly suggest a dehyroxylation of the cellulose molecule. As a result, the water wettability of pure cellulose is reduced due to the lower polarity of the surface. TFM, on the other hand, was used in combination with oxygen to generate a plasma with even higher etching efficiency than that of a pure oxygen plasma. This type of plasma was used as a

microtome to study the cross-sectional microstructure of cellulose-based materials. Sapieha et al. [251] investigated the relationship between etch rate and two principal parameters: gas concentration and pressure; results are shown in Figures A.4 (a) and (b). For pressures less than 250 mTorr, the etch rate increased with pressure. This observation can be attributed to a rise in the production rate of atomic oxygen. However, the etch rate dropped at a higher pressure, which is likely due to an increased rate of recombination of oxygen and fluorine atoms. The plot of etch rate *versus* CF_4 concentration follows the same trend. At low concentration, CF_4 increased the etch rate because the fluorine atoms produced via dissociation of CF_4 can abstract hydrogen atoms from the cellulose, producing radical sites. However, high CF_4 concentrations can result in surface passivation via formation of a fluorinated surface layer on cellulose which inhibits attack by oxygen atoms. This explanation was also supported by XPS data. Cellulose subjected to plasmas with high concentrations of CF_4 developed a new fluorine F_{1a} peak, which was not observed on paper treated with low CF_4 concentrations.

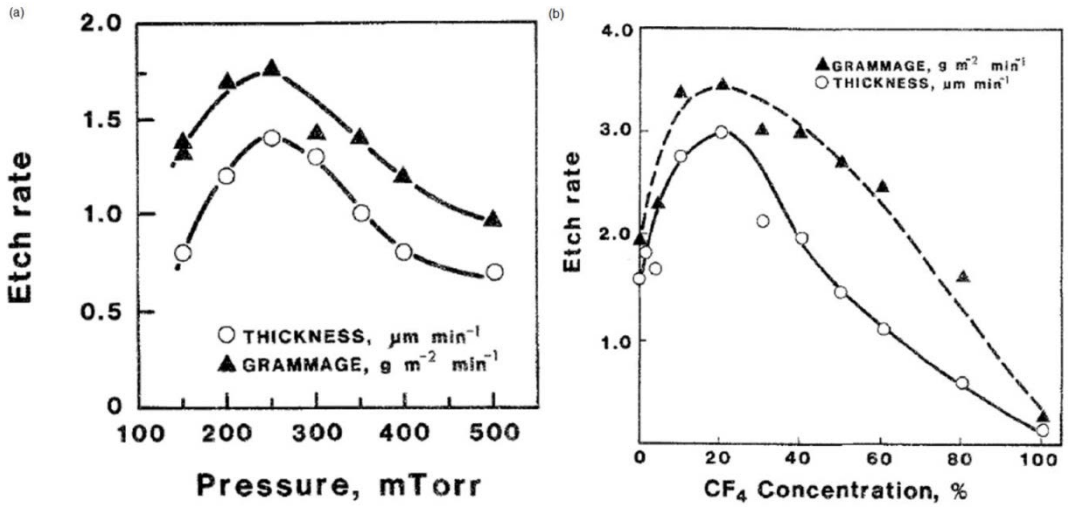

Figure A. 4. Etch rate of kraft paper under a CF_4/O_2 mixture plasma (a) as a function of plasma gas pressure at a fixed flow ratio (CF_4/O_2=0.2) (b) as a function of CF_4 concentration in plasma (by flow rate) at a fixed total gas pressure (250 mTorr).

A.3 Plasma Inducted Radical Formation and Graft Polymerization

Another important result of plasma exposure is the generation of radicals on substrate surfaces. Non-polymerizable gases are commonly used as feed gases for this purpose. Free radicals are highly reactive because of the strong tendency of their unpaired electrons to interact with other electrons and form electron pairs. In fact, radical reactions are heavily involved in every surface modification process described in the previous section. This section, however, will focus specifically on the generation of surface free radicals and their ability to initiate graft polymerization on cellulose-based materials.

Plasma induced graft polymerization usually follows a two-step process. The first step involves the generation of free radicals on the substrate surface due to ion/electron bombardment from non-polymerizable gas plasmas. This step is also called the

"activation" step. After the activation step, the activated sample is then grafted with specific monomers introduced by gases that are not subjected to a plasma environment; reaction of these gases with surface free radicals initiates the polymerization process. In some cases, the sequence is reversed, and the substrate is first immersed into a monomer solution, after which the pre-treated substrate is exposed to a plasma to begin the reaction. The functions of free radicals in this process are to initiate the polymerization process of grafted monomers and to create bonding between substrate and grafted material. The quantity and reactivity of free radicals generated upon plasma exposure are therefore important, because they determine the probability of grafting with appropriate monomers. [252] Compared with conventional grafting methods, plasma induced graft polymerization offers many advantages: low environmental impact, low cost, low temperature, and ease of integration into a continuous process. Also, due to the low penetration depth of ions and electrons, the bulk of the material is not affected by the treatment, so that structural integrity is maintained. The ability of cellulose to trap and stabilize free radicals makes this process particularly suitable for cellulose-based material. [253] Plasma induced graft polymerization has been used to increase the adhesion of cellulose with other non-polar polymers [222, 228, 254], improve the dyeability [224, 255], increase binding between cellulose and metal oxide nanoparticles [256, 257], improve the electric conductivity [258, 259], and impart flame retardancy [253, 260] and hydrophobicity to cellulose.[261] The following paragraphs will first discuss generation of radicals and then address the graft polymerization of various kinds of monomers on cellulose-based materials.

The stability of free radicals formed by plasmas is a key aspect of a successful graft polymerization process. Ward et al. [246, 262] conducted a series of experiments to study the stability of free radicals. The substrates used were cotton and pure cellulose fibers, and the plasma was generated in a low pressure environment using argon. All substrates were exposed to the plasma for 30 minutes. The formation of radicals was confirmed by electron spin resonance (ESR) immediately after plasma exposure. The strong ESR signal of both substrates indicated formation of radicals within the cellulose matrix. In addition, the ESR peak intensity increased with increasing reactor residence time, indicating a direct relationship between treatment time and free radical formation. The ESR signal decayed slowly when activated substrates were exposed to ambient air, but detectable radical levels still remained after 24 hr. This observation clearly confirmed the relative stability of free radicals generated by plasma treatment of cellulose-based substrates. Chen et al. [263] studied the formation of free radicals using different plasma processing gases such as TFM, CO, argon, oxygen and nitrogen. It was found that more "complex" molecules like TFM or CO generated higher concentrations of free radicals compared to argon, nitrogen and oxygen. Among argon, nitrogen and oxygen, argon plasmas generated the most free radicals. Chen et al. also found that more free radicals could be generated on linen surfaces than on cotton surfaces, indicating a strong dependence on substrate. However, due to the high reactivity of free radicals and the lack of in-situ experimental data, the detailed mechanism of free radical formation is unclear.

After the activation step, substrates can be grafted with various monomers to establish different surface chemical functionalities. One important application of plasma

initiated graft polymerization is to increase the dyeability of cotton. Cellulose-based textiles are usually dyed with direct or reactive dyes, neither of which have a high affinity for cellulose fibers. Therefore, the dying process is highly water and energy intensive. This situation can be improved by grafting the cotton surface with materials that can react with dyes. In one study, Karahan et al. [224] treated cotton with air and argon plasmas using a DBD set up. The activated cotton was subsequently immersed into ethylenendiamine (EDA) or triethylenetetramine (TETA) to initiate the grafting process. These two materials were chosen because they contain amine groups, which are suitable for attaching anionic dye molecules to the fiber surface. Control samples were also prepared by exposing samples to a plasma under the same conditions but without carrying out the graft polymerization step. After treatment, the presence of amine groups was confirmed by ATR-FTIR on grafted samples, indicating a successful grafting process. The dyeability was evaluated by relative color strength (K/S) values. An increase in K/S value is indicative of a higher amount of dye on a cotton surface. The results of this study are shown in Figure A.5. It can be seen that the plasma treatment alone (first 3 data points) yielded no positive effect on the dyeability of cotton fabrics regardless of plasma power, probably due to the insufficient formation of new groups to allow acid dye molecules to attach to the cotton fiber surface. However, the dyeability of cotton fabrics significantly increased after the amine grafting step was combined with plasma exposure. In general, samples treated with argon plasmas showed better dyeability than those treated with air plasmas. This is likely due to the fact that argon plasmas generate more radicals than do air plasmas, as discussed above; samples activated by argon plasma are therefore expected to have a higher grafting density.

Better K/S results were also obtained with TETA than with EDA, simply because of the larger number of amine groups. Ren et al. [255] performed a similar study on linen fibers. The linen fabric was activated using a dielectric barrier discharge in ambient air and the activated fabrics were then grafted with acrylic acid. The graft process greatly improved the dyeability of linen fibers.

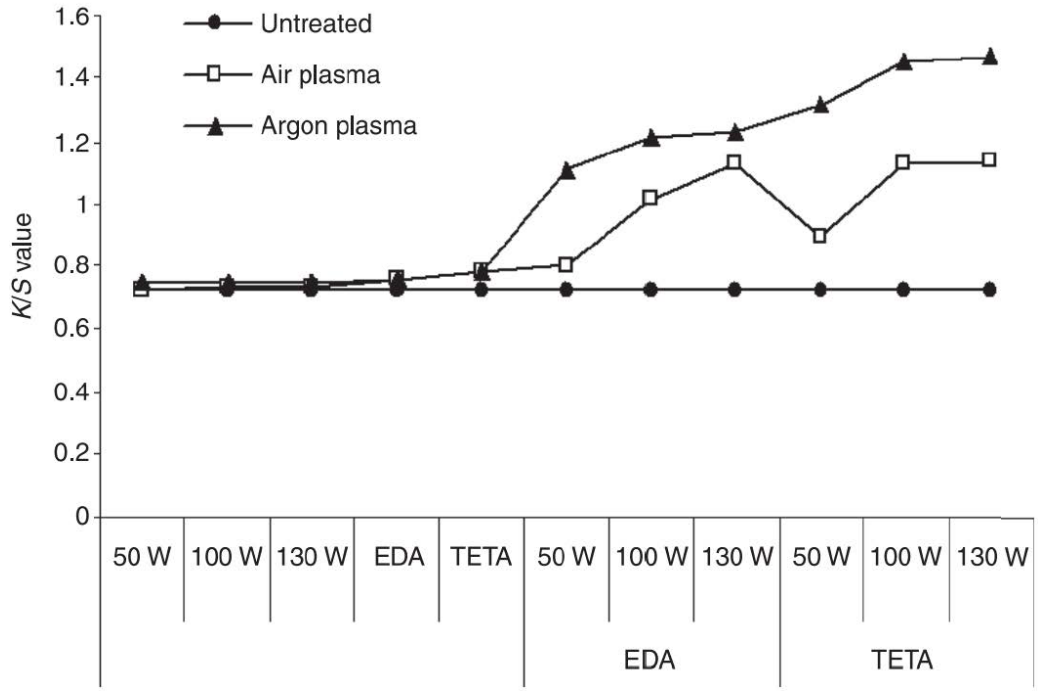

Figure. A.5: Relative color strength values (K/S value) of samples with acid dye agent. EDA and TETA were grafted on cotton by either an argon plasma or an air plasma to enhance dyeability. Control samples received only plasma treatment or only impregnation of EDA/TETA on the cotton surface (first five data points). K/S value of untreated cotton with acid dye was also shown for comparison.

Tsafack et al. [253, 260] developed a process to reduce the flammability of cotton fabrics through the grafting of phosphorous-based compounds. In the first step, bleached cotton fabrics were immersed in a solution containing various monomers and different amounts of crosslinking agent in the presence of a photoinitiator. These impregnated fabrics were then pressed to remove excess solution and subjected to a microwave argon plasma for 15 minutes. Grafting yields depended upon monomer type and amount of crosslinking agent. The flame retardancy of the fabrics grafted with monomers significantly increased compared with non-treated samples. After accelerated laundering procedures, the flame retardancy diminished slightly, but still remained much higher compared with that of untreated cotton fabrics. This is an indication of strong bonding between the fabrics and grafted polymers.

Plasma initiated graft polymerization can also be used to impart hydrophobicity on cellulose-based materials such as cotton. Abidi et al. [222, 228] used a low pressure microwave argon plasma to graft vinyl laurate monomer onto the cotton fabric surface. The objective of this treatment was to attach pending hydrocarbon chains to the surface, thus providing a barrier for water penetration. Due to the small penetration depth of the plasma, the bulk of the cotton fabric was not affected, so the natural comfort of the cotton fabric was retained. During treatment, the sample was first pre-activated in an argon plasma at low pressure. Subsequently, the fabrics were immediately immersed in the monomer solution for 1 hour, and then placed in the plasma chamber for treatment with a microwave plasma. The plasma pretreatment cleaned the fabric surface, increasing the hydrophilicity of the surface, and creating active sites. In the second step, treatment of both the fabric and the monomer in the chamber resulted in grafting and polymerization.

The success of grafting was confirmed by ATR-FTIR data. The hydrophobicity of fabrics was evaluated by measuring the water contact angle, which increased from less than 5^{o} for untreated fabric to 119^{o} for grafted fabric, a significant increase in hydrophobicity. The high water contact angle was retained after repeated home laundering, again indicating a strong adhesion between grafted polymer and the cotton fabric.

A.4 Plasma Enhanced Chemical Vapor Deposition

An important use of plasmas for surface modification involves the deposition of thin polymeric films on a substrate using organic, organo-silicone, or organo-metallic polymerizable vapors. This class of processes is referred to as plasma enhanced chemical vapor deposition (PECVD). The plasma environment enables non-thermal chemical reactions that differ significantly from traditional chemical reaction sequences. For example, when a gas such as ethylene is subjected to a plasma process, it forms a highly cross-linked polymer that is quite different from conventional polyethylene. [264] Compared with plasma initiated grafting, which is a two stage process involving plasma activation and then monomer grafting/polymerization, PECVD is a one stage process. Consequentially, PECVD offers advantages such as reduced processing time, lower cost and reduced chemical waste because no solvents are needed. In addition, due to the bond breaking that occurs at the substrate surface, PECVD films are chemically bonded to the substrate, thereby enhancing adhesion and interface stability. For purposes of the following discussion, we will consider PECVD in two categories: non-fluorinated and fluorinated gas deposition.

For cellulose substrates, non-fluorinated PECVD can be used to increase adhesion between cellulose and other non-polar polymers, [265] increase the dyeability, [266]and impart hydrophobicity on substrates. [267] Tu et al. [265] modified the surface of filter paper by performing a plasma deposition with cyclohexane as the processing gas. The objective of their research was to improve the adhesion between cellulose and polypropylene by depositing a thin hydrocarbon film on the cellulose surface. The plasma deposition was carried out in a radio frequency plasma at low pressure. The presence of a thin hydrocarbon film was confirmed by XPS, FTIR and SEM (Figure A.6 (a) and (b)). An increase in water contact angle was also observed, indicating the presence of a thin non-polar layer on the paper surface. However, the adhesion between treated filter paper and polypropylene was not improved. This result may be due to insufficient intermolecular forces between hydrocarbon film and the polymer. Li et al. exposed paper to an acetylene plasma, thereby depositing a thin film of diamond-like carbon (DLC) onto the paper surface. [38] This coated paper displayed hydrophobicity with high hysteresis. To further improve hydrophobicity and reduce hysteresis, an oxygen plasma etch was used to create additional nanoscale roughness on the fibers prior to DLC deposition. By combining plasma etching and deposition, superhydrophobic paper (water contact angle 162.0°) with low hysteresis (8.7°) was successfully fabricated by invoking non-fluorinated materials.

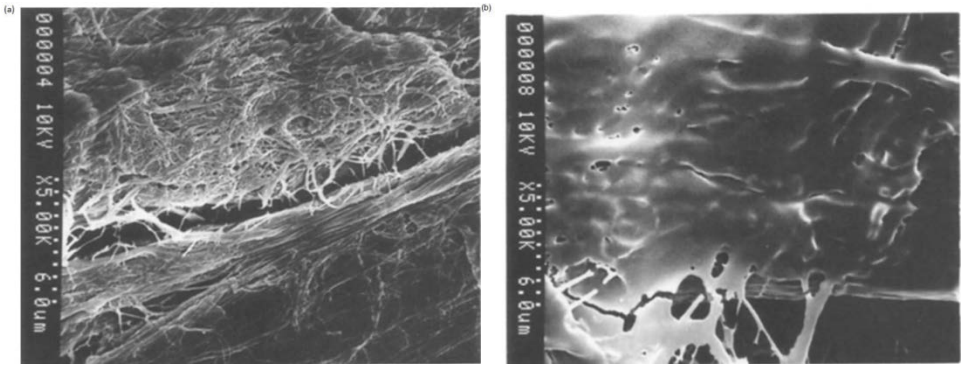

Figure A.6: SEM images of (a) the surface of untreated filter paper and (b) filter paper treated with cyclohexane plasma for 5 minutes at 100 W.

On the other hand, the majority of PECVD processes on cellulose has been performed using fluorinated gas sources. One distinctive property of fluoropolymers is their low surface energy. Fluorinated surfaces have long been known to have the lowest surface energies, and, therefore the lowest degree of wettability of all materials. [268] Consequently, fluorinated PECVD has been used to impart hydrophobicity and oleophobicity to cotton [269-271] and paper, [37, 68, 268, 272, 273]. Cellulose-based hydrophobic material has attracted more attention recently due to its relatively low cost and flexibility. Hydrophobic cotton offers a huge potential for generating hydrophobic yet breathable textiles, while hydrophobic paper can also be used in a vast array of products, including fast food and microwavable food packages, beverage containers, self-cleaning cartons, labels, and paper boards. [37]

McCord et al. [269] conducted research with the aim to enhance the hydrophobicity of cotton fabrics using CF_4 and C_3F_6 gas plasma treatments. Fabrics were treated by low pressure radio frequency plasma. Cotton fabrics treated with fluorocarbon gas plasmas had significantly higher water contact angles than did untreated samples,

with C_3F_6 gas plasmas yielding higher contact angles than CF_4. According to XPS data, the C_3F_6 plasma resulted in a higher concentration of $–CF_3$ groups on the surface, which have a lower surface energy than $–CF_2$ groups. This result indicates that surface fluorocarbon chemical composition rather than the overall surface atomic fluorine content determine hydrophobicity.

In a similar study, Sahin et al. [272] investigated surface fluorination of paper in CF_4 rf plasma environments. According to XPS data, plasma treatment times as low as 30 s can generate surfaces with atomic fractions of fluorine as high as 30%, underlining the high efficiency of plasma fluorination. Not surprisingly, high water contact angle values correlated with high atomic concentrations of fluorine, as measured by XPS. Under specific plasma parameter conditions, contact angles as high as 130^o-140^o could be achieved. While these high contact angles were partially due to the surface chemistry (high fluorine content), the surface micro-topographies also played an important role. AFM images of plasma treated paper showed a significantly rougher topography compared with non-treated samples, which can be attributed to surface etching during the plasma treatment, since increased roughness is known to affect the wetting properties of surfaces.

Vaswani et al. [68] also modified paper and cellulose by plasma assisted deposition of fluorocarbon films using a parallel plate radio frequency plasma reactor at a temperature of 120 ^{o}C. The precursor gases used in this study were pentafluoroethane (PFE) and octafluorocyclobutane (OFB). In order to obtain accurate measurements of film thickness, spectroscopic ellipsometry was used to characterize the fluorocarbon film deposited on a silicon wafer which was placed adjacent to the paper substrate. Water

contact angles were measured for treated paper samples over extended times by placing the substrates in a controlled humidity environment to prevent evaporation of the water droplet. The relation between water contact angle and film thickness is shown in Figure A.7. For fluorocarbon film thicknesses less than 70 nm, the water contact angle was unstable as the water droplets slowly absorbed into the porous paper within less than one hour, suggesting that the surface and near surface fibers were not completely covered at this thickness. To evaluate the barrier properties of fluorocarbon coated paper towards lipophilic materials, the penetration of oleic acid through fluorocarbon layers was studied. It was found that although thicker fluorocarbon layer were helpful to decrease the penetration rate, a small amount of oleic acid was still able to penetrate even the sample with the thickest layer (1 μm) in 1 minute, although water was fully repelled. To investigate this further, SEM studies were conducted on coated paper samples; the images indicate no significant change in pore size after the film deposition. In spite of the high fluorocarbon content on the surface, the porous morphology of coated samples allowed permeation by lipophilic materials despite the high fluorocarbon surface content. Compared with conventional fluoropolymers like PTFE, fluoropolymers formed by PECVD display improved permeability by gases. This unique feature makes this process suitable for the textile and paper industries where water vapor penetration can be advantageous, while liquid water must often be repelled.

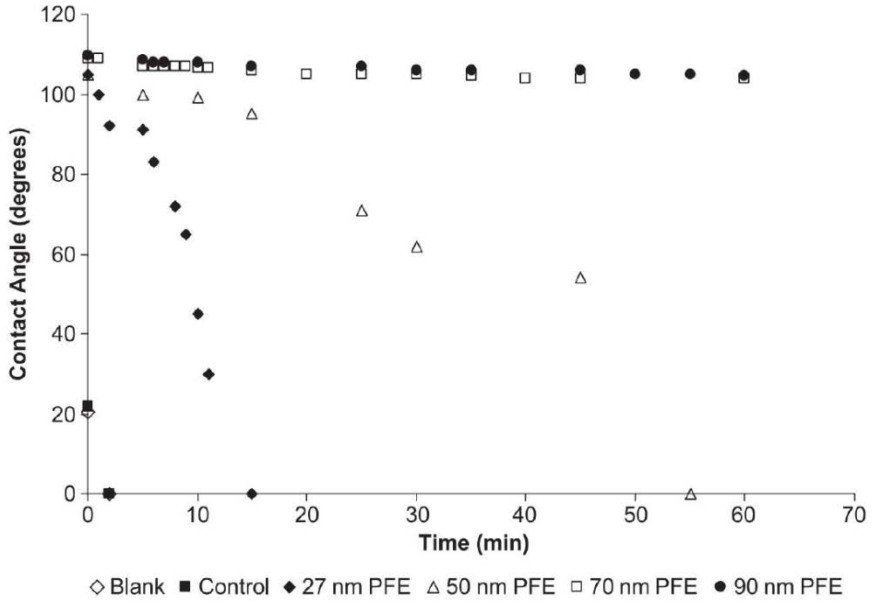

Figure A.7: Variation of water contact angle with time for PFE films of different thicknesses deposited on cellulose. The blank sample is paper without any specific treatment, and the control sample was subjected to the same temperature, pressure, and time conditions, without depositing a film.

Balu et al.[37] created superhydrophobic surfaces (water contact angle >150^{o}) on paper by using two sequential plasma processes. Superhydrophobicity requires a unique combination of two attributes: 1) micron-scale and nano-scale roughness; 2) low surface energy. While paper has a micron-scale roughness due to the fibers present, Balu et al. used an oxygen plasma to generate desirable nano-scale roughness by selectively etching away the amorphous part of the cellulose structure, and uncovering the nanofibrils. A thin fluoropolymer layer was then deposited by PECVD to lower the surface energy. The treated paper not only displayed a high water contact angle (167^{o}), but also showed a low hysteresis (3^{o}), which ensured that the water droplet could readily roll off the paper surface.

A.5 Conclusion

Cellulose-based materials offer numerous advantages for commercial products. However, the hydrophilic properties of these materials limit their range of applications. Treatment of cellulose surfaces with low temperature, non-equilibrium plasmas provides an approach to alter surface properties while maintaining the bulk properties and advantages of this low cost, readily available and bio-renewable material. Furthermore, relative to solution processing methods, plasma treatments have low environmental impact and are amenable to continuous, large scale processing. By switching the processing gas and conditions, plasmas offer great versatility to create different surface properties on cellulose-based material. Non-polymerizable gases such as oxygen, nitrogen, hydrogen and argon, can be used to alter the surface properties of cellulose-based materials through incorporation of new functional groups or by etching or removing material. Plasmas with non-polymerizable gases can also be used to generate free radicals on cellulose surfaces, which can then act as initiators for graft-polymerization processes to change the surface properties of cellulose-based materials, e.g. hydrophobicity, fire retardance, and dyeability. Finally, plasma treatment with polymerizable gases can be used to create thin, strongly bonded polymer layers on cellulose substrates.

REFERENCES

[1] Owens, D.K.; Wendt, R.C. "Estimation of surface free energy of polymers," Journal of Applied Polymer Science, **1969,** *13*, (8), 1741-1748.

[2] Holme, I. "Adhesion to textile fibres and fabrics," International Journal of Adhesion and Adhesives, **1999,** *19*, (6), 455-463.

[3] Furstner, R.; Barthlott, W.; Neinhuis, C.; Walzel, P. "Wetting and self-cleaning properties of artificial superhydrophobic surfaces," Langmuir, **2005,** *21*, (3), 956-961.

[4] Hopken, J.; Moller, M. "Low surface-energy polystyrene," Macromolecules, **1992,** *25*, (5), 1461-1467.

[5] Fox, H.W.; Zisman, W.A. "The spreading of liquids on low energy surfaces .1. Polytetrafluoroethylene," Journal of Colloid Science, **1950,** *5*, (6), 514-531.

[6] Li, M.Y.; Acero, A.A.; Huang, Z.Q.; Rice, S.A. "Formation of an ordered langmuir monolayer by a nonpolar chain molecule," Nature, **1994,** *367*, (6459), 151-153.

[7] Marmur, A. "Wetting on hydrophobic rough surfaces: To be heterogeneous or not to be?," Langmuir, **2003,** *19*, (20), 8343-8348.

[8] Wenzel, R.N. "Resistance of solid surfaces to wetting by water," Industrial and Engineering Chemistry, **1936,** *28*, 988-994.

[9] Cassie, A.B.D.; Baxter, S. "Wettability of porous surfaces," Transactions of the Faraday Society, **1944,** *40*, 546-550.

[10] Chen, W.; Fadeev, A.Y.; Hsieh, M.C.; Oner, D.; Youngblood, J.; McCarthy, T.J. "Ultrahydrophobic and ultralyophobic surfaces: Some comments and examples," Langmuir, **1999,** *15*, (10), 3395-3399.

[11] Nishino, T.; Meguro, M.; Nakamae, K.; Matsushita, M.; Ueda, Y. "The lowest surface free energy based on -cf3 alignment," Langmuir, **1999,** *15*, (13), 4321-4323.

[12] Sun, T.L.; Feng, L.; Gao, X.F.; Jiang, L. "Bioinspired surfaces with special wettability," Accounts of Chemical Research, **2005,** *38*, (8), 644-652.

[13] Zhang, X.; Shi, F.; Niu, J.; Jiang, Y.; Wang, Z. "Superhydrophobic surfaces: From structural control to functional application," Journal of Materials Chemistry, **2008,** *18*, (6), 621-633.

[14] Li, X.-M.; Reinhoudt, D.; Crego-Calama, M. "What do we need for a superhydrophobic surface? A review on the recent progress in the preparation of superhydrophobic surfaces," Chemical Society Reviews, **2007,** *36*, (8), 1350-1368.

[15] Hsu, S.H.; Chang, Y.L.; Tu, Y.C.; Tsai, C.M.; Su, W.F. "Omniphobic low moisture permeation transparent polyacrylate/silica nanocomposite," ACS Applied Materials & Interfaces, **2013,** *5*, (8), 2991-2998.

[16] Sung, G.; Choi, M.C.; Nagappan, S.; Lee, W.K.; Han, M.; Ha, C.S. "Polynorbornene/fluorosilica hybrids for hydrophobic and oleophobic coatings," Polymer Bulletin, **2013,** *70*, (2), 619-630.

[17] Tuteja, A.; Choi, W.; Ma, M.; Mabry, J.M.; Mazzella, S.A.; Rutledge, G.C.; McKinley, G.H.; Cohen, R.E. "Designing superoleophobic surfaces," Science, **2007,** *318*, (5856), 1618-1622.

[18] Lu, Y.; Song, J.; Liu, X.; Xu, W.; Xing, Y.; Wei, Z. "Preparation of superoleophobic and superhydrophobic titanium surfaces via an environmentally friendly electrochemical etching method," Acs Sustainable Chemistry & Engineering, **2013,** *1*, (1), 102-109.

[19] Bellanger, H.; Darmanin, T.; de Givenchy, E.T.; Guittard, F. "Robustness tests on superoleophobic pedop films," Colloids and Surfaces a-Physicochemical and Engineering Aspects, **2013,** *433*, 47-54.

[20] Li, L.; Breedveld, V.; Hess, D.W. "Design and fabrication of superamphiphobic paper surfaces," ACS Applied Materials & Interfaces, **2013,** *5*, (11), 5381-5386.

[21] Yang, J.; Zhang, Z.Z.; Xu, X.H.; Zhu, X.T.; Men, X.H.; Zhou, X.Y. "Superhydrophilic-superoleophobic coatings," Journal of Materials Chemistry, **2012,** *22*, (7), 2834-2837.

[22] Howarter, J.A.; Youngblood, J.P. "Self-cleaning and anti-fog surfaces via stimuli-responsive polymer brushes," Advanced Materials, **2007,** *19*, (22), 3838-3843.

[23] Howarter, J.A.; Youngblood, J.P. "Self-cleaning and next generation anti-fog surfaces and coatings," Macromolecular Rapid Communications, **2008,** *29*, (6), 455-466.

[24] Nevell, T.; Zdernian, S.H. *Cellulose chemistry and its applications*; Ellis horwood series in chemical science, 1st Ed.; John Wiley & Sons: New York, 1985.

[25] Hubbe, M.A. "Paper's resistance to wetting - a review of internal sizing chemicals and their effects," Bioresources, **2007,** *2*, (1), 106-145.

[26] Gess, J.M.; Rende, D.S. "Alkenyl succinic anhydride (asa)," Tappi Journal, **2005,** *4*, (9), 25-30.

[27] Bottorff, K.J. "Akd sizing mechanism - a more definitive description," Tappi Journal, **1994,** *77*, (4), 105-116.

[28] Garnier, G.; Wright, J.; Godbout, L.; Yu, L. "Wetting mechanism of alkyl ketene dimers on cellulose films," Colloids and Surfaces a-Physicochemical and Engineering Aspects, **1998,** *145*, (1-3), 153-165.

[29] Li, X.; Tian, J.F.; Shen, W. "Progress in patterned paper sizing for fabrication of paper-based microfluidic sensors," Cellulose, **2010,** *17*, (3), 649-659.

[30] Shen, W.; Filonanko, Y.; Truong, Y.; Parker, I.H.; Brack, N.; Pigram, P.; Liesegang, J. "Contact angle measurement and surface energetics of sized and unsized paper," Colloids and Surfaces a-Physicochemical and Engineering Aspects, **2000,** *173*, (1-3), 117-126.

[31] Espy, H.H. "The mechanism of wet-strength development in paper - a review," Tappi Journal, **1995,** *78*, (4), 90-99.

[32] Yang, H.; Deng, Y. "Preparation and physical properties of superhydrophobic papers," Journal of Colloid and Interface Science, **2008,** *325*, (2), 588-593.

[33] Hu, Z.; Zen, X.; Gong, J.; Deng, Y. "Water resistance improvement of paper by superhydrophobic modification with microsized caco3 and fatty acid coating," Colloids and Surfaces a-Physicochemical and Engineering Aspects, **2009,** *351*, (1-3), 65-70.

[34] Gao, Z.I.; Zhai, X.L.; Liu, F.; Zhang, M.; Zang, D.L.; Wang, C.Y. "Fabrication of tio2/ep super-hydrophobic thin film on filter paper surface," Carbohydrate Polymers, **2015,** *128*, 24-31.

[35] Teisala, H.; Tuominen, M.; Aromaa, M.; Makela, J.M.; Stepien, M.; Saarinen, J.J.; Toivakka, M.; Kuusipalo, J. "Development of superhydrophobic coating on paperboard surface using the liquid flame spray," Surface & Coatings Technology, **2010,** *205*, (2), 436-445.

[36] Stepien, M.; Chinga-Carrasco, G.; Saarinen, J.J.; Teisala, H.; Tuominen, M.; Aromaa, M.; Haapanen, J.; Kuusipalo, J.; Makela, J.M.; Toivakka, M. "Wear resistance of nanoparticle coatings on paperboard," Wear, **2013,** *307*, (1-2), 112-118.

[37] Balu, B.; Breedveld, V.; Hess, D.W. "Fabrication of "roll-off" and "sticky" superhydrophobic cellulose surfaces via plasma processing," Langmuir, **2008,** *24*, (9), 4785-4790.

[38] Li, L.; Roethel, S.; Breedveld, V.; Hess, D.W. "Creation of low hysteresis superhydrophobic paper by deposition of hydrophilic diamond-like carbon films," Cellulose, **2013,** *20*, (6), 3219-3226.

[39] Jin, C.F.; Jiang, Y.F.; Niu, T.; Huang, J.G. "Cellulose-based material with amphiphobicity to inhibit bacterial adhesion by surface modification," Journal of Materials Chemistry, **2012,** *22*, (25), 12562-12567.

[40] Glavan, A.C.; Martinez, R.V.; Maxwell, E.J.; Subramaniam, A.B.; Nunes, R.M.D.; Soh, S.; Whitesides, G.M. "Rapid fabrication of pressure-driven open-channel microfluidic devices in omniphobic rf paper," Lab on a Chip, **2013,** *13*, (15), 2922-2930.

[41] Bongiovanni, R.; Zeno, E.; Pollicino, A.; Serafini, P.; Tonelli, C. "Uv light-induced grafting of fluorinated monomer onto cellulose sheets," Cellulose, **2011,** *18*, (1), 117-126.

[42] Glavan, A.C.; Martinez, R.V.; Subramaniam, A.B.; Yoon, H.J.; Nunes, R.M.D.; Lange, H.; Thuo, M.M.; Whitesides, G.M. "Omniphobic "r-f paper" produced by silanization of paper with fluoroalkyltrichlorosilanes," Advanced Functional Materials, **2014,** *24*, (1), 60-70.

[43] Robertso.Aa "Interactions of liquids with cellulose," Tappi, **1970,** *53*, (7), 1331-&.

[44] Molina, R.; Gomez, M.; Kan, C.W.; Bertran, E. "Hydrophilic-oleophobic coatings on cellulosic materials by plasma assisted polymerization in liquid phase and fluorosurfactant complexation," Cellulose, **2014,** *21*, (1), 729-739.

[45] Sawada, H.; Ikematsu, Y.; Kawase, T.; Hayakawa, Y. "Synthesis and surface properties of novel fluoroalkylated flip-flop-type silane coupling agents," Langmuir, **1996,** *12*, (15), 3529-3530.

[46] Vaidya, A.; Chaudhury, M.K. "Synthesis and surface properties of environmentally responsive segmented polyurethanes," Journal of Colloid and Interface Science, **2002,** *249*, (1), 235-245.

[47] Kota, A.K.; Kwon, G.; Choi, W.; Mabry, J.M.; Tuteja, A. "Hygro-responsive membranes for effective oil-water separation," Nature Communications, **2012,** *3*, 1-8.

[48] Howarter, J.A.; Genson, K.L.; Youngblood, J.P. "Wetting behavior of oleophobic polymer coatings synthesized from fluorosurfactant-macromers," ACS Applied Materials & Interfaces, **2011,** *3*, (6), 2022-2030.

[49] Hutton, S.J.; Crowther, J.M.; Badyal, J.P.S. "Complexation of fluorosurfactants to functionalized solid surfaces: Smart behavior," Chemistry of Materials, **2000,** *12*, (8), 2282-2286.

[50] Skutlarek, D.; Exner, M.; Farber, H. "Perfluorinated surfactants in surface and drinking water," Environmental Science and Pollution Research, **2006,** *13*, (5), 299-307.

[51] Zhu, Z.Y.; Wang, T.Y.; Meng, J.; Wang, P.; Li, Q.F.; Lu, Y.L. "Perfluoroalkyl substances in the daling river with concentrated fluorine industries in china: Seasonal

variation, mass flow, and risk assessment," Environmental Science and Pollution Research, **2015,** *22*, (13), 10009-10018.

[52] Pal, A.; He, Y.L.; Jekel, M.; Reinhard, M.; Gin, K.Y.H. "Emerging contaminants of public health significance as water quality indicator compounds in the urban water cycle," Environment International, **2014,** *71*, 46-62.

[53] Brambilla, G.; D'Hollander, W.; Oliaei, F.; Stahl, T.; Weber, R. "Pathways and factors for food safety and food security at pfos contaminated sites within a problem based learning approach," Chemosphere, **2015,** *129*, 192-202.

[54] Chen, H.L.; Yao, J.; Wang, F.; Cai, M.M.; Liu, H.J. "Toxicity of perfluorooctanoic acid to pseudomonas putida in the aquatic environment," Journal of Hazardous materials, **2013,** *262*, 726-731.

[55] MiraIles-Marco, A.; Harrad, S. "Perfluorooctane sulfonate: A review of human exposure, biomonitoring and the environmental forensics utility of its chirality and isomer distribution," Environment International, **2015,** *77*, 148-159.

[56] Chen, K.C.; Li, H.T.; Huang, S.C.; Chen, W.B.; Sun, K.W.; Chang, F.C. "Synthesis and performance enhancement of novel polybenzoxazines with low surface free energy," Polymer International, **2011,** *60*, (7), 1089-1096.

[57] Ishida, H. *Handbook of benxoazine resins*; 1st Ed.; Elsevier: 2011.

[58] Wang, Y.X.; Ishida, H. "Cationic ring-opening polymerization of benzoxazines," Polymer, **1999,** *40*, (16), 4563-4570.

[59] Ishida, H.; Kanchanasopa, M.; Yanumet, N. "The effect of curing conditions on the volumetric expansion of bisphenol-a and aniline-based polybenzoxazine," Abstracts of Papers of the American Chemical Society, **1996,** *212*, 61-PMSE.

[60] Ghosh, N.N.; Kiskan, B.; Yagci, Y. "Polybenzoxazines - new high performance thermosetting resins: Synthesis and properties," Progress in Polymer Science, **2007,** *32*, (11), 1344-1391.

[61] Wang, C.F.; Su, Y.C.; Kuo, S.W.; Huang, C.F.; Sheen, Y.C.; Chang, F.C. "Low-surface-free-energy materials based on polybenzoxazines," Angewandte Chemie-International Edition, **2006,** *45*, (14), 2248-2251.

[62] Kim, H.D.; Ishida, H. "A study on hydrogen-bonded network structure of polybenzoxazines," Journal of Physical Chemistry A, **2002,** *106*, (14), 3271-3280.

[63] Goward, G.R.; Sebastiani, D.; Schnell, I.; Spiess, H.W.; Kim, H.D.; Ishida, H. "Benzoxazine oligomers: Evidence for a helical structure from solid-state nmr

spectroscopy and dft-based dynamics and chemical shift calculations," Journal of the American Chemical Society, **2003,** *125*, (19), 5792-5800.

[64] Zhou, C.; Lu, X.; Xin, Z.; Liu, J.; Zhang, Y. "Polybenzoxazine/sio2 nanocomposite coatings for corrosion protection of mild steel," Corrosion Science, **2014,** *80*, 269-275.

[65] Selvi, M.; Vengatesan, M.R.; Devaraju, S.; Kumar, M.; Alagar, M. "In situ sol-gel synthesis of silica reinforced polybenzoxazine hybrid materials with low surface free energy," Rsc Advances, **2014,** *4*, (17), 8446-8452.

[66] Kao, T.H.; Chen, J.K.; Cheng, C.C.; Su, C.J.; Chang, F.C. "Low-surface-free-energy polybenzoxazine/polyacrylonitrile fibers for biononfouling membrane," Polymer, **2013,** *54*, (1), 258-268.

[67] Gogoi, N.; Rastogi, D.; Jassal, M.; Agrawal, A.K. "Low-surface-energy materials based on polybenzoxazines for surface modification of textiles," Journal of the Textile Institute, **2014,** *105*, (11), 1212-1220.

[68] Vaswani, S.; Koskinen, J.; Hess, D.W. "Surface modification of paper and cellulose by plasma-assisted deposition of fluorocarbon films," Surface and Coatings Technology, **2005,** *195*, (2-3), 121-129.

[69] Aulin, C.; Gallstedt, M.; Lindstrom, T. "Oxygen and oil barrier properties of microfibrillated cellulose films and coatings," Cellulose, **2010,** *17*, (3), 559-574.

[70] He, Q.H.; Ma, C.C.; Hu, X.Q.; Chen, H.W. "Method for fabrication of paper-based microfluidic devices by alkylsilane self-assembling and uv/o-3-patterning," Analytical Chemistry, **2013,** *85*, (3), 1327-1331.

[71] Kulkarni, S.A.; Vijayamohanan, K.P. "Interfacial behavior of alkyltrichlorosilane monolayers on silicon: Control of flat-band potential and surface state distribution using chain length variation," Surface Science, **2007,** *601*, (14), 2983-2993.

[72] Zhu, Z.; Xu, G.; An, Y.; He, C. "Construction of octadecyltrichlorosilane self-assembled monolayer on stainless steel 316l surface," Colloids and Surfaces a-Physicochemical and Engineering Aspects, **2014,** *457*, 408-413.

[73] Sagiv, J. "Organized monolayers by adsorption .1. Formation and structure of oleophobic mixed monolayers on solid-surfaces," Journal of the American Chemical Society, **1980,** *102*, (1), 92-98.

[74] Jesionowski, T.; Krysztafkiewicz, A. "Influence of silane coupling agents on surface properties of precipitated silicas," Applied Surface Science, **2001,** *172*, (1-2), 18-32.

[75] Kulkami, S.A.; Ogale, S.B.; Vijayamohanan, K.P. "Tuning the hydrophobic properties of silica particles by surface silanization using mixed self-assembled monolayers," Journal of Colloid and Interface Science, **2008,** *318*, (2), 372-379.

[76] Szczepanski, V.; Vlassiouk, I.; Smirnov, S. "Stability of silane modifiers on alumina nanoporous membranes," Journal of Membrane Science, **2006,** *281*, (1-2), 587-591.

[77] Yu, M.; Gu, G.; Meng, W.-D.; Qing, F.-L. "Superhydrophobic cotton fabric coating based on a complex layer of silica nanoparticles and perfluorooctylated quaternary ammonium silane coupling agent," Applied Surface Science, **2007,** *253*, (7), 3669-3673.

[78] Taipina, M.d.O.; Favaro Ferrarezi, M.M.; Pagotto Yoshida, I.V.; Goncalves, M.d.C. "Surface modification of cotton nanocrystals with a silane agent," Cellulose, **2013,** *20*, (1), 217-226.

[79] Saraji, M.; Farajmand, B. "Chemically modified cellulose paper as a thin film microextraction phase," Journal of Chromatography A, **2013,** *1314*, 24-30.

[80] Cunha, A.G.; Gandini, A. "Turning polysaccharides into hydrophobic materials: A critical review. Part 1. Cellulose," Cellulose, **2010,** *17*, (5), 875-889.

[81] Cunha, A.G.; Freire, C.; Silvestre, A.; Pascoal Neto, C.; Gandini, A.; Belgacem, M.N.; Chaussy, D.; Beneventi, D. "Preparation of highly hydrophobic and lipophobic cellulose fibers by a straightforward gas-solid reaction," Journal of Colloid and Interface Science, **2010,** *344*, (2), 588-595.

[82] Tang, Z.; Hess, D.W.; Breedveld, V. "Fabrication of oleophobic paper with tunable hydrophilicity by treatment with non-fluorinated chemicals," Journal of Materials Chemistry A, **2015,** *3*, (28), 14651-14660.

[83] Fadeev, A.Y.; McCarthy, T.J. "Self-assembly is not the only reaction possible between alkyltrichlorosilanes and surfaces: Monomolecular and oligomeric covalently attached layers of dichloro- and trichloroalkylsilanes on silicon," Langmuir, **2000,** *16*, (18), 7268-7274.

[84] Verzele, M.; Mussche, P. "Monomeric and polymeric derivatization in reversed-phase high-performance liquid-chromatographic materials," Journal of Chromatography, **1983,** *254*, (JAN), 117-122.

[85] Gao, L.; McCarthy, T.J. "A perfectly hydrophobic surface (theta(a)/theta(r)=180 degrees/180 degrees)," Journal of the American Chemical Society, **2006,** *128*, (28), 9052-9053.

[86] Kessel, C.R.; Granick, S. "Formation and characterization of a highly ordered and well-anchored alkylsilane monolayer on mica by self-assembly," Langmuir, **1991,** *7*, (3), 532-538.

[87] Brzoska, J.B.; Benazouz, I.; Rondelez, F. "Silanization of solid substrates - a step toward reproducibility," Langmuir, **1994,** *10*, (11), 4367-4373.

[88] McGovern, M.E.; Kallury, K.M.R.; Thompson, M. "Role of solvent on the silanization of glass with octadecyltrichlorosilane," Langmuir, **1994,** *10*, (10), 3607-3614.

[89] Chen, L.J.; Tsai, Y.H.; Liu, C.S.; Chiou, D.R.; Yeh, M.C. "Effect of water content in solvent on the critical temperature in the formation of self-assembled hexadecyltrichlorosilane monolayers on mica," Chemical Physics Letters, **2001,** *346*, (3-4), 241-245.

[90] Desbief, S.; Patrone, L.; Goguenheim, D.; Guerin, D.; Vuillaume, D. "Impact of chain length, temperature, and humidity on the growth of long alkyltrichlorosilane self-assembled monolayers," Physical Chemistry Chemical Physics, **2011,** *13*, (7), 2870-2879.

[91] Shirgholami, M.A.; Shateri-Khalilabad, M.; Yazdanshenas, M.E. "Effect of reaction duration in the formation of superhydrophobic polymethylsilsesquioxane nanostructures on cotton fabric," Textile Research Journal, **2013,** *83*, (1), 100-110.

[92] Makowski, T.; Kowalczyk, D.; Fortuniak, W.; Jeziorska, D.; Brzezinski, S.; Tracz, A. "Superhydrophobic properties of cotton woven fabrics with conducting 3d networks of multiwall carbon nanotubes, mwcnts," Cellulose, **2014,** *21*, (6), 4659-4670.

[93] Liu, F.; Ma, M.L.; Zang, D.L.; Gao, Z.X.; Wang, C.Y. "Fabrication of superhydrophobic/superoleophilic cotton for application in the field of water/oil separation," Carbohydrate Polymers, **2014,** *103*, 480-487.

[94] Zang, D.L.; Liu, F.; Zhang, M.; Niu, X.G.; Gao, Z.X.; Wang, C.Y. "Superhydrophobic coating on fiberglass cloth for selective removal of oil from water," Chemical Engineering Journal, **2015,** *262*, 210-216.

[95] Kulkarni, S.A.; Mirji, S.A.; Mandale, A.B.; Gupta, R.P.; Vijayamohanan, K.P. "Growth kinetics and thermodynamic stability of octadecyltrichlorosilane self-assembled monolayer on si (100) substrate," Materials Letters, **2005,** *59*, (29-30), 3890-3895.

[96] Fadeev, A.Y.; McCarthy, T.J. "Trialkylsilane monolayers covalently attached to silicon surfaces: Wettability studies indicating that molecular topography contributes to contact angle hysteresis," Langmuir, **1999,** *15*, (11), 3759-3766.

[97] Bierbaum, K.; Kinzler, M.; Woll, C.; Grunze, M.; Hahner, G.; Heid, S.; Effenberger, F. "A near-edge x-ray-absorption fine structure spectroscopy and x-ray photoelectron-spectroscopy study of the film properties of self-assembled monolayers of organosilanes on oxidized si(100)," Langmuir, **1995,** *11*, (2), 512-518.

[98] Launer, P.J., . In *Silicon compounds: Silanes & silicones*; 3rd ed.; Arkles, B., Larson, G.L., Eds. Gelest Inc.: Morrisville, PA, 2013; Vol. 1, pp 175-178.

[99] Passoni, L.; Bonvini, G.; Luzio, A.; Facibeni, A.; Bottani, C.E.; Di Fonzo, F. "Multiscale effect of hierarchical self-assembled nanostructures on superhydrophobic surface," Langmuir, **2014,** *30*, (45), 13581-13587.

[100] Chibowski, E. "Apparent surface free energy of superhydrophobic surfaces," Journal of Adhesion Science and Technology, **2011,** *25*, (12), 1323-1336.

[101] Zettlemoyer, A.C. "Hydrophobic surfaces," Journal of Colloid and Interface Science, **1968,** *28*, (3-4), 343-369.

[102] Raghavanpillai, A.; Reinartz, S.; Hutchenson, K.W. "Hydrophobic and oleophobic surface modification using fluorinated bis-urea and bis-amide gelators," Journal of Fluorine Chemistry, **2009,** *130*, (4), 410-417.

[103] Kahan, G.J. "Hydrophobic films on solid surfaces," Journal of Colloid and Interface Science, **1951,** *6*, (6), 571-575.

[104] Feng, L.; Li, S.H.; Li, Y.S.; Li, H.J.; Zhang, L.J.; Zhai, J.; Song, Y.L.; Liu, B.Q.; Jiang, L.; Zhu, D.B. "Super-hydrophobic surfaces: From natural to artificial," Advanced Materials, **2002,** *14*, (24), 1857-1860.

[105] Dong, F.; Ha, C.-S. "Superhydrophobic and oleophobic surfaces fabricated from incompletely condensed polyhedral oligomeric silsesquioxane," Macromolecular Research, **2011,** *19*, (2), 101-104.

[106] Aulin, C.; Yun, S.H.; Wagberg, L.; Lindstrom, T. "Design of highly oleophobic cellulose surfaces from structured silicon templates," ACS Applied Materials & Interfaces, **2009,** *1*, (11), 2443-2452.

[107] Wang, B.; Li, J.; Wang, G.; Liang, W.; Zhang, Y.; Shi, L.; Guo, Z.; Liu, W. "Methodology for robust superhydrophobic fabrics and sponges from in situ growth of transition metal/metal oxide nanocrystals with thiol modification and their applications in oil/water separation," ACS Applied Materials & Interfaces, **2013,** *5*, (5), 1827-1839.

[108] Verplanck, N.; Galopin, E.; Camart, J.-C.; Thomy, V.; Coffinier, Y.; Boukherroub, R. "Reversible electrowetting on superhydrophobic silicon nanowires," Nano Letters, **2007,** *7*, (3), 813-817.

[109] Nguyen, J.G.; Cohen, S.M. "Moisture-resistant and superhydrophobic metal-organic frameworks obtained via postsynthetic modification," Journal of the American Chemical Society, **2010,** *132*, (13), 4560-4561.

[110] Li, S.; Zhang, S.; Wang, X. "Fabrication of superhydrophobic cellulose-based materials through a solution-immersion process," Langmuir, **2008,** *24*, (10), 5585-5590.

[111] Dorrer, C.; Ruehe, J. "Wetting of silicon nanograss: From superhydrophilic to superhydrophobic surfaces," Advanced Materials, **2008,** *20*, (1), 159-163.

[112] Amigoni, S.; de Givenchy, E.T.; Dufay, M.; Guittard, F. "Covalent layer-by-layer assembled superhydrophobic organic-inorganic hybrid films," Langmuir, **2009,** *25*, (18), 11073-11077.

[113] Zhang, J.; Seeger, S. "Superoleophobic coatings with ultralow sliding angles based on silicone nanofilaments," Angewandte Chemie-International Edition, **2011,** *50*, (29), 6652-6656.

[114] Leng, B.; Shao, Z.; de With, G.; Ming, W. "Superoleophobic cotton textiles," Langmuir, **2009,** *25*, (4), 2456-2460.

[115] Zhou, H.; Wang, H.X.; Niu, H.T.; Lin, T. "Superphobicity/philicity janus fabrics with switchable, spontaneous, directional transport ability to water and oil fluids," Scientific Reports, **2013,** *3*, 1-6.

[116] Liu, K.S.; Tian, Y.; Jiang, L. "Bio-inspired superoleophobic and smart materials: Design, fabrication, and application," Progress in Materials Science, **2013,** *58*, (4), 503-564.

[117] Lampitt, R.A.; Crowther, J.M.; Badyal, J.P.S. "Switching liquid repellent surfaces," Journal of Physical Chemistry B, **2000,** *104*, (44), 10329-10331.

[118] Howarter, J.A.; Youngblood, J.P. "Amphiphile grafted membranes for the separation of oil-in-water dispersions," Journal of Colloid and Interface Science, **2009,** *329*, (1), 127-132.

[119] Rohrbach, K.; Li, Y.Y.; Zhu, H.L.; Liu, Z.; Dai, J.Q.; Andreasen, J.L.; Hu, L.B. "A cellulose based hydrophilic, oleophobic hydrated filter for water/oil separation," Chemical Communications, **2014,** *50*, (87), 13296-13299.

[120] Brown, P.S.; Atkinson, O.; Badyal, J.P.S. "Ultrafast oleophobic-hydrophilic switching surfaces for antifogging, self-cleaning, and oil water separation," ACS Applied Materials & Interfaces, **2014,** *6*, (10), 7504-7511.

[121] Shafrin, E.G.; Zisman, W.A. "Constitutive relations in the wetting of low energy surfaces and the theory of the retraction method of preparing monolayers," Journal of Physical Chemistry, **1960,** *64*, (5), 519-524.

[122] Siriviriyanun, A.; Imae, T. "Anti-fingerprint properties of non-fluorinated organosiloxane self-assembled monolayer-coated glass surfaces," Chemical Engineering Journal, **2014,** *246*, 254-259.

[123] Zhang, Z.; Sebe, G.; Rentsch, D.; Zimmermann, T.; Tingaut, P. "Ultralightweight and flexible silylated nanocellulose sponges for the selective removal of oil from water," Chemistry of Materials, **2014,** *26*, (8), 2659-2668.

[124] Tshabalala, M.A.; Kingshott, P.; VanLandingham, M.R.; Plackett, D. "Surface chemistry and moisture sorption properties of wood coated with multifunctional alkoxysilanes by sol-gel process," Journal of Applied Polymer Science, **2003,** *88*, (12), 2828-2841.

[125] Miyafuji, H.; Saka, S. "Topochemistry of sio_2 wood-inorganic composites for enhancing water-repellency," Materials Science Research International, **1999,** *5*, (4), 270-275.

[126] Hochmanska, P.; Mazela, B.; Krystofiak, T. "Hydrophobicity and weathering resistance of wood treated with silane-modified protective systems," Drewno, **2014,** *57*, (191), 99-110.

[127] Kulkarni, M.M.; Bandyopadhyaya, R.; Sharma, A. "Janus silica film with hydrophobic and hydrophilic surfaces grown at an oil-water interface," Journal of Materials Chemistry, **2008,** *18*, (9), 1021-1028.

[128] Jang, K.O.; Yeh, K. "Effects of silicone softeners and silane coupling agents on the performance properties of cotton fabrics," Textile Research Journal, **1993,** *63*, (10), 557-565.

[129] Fei, T.; Chen, H.; Lin, J. "Transparent superhydrophobic films possessing high thermal stability and improved moisture resistance from the deposition of mtms-based aerogels," Colloids and Surfaces, A: Physicochemical and Engineering Aspects, **2014,** *443*, 255-264.

[130] Wang, J.T.; Zheng, Y.A.; Wang, A.Q. "Superhydrophobic kapok fiber oil-absorbent: Preparation and high oil absorbency," Chemical Engineering Journal, **2012,** *213*, 1-7.

[131] Li, S.H.; Zhang, S.B.; Wang, X.H. "Fabrication of superhydrophobic cellulose-based materials through a solution-immersion process," Langmuir, **2008,** *24*, (10), 5585-5590.

[132] Girardi, F.; Maggini, S.; Della Volpe, C.; Cappelletto, E.; Mueller, K.; Siboni, S.; Di Maggio, R. "Hybrid organic-inorganic materials on paper: Surface and thermo-mechanical properties," Journal of Sol-Gel Science and Technology, **2011,** *60*, (3), 315-323.

[133] Yagi, O.; Iwamiya, Y.; Suzuki, K.; Funane, R.; Ohishi, F. "Improvement in tensile strength and water repellency of paper after treatment with methyltrimethoxysilane oligomer using titanium butoxide as a catalyst," Journal of Sol-Gel Science and Technology, **2005,** *36*, (1), 69-75.

[134] Wang, J.Y.; Monton, M.R.N.; Zhang, X.; Filipe, C.D.M.; Pelton, R.; Brennan, J.D. "Hydrophobic sol-gel channel patterning strategies for paper-based microfluidics," Lab on a Chip, **2014,** *14*, (4), 691-695.

[135] Yang, J.; Song, H.J.; Yan, X.H.; Tang, H.; Li, C.S. "Superhydrophilic and superoleophobic chitosan-based nanocomposite coatings for oil/water separation," Cellulose, **2014,** *21*, (3), 1851-1857.

[136] Ragesh, P.; Ganesh, V.A.; Naira, S.V.; Nair, A.S. "A review on 'self-cleaning and multifunctional materials'," Journal of Materials Chemistry A, **2014,** *2*, (36), 14773-14797.

[137] Zhu, X.Y.; Tu, W.T.; Wee, K.H.; Bai, R.B. "Effective and low fouling oil/water separation by a novel hollow fiber membrane with both hydrophilic and oleophobic surface properties," Journal of Membrane Science, **2014,** *466*, 36-44.

[138] Graiver, D.; Farminer, K.W.; Narayan, R. "A review of the fate and effects of silicones in the environment," Journal of Polymers and the Environment, **2003,** *11*, (4), 129-136.

[139] Rowe, V.K.; Spencer, H.C.; Bass, S.L. "Toxicological studies on certain commercial silicones and hydrolyzable silane intermediates," Journal of Industrial Hygiene and Toxicology, **1948,** *30*, (6), 332-352.

[140] Ciapetti, G.; Granchi, D.; Stea, S.; Savarino, L.; Verri, E.; Gori, A.; Savioli, F.; Montanaro, L. "Cytotoxicity testing of materials with limited in vivo exposure is affected by the duration of cell-material contact," Journal of Biomedical Materials Research, **1998,** *42*, (4), 485-490.

[141] TAPPI *Forming handsheets for physical tests of pulp*; Technical Association of Paper and Pulp Industry: Atlanta, GA, 2002.

[142] TAPPI *Air resistance of paper (gurley method)*; Technical Association of Paper and Pulp Industry: Atlanta, GA, 2006.

[143] ANSI *Surface texture (surface roughness, waviness, and lay)*; Americal National Standard Institution: Washington, DC, 1995.

[144] Alam, T.M.; Assink, R.A.; Loy, D.A. "Hydrolysis and esterification in organically modified alkoxysilanes: A si-29 nmr investigation of methyltrimethoxysilane," Chemistry of Materials, **1996,** *8*, (9), 2366-2374.

[145] Dong, H.J.; Lee, M.; Thomas, R.D.; Zhang, Z.P.; Reidy, R.F.; Mueller, D.W. "Methyltrimethoxysilane sol-gel polymerization in acidic ethanol solutions studied by si-29 nmr spectroscopy," Journal of Sol-Gel Science and Technology, **2003,** *28*, (1), 5-14.

[146] Zhang, Z.P.; Gorman, B.P.; Dong, H.J.; Orozco-Teran, R.A.; Mueller, D.W.; Reidy, R.F. "Investigation of polymerization and cyclization of dimethyldiethoxysilane by si-29 nmr and ftir," Journal of Sol-Gel Science and Technology, **2003,** *28*, (2), 159-165.

[147] Dong, H.J.; Zhang, Z.P.; Lee, M.H.; Mueller, D.W.; Reidy, R.F. "Sol-gel polycondensation of methyltrimethoxysilane in ethanol studied by si-29 nmr spectroscopy using a two-step acid/base procedure," Journal of Sol-Gel Science and Technology, **2007,** *41*, (1), 11-17.

[148] Alexander, M.R.; Short, R.D.; Jones, F.R.; Michaeli, W.; Blomfield, C.J. "A study of hmdso/o-2 plasma deposits using a high-sensitivity and -energy resolution xps instrument: Curve fitting of the si 2p core level," Applied Surface Science, **1999,** *137*, (1-4), 179-183.

[149] O'Hare, L.A.; Parbhoo, B.; Leadley, S.R. "Development of a methodology for xps curve-fitting of the si 2p core level of siloxane materials," Surface and Interface Analysis, **2004,** *36*, (10), 1427-1434.

[150] Rao, A.V.; Kulkarni, M.M.; Amalnerkar, D.P.; Seth, T. "Superhydrophobic silica aerogels based on methyltrimethoxysilane precursor," Journal of Non-Crystalline Solids, **2003,** *330*, (1-3), 187-195.

[151] Sawada, H.; Yoshioka, H.; Kawase, T.; Takahashi, H.; Abe, A.; Ohashi, R. "Synthesis and applications of a variety of fluoroalkyl end-capped oligomers/silica gel polymer hybrids," Journal of Applied Polymer Science, **2005,** *98*, (1), 169-177.

[152] Tian, D.; Zhang, X.; Tian, Y.; Wu, Y.; Wang, X.; Zhai, J.; Jiang, L. "Photo-induced water-oil separation based on switchable superhydrophobicity-superhydrophilicity and underwater superoleophobicity of the aligned zno nanorod array-coated mesh films," Journal of Materials Chemistry, **2012,** *22*, (37), 19652-19657.

[153] Lavoine, N.; Desloges, I.; Dufresne, A.; Bras, J. "Microfibrillated cellulose - its barrier properties and applications in cellulosic materials: A review," Carbohydrate Polymers, **2012,** *90*, (2), 735-764.

[154] Han, J.; Salmieri, S.; Le Tien, C.; Lacroix, M. "Improvement of water barrier property of paperboard by coating application with biodegradable polymers," Journal of Agricultural and Food Chemistry, **2010,** *58*, (5), 3125-3131.

[155] Havimo, M.; Jalomaki, J.; Granstrom, M.; Rissanen, A.; Iivanainen, T.; Kemell, M.; Heikkila, M.; Sipi, M.; Kilpelainen, I. "Mechanical strength and water resistance of paperboard coated with long chain cellulose esters," Packaging Technology and Science, **2011,** *24*, (4), 249-258.

[156] Paunonen, S. "Strength and barrier enhancements of composites and packaging boards by nanocelluloses - a literature review," Nordic Pulp & Paper Research Journal, **2013,** *28*, (2), 165-181.

[157] Campbell, W.G.; McDonald, I.R.C. "The chemistry of the wood cell wall .2. The isolation of beech and spruce acid-soluble and modified lignins," Journal of the Chemical Society, **1952**, (AUG), 3180-3183.

[158] *Handbook of wood chemistry and wood composites, 2nd edition*; Handbook of wood chemistry and wood composites, 2nd edition,Crc Press-Taylor & Francis Group: Boca Raton, 2013.

[159] Hon, D.N.-S., Weathering and photochemistry of wood. In *Wood and cellulosic chemistry*; Hon, D.N.-S., Shiraishi, N., Eds. Marcel Dekker, Inc.: Basel, NY, 2001; pp 513-546.

[160] Rowell, R.M. "Penetration and reactivity of wood cell-wall components," Abstracts of Papers of the American Chemical Society, **1983,** *185*, (MAR), 4-CELL.

[161] Sevanto, S.; Holtta, T.; Hirsikko, A.; Vesala, T.; Nikinmaa, E. "Determination of thermal expansion of green wood and the accuracy of tree stem diameter variation measurements," Boreal Environment Research, **2005,** *10*, (5), 437-445.

[162] Kloiber, M.; Drdacky, M.; Tippner, J.; Hrivnak, J. "Conventional compressive strength parallel to the grain and mechanical resistance of wood against pin penetration and microdrilling established by in-situ semidestructive devices," Materials and Structures, **2015,** *48*, (10), 3217-3229.

[163] de Melo, J.E.; de Souza, M.R.; da Costa, A.F. "Influence of the specimen size and test speed in static bending strength of three tropical wood species," Ciencia Florestal, **2015,** *25*, (2), 415-424.

[164] Srivaro, S.; Matan, N.; Lam, F. "Stiffness and strength of oil palm wood core sandwich panel under center point bending," Materials & Design, **2015,** *84*, 154-162.

[165] Sebe, G.; Brook, M.A. "Hydrophobization of wood surfaces: Covalent grafting of silicone polymers," Wood Science and Technology, **2001,** *35*, (3), 269-282.

[166] Evans, P.D.; Thay, P.D.; Schmalzl, K.J. "Degradation of wood surfaces during natural weathering. Effects on lignin and cellulose and on the adhesion of acrylic latex primers," Wood Science and Technology, **1996,** *30*, (6), 411-422.

[167] Ayadi, N.; Lejeune, F.; Charrier, F.; Charrier, B.; Merlin, A. "Color stability of heat-treated wood during artificial weathering," Holz Als Roh-Und Werkstoff, **2003,** *61*, (3), 221-226.

[168] Anderson, E.L.; Pawlak, Z.; Owen, N.L.; Feist, W.C. "Infrared studies of wood weathering .1. Softwoods," Applied Spectroscopy, **1991,** *45*, (4), 641-647.

[169] Wang, Z.; Chen, T.; Gao, Y.; Breuil, C.; Hiratsuka, Y. "Biological degradation of resin acids in wood chips by wood-inhabiting fungi," Applied and Environmental Microbiology, **1995,** *61*, (1), 222-225.

[170] Brelid, P.L.; Simonson, R.; Bergman, O.; Nilsson, T. "Resistance of acetylated wood to biological degradation," Holz Als Roh-Und Werkstoff, **2000,** *58*, (5), 331-337.

[171] Blanchette, R.A.; Nilsson, T.; Daniel, G.; Abad, A. "Biological degradation of wood," Advances in Chemistry Series, **1990**, (225), 141-174.

[172] Weichelt, F.; Emmler, R.; Flyunt, R.; Beyer, E.; Buchmeiser, M.R.; Beyer, M. "Zno-based uv nanocomposites for wood coatings in outdoor applications," Macromolecular Materials and Engineering, **2010,** *295*, (2), 130-136.

[173] Marney, D.C.O.; Russell, L.J. "Combined fire retardant and wood preservative treatments for outdoor wood applications - a review of the literature," Fire Technology, **2008,** *44*, (1), 1-14.

[174] Gao, J.S.; Zhang, Z.F., Research on the rationality of the combined application of bamboo and wood in outdoor furniture. In *Mechanical engineering, materials and energy iii*; Abdullah, M.Z., Ed. 2014; Vol. 483, pp 142-145.

[175] Hsieh, C.T.; Chang, B.S.; Lin, J.Y. "Improvement of water and oil repellency on wood substrates by using fluorinated silica nanocoating," Applied Surface Science, **2011,** *257*, (18), 7997-8002.

[176] Yasuda, R.; Minato, K.; Norimoto, M. "Moisture adsorption thermodynamics of chemically-modified wood," Holzforschung, **1995,** *49*, (6), 548-554.

[177] Zanini, S.; Riccardi, C.; Orlandi, M.; Fornara, V.; Colombini, M.P.; Donato, D.I.; Legnaioli, S.; Palleschi, V. "Wood coated with plasma-polymer for water repellence," Wood Science and Technology, **2008,** *42*, (2), 149-160.

[178] Poaty, B.; Riedl, B.; Blanchet, P.; Blanchard, V.; Stafford, L. "Improved water repellency of black spruce wood surfaces after treatment in carbon tetrafluoride plasmas," Wood Science and Technology, **2013,** *47*, (2), 411-422.

[179] Xie, L.; Tang, Z.; Jiang, L.; Breedveld, V.; Hess, D.W. "Creation of superhydrophobic wood surfaces by plasma etching and thin-film deposition," Surface and Coatings Technology, **2015,** *281*, 125-132.

[180] Hakkou, M.; Petrissans, M.; Zoulalian, A.; Gerardin, P. "Investigation of wood wettability changes during heat treatment on the basis of chemical analysis," Polymer Degradation and Stability, **2005,** *89*, (1), 1-5.

[181] Wang, X.Q.; Chai, Y.B.; Liu, J.L. "Formation of highly hydrophobic wood surfaces using silica nanoparticles modified with long-chain alkylsilane," Holzforschung, **2013,** *67*, (6), 667-672.

[182] Levasseur, O.; Stafford, L.; Gherardi, N.; Naude, N.; Blanchard, V.; Blanchet, P.; Riedl, B.; Sarkissian, A. "Deposition of hydrophobic functional groups on wood surfaces using atmospheric-pressure dielectric barrier discharge in helium-hexamethyldisiloxane gas mixtures," Plasma Processes and Polymers, **2012,** *9*, (11-12), 1168-1175.

[183] Fu, Y.C.; Li, G.; Yu, H.P.; Liu, Y.X. "Hydrophobic modification of wood via surface-initiated arget atrp of mma," Applied Surface Science, **2012,** *258*, (7), 2529-2533.

[184] Adcock, T.; Shah, V.; Chen, M.J.; Meister, J.J. "Graft copolymers of lignin as hydrophobic agents for plastic (wood-filled) composites," Journal of Applied Polymer Science, **2003,** *89*, (5), 1266-1276.

[185] Jin, C.D.; Li, J.P.; Han, S.J.; Wang, J.; Sun, Q.F. "A durable, superhydrophobic, superoleophobic and corrosion-resistant coating with rose-like zno nanoflowers on a bamboo surface," Applied Surface Science, **2014,** *320*, 322-327.

[186] Landry, V.; Blanchet, P. "Weathering resistance of opaque pvdf-acrylic coatings applied on wood substrates," Progress in Organic Coatings, **2012,** *75*, (4), 494-501.

[187] Valentine, R.; Baker, B.B.; Bonesteel, J.K.; Pinto, J.G.; Kasprzak, D.J.; Makovec, G.T.; Seidel, W.C.; Clarke, F.B.; Herpol, C.H.; Jannssens, M. "Inhalation toxicity of fluoropolymer wood smokes in full-scale fires," Abstracts of Papers of the American Chemical Society, **1989,** *197*, 8-MACR.

[188] Siriviriyanun, A.; Imae, T. "Anti-fingerprint properties of non-fluorinated organosiloxane self-assembled monolayer-coated glass surfaces," Chemical Engineering Journal, **2014,** *246*, (0), 254-259.

[189] Lee, S.B.; Luner, P. "Wetting and interfacial properties of lignin," Tappi, **1972,** *55*, (1), 116-&.

[190] Tang, L.J.; Zhang, R.; Zhou, X.Y.; Pan, M.Z.; Chen, M.Z.; Yang, X.H.; Zhou, P.; Chen, Z. "Dynamic adhesive wettability of poplar veneer with cold oxygen plasma treatment," Bioresources, **2012,** *7*, (3), 3327-3339.

[191] Aydin, I.; Demirkir, C. "Activation of spruce wood surfaces by plasma treatment after long terms of natural surface inactivation," Plasma Chemistry and Plasma Processing, **2010,** *30*, (5), 697-706.

[192] Konnerth, J.; Weigl, M.; Gindl-Altmutter, W.; Avramidis, G.; Wolkenhauer, A.; Viol, W.; Gilge, M.; Obersriebnig, M. "Effect of plasma treatment on cell-wall adhesion of urea-formaldehyde resin revealed by nanoindentation," Holzforschung, **2014,** *68*, (6), 707-712.

[193] Tang, L.J.; Yang, X.H.; Zhang, R.; Wang, X.M.; Zhou, X.Y. "Surface modification of poplar veneer by means of radio frequency oxygen plasma (rf-op) to improve interfacial adhesion with urea-formaldehyde resin," Holzforschung, **2015,** *69*, (2), 193-198.

[194] Liu, W.D.; Chen, T.T.; Xie, T.S.; Lai, F.W.; Qiu, R.H. "Oxygen plasma treatment of bamboo fibers (bf) and its effects on the static and dynamic mechanical properties of bf-unsaturated polyester composites," Holzforschung, **2015,** *69*, (4), 449-455.

[195] Lang, Q.; Bi, Z.; Pu, J.W. "Poplar wood-methylol urea composites prepared by in situ polymerization. Ii. Characterization of the mechanism of wood modification by methylol urea," Journal of Applied Polymer Science, **2015,** *132*, (42).

[196] Cappelletto, E.; Maggini, S.; Girardi, F.; Bochicchio, G.; Tessadri, B.; Di Maggio, R. "Wood surface protection with different alkoxysilanes: A hydrophobic barrier," Cellulose, **2013,** *20*, (6), 3131-3141.

[197] Schaum, J.; Cohen, M.; Perry, S.; Artz, R.; Draxler, R.; Frithsen, J.B.; Heist, D.; Lorber, M.; Phillips, L. "Screening level assessment of risks due to dioxin emissions from burning oil from the bp deepwater horizon gulf of mexico spill," Environmental Science & Technology, **2010,** *44*, (24), 9383-9389.

[198] Zouboulis, A.I.; Avranas, A. "Treatment of oil-in-water emulsions by coagulation and dissolved-air flotation," Colloids and Surfaces a-Physicochemical and Engineering Aspects, **2000,** *172*, (1-3), 153-161.

[199] Zhang, L.; Zhang, Z.; Wang, P. "Smart surfaces with switchable superoleophilicity and superoleophobicity in aqueous media: Toward controllable oil/water separation," Npg Asia Materials, **2012,** *4*.

[200] Calcagnile, P.; Fragouli, D.; Bayer, I.S.; Anyfantis, G.C.; Martiradonna, L.; Cozzoli, P.D.; Cingolani, R.; Athanassiou, A. "Magnetically driven floating foams for the removal of oil contaminants from water," Acs Nano, **2012,** *6*, (6), 5413-5419.

[201] Yuan, J.; Liu, X.; Akbulut, O.; Hu, J.; Suib, S.L.; Kong, J.; Stellacci, F. "Superwetting nanowire membranes for selective absorption," Nature Nanotechnology, **2008,** *3*, (6), 332-336.

[202] Adebajo, M.O.; Frost, R.L.; Kloprogge, J.T.; Carmody, O.; Kokot, S. "Porous materials for oil spill cleanup: A review of synthesis and absorbing properties," Journal of Porous Materials, **2003,** *10*, (3), 159-170.

[203] Meininghaus, C.K.W.; Prins, R. "Sorption of volatile organic compounds on hydrophobic zeolites," Microporous and Mesoporous Materials, **2000,** *35-6*, 349-365.

[204] Alther, G.R. "Organically modified clay removes oil from water," Waste Management, **1995,** *15*, (8), 623-628.

[205] Bayat, A.; Aghamiri, S.F.; Moheb, A.; Vakili-Nezhaad, G.R. "Oil spill cleanup from sea water by sorbent materials," Chemical Engineering & Technology, **2005,** *28*, (12), 1525-1528.

[206] Teas, C.; Kalligeros, S.; Zanikos, F.; Stournas, S.; Lois, E.; Anastopoulos, G. "Investigation of the effectiveness of absorbent materials in oil spills clean up," Desalination, **2001,** *140*, (3), 259-264.

[207] Zhu, Q.; Pan, Q.; Liu, F. "Facile removal and collection of oils from water surfaces through superhydrophobic and superoleophilic sponges," Journal of Physical Chemistry C, **2011,** *115*, (35), 17464-17470.

[208] Wang, S.; Li, M.; Lu, Q. "Filter paper with selective absorption and separation of liquids that differ in surface tension," ACS Applied Materials & Interfaces, **2010,** *2*, (3), 677-683.

[209] Lee, C.H.; Johnson, N.; Drelich, J.; Yap, Y.K. "The performance of superhydrophobic and superoleophilic carbon nanotube meshes in water-oil filtration," Carbon, **2011,** *49*, (2), 669-676.

[210] Feng, L.; Zhang, Z.Y.; Mai, Z.H.; Ma, Y.M.; Liu, B.Q.; Jiang, L.; Zhu, D.B. "A super-hydrophobic and super-oleophilic coating mesh film for the separation of oil and water," Angewandte Chemie-International Edition, **2004,** *43*, (15), 2012-2014.

[211] Yu, Y.; Chen, H.; Liu, Y.; Craig, V.; Li, L.H.; Chen, Y. "Superhydrophobic and superoleophilic boron nitride nanotube-coated stainless steel meshes for oil and water separation," Advanced Materials Interfaces, **2014,** *1*, (1).

[212] Li, X.; Hu, D.; Cao, L.; Yang, C. "Sensitivity of coalescence separation of oil-water emulsions using stainless steel felt enabled by lbl self-assembly and cvd," Rsc Advances, **2015,** *5*, (87), 71345-71354.

[213] Liu, T.L.; Kim, C.-J.C.J. "Turning a surface superrepellent even to completely wetting liquids," Science, **2014,** *346*, (6213), 1096-1100.

[214] Taylor, N.G. "Cellulose biosynthesis and deposition in higher plants," New Phytologist, **2008,** *178*, (2), 239-252.

[215] Cosgrove, D.J. "Growth of the plant cell wall," Nature Reviews Molecular Cell Biology, **2005,** *6*, (11), 850-861.

[216] Osullivan, A.C. "Cellulose: The structure slowly unravels," Cellulose, **1997,** *4*, (3), 173-207.

[217] Klemm, D.; Heublein, B.; Fink, H.P.; Bohn, A. "Cellulose: Fascinating biopolymer and sustainable raw material," Angewandte Chemie-International Edition, **2005,** *44*, (22), 3358-3393.

[218] Pelton, R. "Bioactive paper provides a low-cost platform for diagnostics," TRAC Trends in Analytical Chemistry, **2009,** *28*, (8), 925-942.

[219] Mohanty, A.K.; Misra, M.; Hinrichsen, G. "Biofibres, biodegradable polymers and biocomposites: An overview," Macromolecular Materials and Engineering, **2000,** *276*, (3-4), 1-24.

[220] Bledzki, A.K.; Gassan, J. "Composites reinforced with cellulose based fibres," Progress in Polymer Science, **1999,** *24*, (2), 221-274.

[221] Beguin, P.; Aubert, J.P. "The biological degradation of cellulose," FEMS Microbiology Review, **1994,** *13*, (1), 25-58.

[222] Abidi, N.; Hequet, E. "Cotton fabric graft copolymerization using microwave plasma. I. Universal attenuated total reflectance-ftir study," Journal of Applied Polymer Science, **2004,** *93*, (1), 145-154.

[223] Inagaki, N. *Plasma surface modification and plasma polymerization*; 1 st Ed.; Technomic Publishing Company: Lancaster, Pennslvania, 1996.

[224] Karahan, H.A.; Ozdogan, E.; Demir, A.; Ayhan, H.; Seventekin, N. "Effects of atmospheric plasma treatment on the dyeability of cotton fabrics by acid dyes," Coloration Technology, **2008,** *124*, (2), 106-110.

[225] Morent, R.; De Geyter, N.; Verschuren, J.; De Clerck, K.; Kiekens, P.; Leys, C. "Non-thermal plasma treatment of textiles," Surface and Coatings Technology, **2008,** *202*, (14), 3427-3449.

[226] Pitt, W.G.; Lakenan, J.E.; Strong, A.B. "The influence of plasma gas species on the adhesion of thermoplastic to organic fibers," Journal of Applied Polymer Science, **1993,** *48*, (5), 845-856.

[227] Sahin, H.T. "Rf-argon plasma induced surface modification of paper," Surface Review and Letters, **2008,** *15*, (4), 503-508.

[228] Abidi, N.; Hequet, E. "Cotton fabric graft copolymerization using microwave plasma. Ii. Physical properties," Journal of Applied Polymer Science, **2005,** *98*, (2), 896-902.

[229] Carlsson, C.M.G.; Strom, G. "Reduction and oxidation of cellulose surfaces by means of cold-plasma," Langmuir, **1991,** *7*, (11), 2492-2497.

[230] Calvimontes, A.; Mauersberger, P.; Nitschke, M.; Dutschk, V.; Simon, F. "Effects of oxygen plasma on cellulose surface," Cellulose, **2011,** *18*, (3), 803-809.

[231] Chan, C.M.; Ko, T.M.; Hiraoka, H. "Polymer surface modification by plasmas and photons," Surface Science Reports, **1996,** *24*, (1-2), 3-54.

[232] Kolarova, K.; Vosmanska, V.; Rimpelova, S.; Svorcik, V. "Effect of plasma treatment on cellulose fiber," Cellulose, **2013,** *20*, (2), 953-961.

[233] Normand, F.; Granier, A.; Leprince, P.; Marec, J.; Shi, M.K.; Clouet, F. "Polymer treatment in the flowing afterglow of an oxygen microwave-discharge - active species profile concentrations and kinetics of the functionalization," Plasma Chemistry and Plasma Processing, **1995,** *15*, (2), 173-198.

[234] Karahan, H.A.; Ozdogan, E. "Improvements of surface functionality of cotton fibers by atmospheric plasma treatment," Fibers and Polymers, **2008,** *9*, (1), 21-26.

[235] Sinha, E.; Panigrahi, S. "Effect of plasma treatment on structure, wettability of jute fiber and flexural strength of its composite," Journal of Composite Materials, **2009,** *43*, (17), 1791-1802.

[236] Vesel, A.; Mozetic, M.; Hladnik, A.; Dolenc, J.; Zule, J.; Milosevic, S.; Krstulovic, N.; Klanjsek-Gunde, M.; Hauptmann, N. "Modification of ink-jet paper by oxygen-plasma treatment," Journal of Physics D: Applied Physics, **2007,** *40*, (12), 3689-3696.

[237] Wong, K.K.; Tao, X.M.; Yuen, C.W.M.; Yeung, K.W. "Wicking properties of linen treated with low temperature plasma," Textile Research Journal, **2001,** *71*, (1), 49-56.

[238] Flynn, C.N.; Byrne, C.P.; Meenan, B.J. "Surface modification of cellulose via atmospheric pressure plasma processing in air and ammonia-nitrogen gas," Surface and Coatings Technology, **2013,** *233*, 108-118.

[239] Sinha, E.; Rout, S.K.; Barhai, P.K. "Study of the structural and thermal properties of plasma treated jute fibre," Applied Physics A, **2008,** *92*, (2), 283-290.

[240] Wu, J.; Zeng, F.C.; Chen, B.Q. "The solubility of natural cellulose after dbd plasma treatment," Plasma Science & Technology, **2008,** *10*, (6), 743-747.

[241] Baltazar-Y-Jimenez, A.; Bistritz, M.; Schulz, E.; Bismarck, A. "Atmospheric air pressure plasma treatment of lignocellulosic fibres: Impact on mechanical properties and adhesion to cellulose acetate butyrate," Composites Science and Technology, **2008,** *68*, (1), 215-227.

[242] Temmerman, E.; Akishev, Y.; Trushkin, N.; Leys, C.; Verschuren, J. "Surface modification with a remote atmospheric pressure plasma: Dc glow discharge and surface streamer regime," Journal of Physics D-Applied Physics, **2005,** *38*, (4), 505-509.

[243] Carneiro, N.; Souto, A.P.; Silva, E.; Marimba, A.; Tena, B.; Ferreira, H.; Magalhaes, V. "Dyeability of corona-treated fabrics," Coloration Technology, **2001,** *117*, (5), 298-302.

[244] Pandiyaraj, K.N.; Selvarajan, V. "Non-thermal plasma treatment for hydrophilicity improvement of grey cotton fabrics," Journal of Materials Processing Technology, **2008,** *199*, (1-3), 130-139.

[245] Inbakumar, S.; Morent, R.; De Geyter, N.; Desmet, T.; Anukaliani, A.; Dubruel, P.; Leys, C. "Chemical and physical analysis of cotton fabrics plasma-treated with a low pressure dc glow discharge," Cellulose, **2010,** *17*, (2), 417-426.

[246] Ward, T.L.; Jung, H.Z.; Hinojosa, O.; Benerito, R.R. "Effect of rf cold-plasmas on polysaccharides," Surface Science, **1978,** *76*, (1), 257-273.

[247] Sun, D.; Stylios, G.K. "Effect of low temperature plasma treatment on the scouring and dyeing of natural fabrics," Textile Research Journal, **2004,** *74*, (9), 751-756.

[248] Wong, K.K.; Tao, X.M.; Yuen, C.W.M.; Yeung, K.W. "Low temperature plasma treatment of linen," Textile Research Journal, **1999,** *69*, (11), 846-855.

[249] Gaiolas, C.; Costa, A.P.; Silva, M.S.; Thielemans, W.; Amaral, M.E. "Cold plasma-assisted paper recycling," Industrial Crops and Products, **2013,** *43*, 114-118.

[250] Jamali, A.; Evans, P.D. "Etching of wood surfaces by glow discharge plasma," Wood Science and Technology, **2011,** *45*, (1), 169-182.

[251] Sapieha, S.; Wrobel, A.M.; Wertheimer, M.R. "Plasma-assited etching of paper," Plasma Chemistry and Plasma Processing, **1988,** *8*, (3), 331-346.

[252] Sabharwal, H.S.; Denes, F.; Nielsen, L.; Young, R.A. "Free-radical formation in jute from argon plasma treatment," Journal of Agricultural and Food Chemistry, **1993,** *41*, (11), 2202-2207.

[253] Tsafack, M.J.; Levalois-Grutzmacher, J. "Towards multifunctional surfaces using the plasma-induced graft-polymerization (pigp) process: Flame and waterproof cotton textiles," Surface & Coatings Technology, **2007,** *201*, (12), 5789-5795.

[254] Wielen, L.C.V.; Ragauskas, A.J. "Grafting of acrylamide onto cellulosic fibers via dielectric-barrier discharge," European Polymer Journal, **2004,** *40*, (3), 477-482.

[255] Ren, C.S.; Wang, D.Z.; Wang, Y.N. "Improvement of the graft and dyeability of linen by dbd treatment in ambient air," Journal of Materials Processing Technology, **2008,** *206*, (1-3), 216-220.

[256] Mihailovic, D.; Saponjic, Z.; Radoicic, M.; Lazovic, S.; Baily, C.J.; Jovancic, P.; Nedeljkovic, J.; Radetic, M. "Functionalization of cotton fabrics with corona/air rf plasma and colloidal tio2 nanoparticles," Cellulose, **2011,** *18*, (3), 811-825.

[257] Mejia, M.I.; Marin, J.M.; Restrepo, G.; Pulgarin, C.; Mielczarski, E.; Mielczarski, J.; Arroyo, Y.; Lavanchy, J.C.; Kiwi, J. "Self-cleaning modified tio2-cotton pretreated by uvc-light (185 nm) and rf-plasma in vacuum and also under atmospheric pressure," Applied Catalysis B, **2009,** *91*, (1-2), 481-488.

[258] Bhat, N.V.; Benjamin, Y.N. "Surface resistivity behavior of plasma treated and plasma grafted cotton and polyester fabrics," Textile Research Journal, **1999,** *69*, (1), 38-42.

[259] Sahin, H.T. "Pyrrole thin films deposited on paper by pulsed rf plasma," Central European Journal of Chemistry, **2007,** *5*, (3), 824-834.

[260] Tsafack, M.J.; Levalois-Grutzmacher, J. "Flame retardancy of cotton textiles by plasma-induced graft-polymerization (pigp)," Surface and Coatings Technology, **2006,** *201*, (6), 2599-2610.

[261] Sahin, H.T. "Application of rf argon plasma to enhance hydrophobic properties of fluoropolymer pre-deposited paper," Journal of Adhesion Science and Technology, **2011,** *25*, (6-7), 685-697.

[262] Ward, T.L.; Jung, H.Z.; Hinojosa, O.; Benerito, R.R. "Characterization and use of radio-frequency plasma-activated natural polymers," Journal of Applied Polymer Science, **1979,** *23*, (7), 1987-2003.

[263] Chen, J.R. "Free-radicals of fibers treated with low-temperature plasma," Journal of Applied Polymer Science, **1991,** *42*, (7), 2035-2037.

[264] Kobayash.H; Bell, A.T.; Shen, M. "Formation of an amorphous powder during polymerization of ethylene in a radio-frequency discharge," Journal of Applied Polymer Science, **1973,** *17*, (3), 885-892.

[265] Tu, X.; Young, R.A.; Denes, F. "Improvement of bonding between cellulose and polypropylene by plasma treatment," Cellulose, **1994,** *1*, (1), 87-106.

[266] Ozdogan, E.; Saber, R.; Ayhan, H.; Seventekin, N. "A new approach for dyeability of cotton fabrics by different plasma polymerisation methods," Coloration Technology, **2002,** *118*, (3), 100-103.

[267] Magalhaes, W.L.E.; de Souza, M.F. "Solid softwood coated with plasma-polymer for water repellence," Surface and Coatings Technology, **2002,** *155*, (1), 11-15.

[268] Sapieha, S.; Verreault, M.; Klembergsapieha, J.E.; Sacher, E.; Wertheimer, M.R. "X-ray photoelectron study of the plasma fluorination of lignocellulose," Applied Surface Science, **1990,** *44*, (2), 165-169.

[269] McCord, M.G.; Hwang, Y.J.; Qiu, Y.; Hughes, L.K.; Bourham, M.A. "Surface analysis of cotton fabrics fluorinated in radio-frequency plasma," Journal of Applied Polymer Science, **2003,** *88*, (8), 2038-2047.

[270] Zhang, J.; France, P.; Radomyselskiy, A.; Datta, S.; Zhao, J.A.; van Ooij, W. "Hydrophobic cotton fabric coated by a thin nanoparticulate plasma film," Journal of Applied Polymer Science, **2003,** *88*, (6), 1473-1481.

[271] Vohrer, U.; Muller, M.; Oehr, C. "Glow-discharge treatment for the modification of textiles," Surface and Coatings Technology, **1998,** *98*, (1-3), 1128-1131.

[272] Sahin, H.T.; Manolache, S.; Young, R.A.; Denes, F. "Surface fluorination of paper in cf_4-rf plasma environments," Cellulose, **2002,** *9*, (2), 171-181.

[273] Mukhopadhyay, S.M.; Joshi, P.; Datta, S.; Zhao, J.G.; France, P. "Plasma assisted hydrophobic coatings on porous materials: Influence of plasma parameters," Journal of Physics D: Applied Physics, **2002,** *35*, (16), 1927-1933.